POLITECNICO DI MILANO

School OF CIVIL, ENVIRONMENTAL AND TERRITORIAL ENGINEERING

Master degree in STRUCTURAL ENGINEERING

Optimization of post-tensioned concrete floor slabs

Supervisor:
Professor Franco MOLA

Co-supervisors:
Eng. Eric Long, **Eng. David Shook**, **Eng. Alessandro Beghini (Skidmore, Owings and Merrill LLP Office of San Francisco)**

Candidate:
Marc Hymans
817514

Politecnico di Milano
School of Civil, Environmental and Territorial Engineering
Building 5
Piazza Leonardo da Vinci, 32
20133 Milano, Italy

Skidmore, Owings & Merrill LLP
One Front Street, Suite 2400
San Francisco, CA 94111, USA

Marc Hymans (Author)
+33 (0)624622187
3, Villa Juge
75015 Paris
marchymans@gmail.com

“Dans la poutre en béton précontraint, l’acier n’est pas une armature, c’est une force.” Yves Guyon [7]

“In the prestressed concrete beam, the steel is not a reinforcement, it is a force. “ translated from french by the author

Table of Contents

Preface

The presented work has been possible thanks to the friendship and professional cooperation between my professor, Franco Mola, and Mark Sarkisian, partner and director of the structural engineering group in the Skidmore, Owings and Merrill LLP office of San Francisco.
Their friendship offered me the chance to have an internship with SOM in San Francisco, providing me the opportunity to deal with an innovative and challenging topic for my thesis research. The internship also, allowed me to observe different approaches to structural engineering design, and to learn from practicing professionals.

The perfect cooperation I observed between architects and engineers made me realize the importance of working in a team with different skills and backgrounds.

First of all, I would like to acknowledge everyone in the structural engineering group of the SOM San Francisco office.

Moreover, my sincere thanks to Professor Mola, Elena Mola and Laura Pellegrini, who gave me their support in creating this great opportunity.
I would also like to thank Mark Sarkisian, and along with him the entire Skidmore Owings and Merrill office of San Francisco, whose experiences and passion were fundamental in approaching the research topic studied.

Particularly I would like to thank the people I worked more closely with: Alessandro Beghini, David Shook and Eric Long, who deserve special thanks for the incredible help they gave me throughout , and through the completion of my research.
Their advice and feedback have been more than helpful when developing my research study.
Finally, I would like to acknowledge the people of the office who advised me on my research, Neville Mathias, Samantha Walker, Lily Rong, Nicole, Yue, Francesco Renaudo and all the members of the structural engineering team of the San Francisco office with whom I had the chance to work with.

Abstract

The proposed study will focus on the design of flat plate slabs, with a particular concern for high-rise buildings. The slab has a crucial role within these structures, acting as a diaphragm to transfer the forces – seismic forces and gravity loads – to the members supporting the floor, providing a "level-to-level redistribution of forces".
The present work aims to formulate a methodology to design thin post-tensioned reinforced concrete slabs for complex architectural projects. Complexities considered include asymmetrical slabs, the non-regularity of columns and, very long spans. For architectural and structural reasons, flat slabs are becoming thinner. This trend can reduce building height and/or allow more floors in a single building. From a structural perspective, the thinning of slabs primarily reduces the amount of material used and allows for a reduction in structural weight. For high-rise constructions, smaller walls and foundations is a crucial factor.

The main objective of the research will focus on the use of post-tensioning in order to reduce:
1. Thickness and weight of slabs by finding the optimal location of post-tensioning.
As we can imagine this will save on the amount of rebar used thanks to the use of post-tensioning.
2. Slab deflections for very long spans.
The goal is to achieve increased structural performance of a building structure and reduce overall cost construction.
The first task requires finding tools to predict optimal post-tensioned layouts/profiles. This can be accomplished by separating the problem into two parts: the in-plane behavior and the out-of-plane behavior. The out-of-plane behavior can be studied using the *force density method*. This method would determine the vertical drape of cable networks defined by the post-tensioning tendons through changing the coordinates of the fixed nodes or the force densities of the cables. The in-plane problem can be analyzed using plate theory. The main objective is to determine the directions of the stresses within the plate. The topology optimization will give a good initial evaluation if applied by scaling the intensity of the stresses to differentiate the banded tendons from the uniform ones.

A complete understanding of the post-tensioning concrete slab behavior is indispensable to perform the optimization procedure, therefore a number of factors, such as cracking, deflection, creep and shrinkage must also be taken into account when finalizing the optimized design.
First, the design criteria used to design post-tensioning concrete slabs, both in a traditional and in an optimized way, will be presented.
Subsequently, topology optimization will be applied to define the optimized tendons profile and layout, which will then be updated using a FEM software in order to evaluate the accuracy of the results and to verify their compliance with the design criteria and code specifications

Finally, an evaluation of the rebar quantities, both for prestressing and ordinary design, for use in the optimized design will be carried out with a comparison between the optimized and traditional layout to be performed.

One step further in the research would consist of considering construction constraints (construction techniques, feasibility, time and cost) to adapt the obtained optimized profiles to a possible utilization on site.

1. Introduction

There are many advantages to the use of post-tensioning which have resulted in it becoming more and more systematically used in construction practices. Post-tensioned flat slabs are a good example as they allow a significant reduction of the slab's thickness by maximizing the spans, and helping to increase the number of floors, which can be of particular interest for high-rise buildings.

The application of post-tensioning is a well mastered and common technique today. The preferred approach for a typical flat slab is to have banded tendons in one direction and distributed tendons in the other. The advantage of this solution is that both directions can be designed with a maximum permissible drape to counteract the maximum bending moment at mid-span between two columns.

On one hand, and thanks to computer advancements, design procedures have radically evolved during the past several decades. Each building can have a unique shape. On the other hand, the conventional approach to applying post-tensioning is currently developed as a trial and error process and can become very time consuming. This approach requires an iterative process, the right intuition of the engineer and to take into account the architectural modifications throughout the design phase.
It becomes crucial to find a way to apply conventional post-tensioning in particular shaped buildings, in order, as a final step, to find the most efficient way to post-tension a regular or complex shaped flat slab.

One way to solve these issues can be found thanks to the use of new optimization methodologies, combined with MatLab codes, to create a specific tool to optimize post-tensioning in concrete flat slabs. This tool could help to provide a better performance of the buildings slabs along with saving time and reducing the cost of the building.
Investigation of topology optimization and force density methods can be used in order to discover these new ways of post-tensioning. Topology optimization is a mathematical approach that optimizes the material layout in a given space, commonly used in in the aeronautical or car industry.
The Force Density Method is a computational method through which a membrane surface is transformed into a discrete cable network; in order to determine the equilibrium geometry of a prestressed membrane subjected to a certain load case and a set of predefined boundary conditions. The method is usually employed for tensile structures, gridshells, etc.

The opportunity to investigate these state-of-the-art methods was possible through an internship with the structural engineering department of the San Francisco branch of Skidmore,

Owings and Merrill LLP. It was a great opportunity to apply these new tools to one of the most challenging high-rise building designs they are currently pursuing in their practice. In fact, during the internship the above mentioned optimization procedure consistency has been tested on a residential building located on the front bay of the San Francisco financial district area.
For this reason, the research that has been carried out intends to achieve a double objective: to satisfy the code requirements, with a better deflection profile of the post-tensioned concrete flat slab and also with the least possible amount of cables.

In this work, a double optimization approach has been investigated, developing in parallel an In-Plan optimization method and a Profiles optimization procedure.

Thanks to the cited optimization tools and some self-development codes, a clear step-by-step procedure has been elaborated and can be inserted into those projects that require optimization.

2. Post-tensioning design for concrete flat slabs

2.1 Advantages of prestressed slabs compared to reinforced concrete slabs

Post-tensioning allows almost any shape of structure to be constructed, while reducing environmental impacts, construction time, materials and costs. The use of post-tensioning allows for thinner concrete sections, longer spans between supports, stiffer walls to resist lateral loads and stiffer foundations to resist the effects of shrinking and swelling soils. Concrete has what engineers call 'compressive' strength- meaning that it happily bears its own weight within a structure. As soon as one introduces the 'live' loads of everyday usage, such as vehicles in a car park or on a bridge, the concrete tends to deflect or sag which leads to cracking, thus weakening the structure.

2.1.1 Savings

Post tensioning (PT) offers non-negligible savings in materials. A decrease in material used directly translates to cost reductions and when also considering the environmental impact or carbon impact by employing less embodied energy for the structure the consequences are significant. The Post tensioning and load balancing effects provided by PT within the concrete elements increases the spans possible with thinner structural elements. A typical post-tensioned floor on average is about 20 % thinner than a classical reinforced concrete (RC) floor (Figure 1). For example, once span length exceeds a threshold value of about 16ft (5m), a post-tensioned slab will be approximately 1/3 thinner than a reinforced concrete slab designed for the same loading.

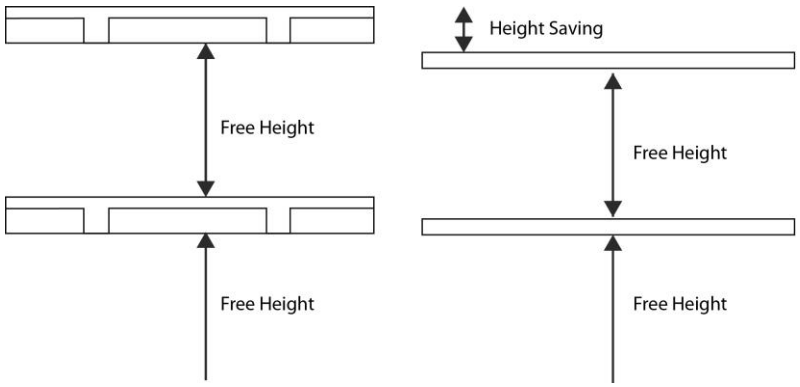

Figure 1: reinforced concrete floor and post-tensioned slab (Source: author, 2015)

The study by Dane Miller [12] confirms that the reduction of concrete usage or steel mass through the use of post-tensioning increases with span length, ranging for concrete to be about a 21.5 % reduction for a 6.67 m span up to 34.4% for a 13.33 m span. PT also reduces the steel mass by between 23% and 44%. (See figures below)
In fact, reducing the floor thickness impacts the entire dead load of the building, which means less concrete material required for the slab, the columns, the walls and the foundations.
That is to say it reduces almost 20% [8] of the total dead load of the entire structure.

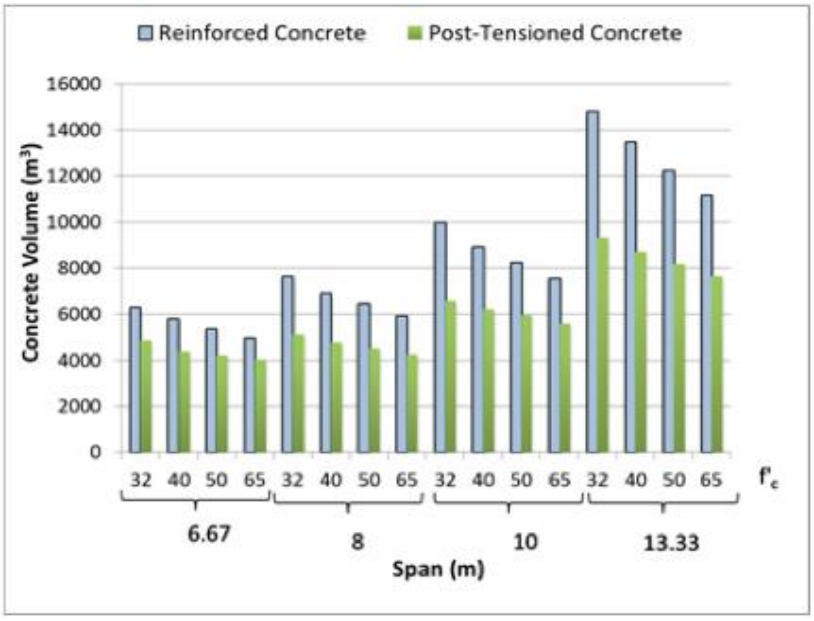

Figure 2: concrete volume of building (Source: Miller, Dane, June 2013)

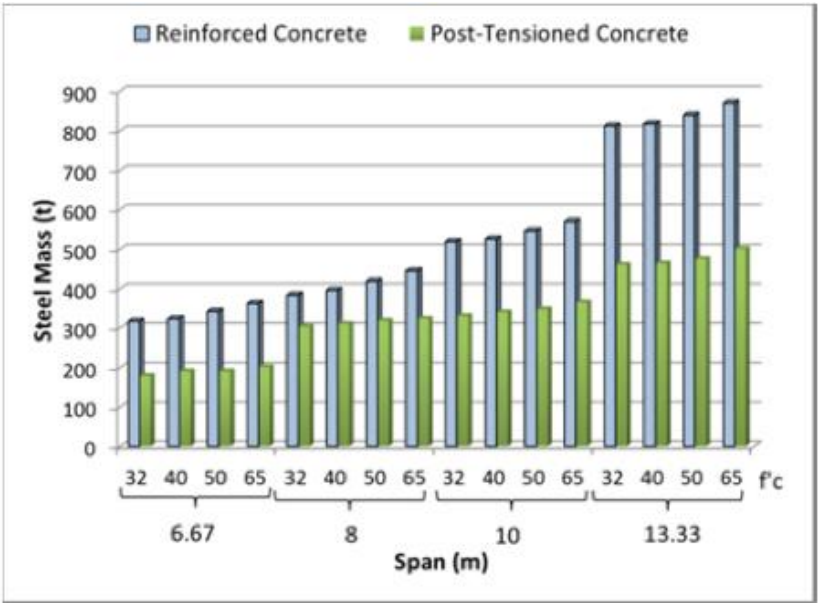

Figure 3: Total steel mass of building (Source: Miller, Dane, June 2013)

Also, a thinner slab, primarily in high-rise buildings, allows as many floors as possible with no increase of the final building total height.

A study [8] made by Pakwan Gupta has shown that PT concrete slabs generally contain 30 % to 50 % less steel than RC elements when designed for equivalent load, span and performance (Table 1).

Bay size, ft x ft	Slab thickness, in.	Span-to-thickness ratio	Material quantities per ft²			Costs		
			Concrete, in.	Reinforcing bars, lb	PT steel, lb	Concrete, $/ft²	Steel, $/ft²	Total, $/ft²
RC floor system								
30 x 30	10+4*	36	10.3†	4	0	5.56	3.60	9.16
PT floor System								
30 x 30	8.5	42.4	8.6	0.8	0.9	4.65	2.79	7.44
30 x 30	8	45	8.2	1.6	0.95	4.42	3.63	8.05

Table 1: Cost comparison of RC and PT floor systems (Source: Gupta, Pakwan R., October 2012)

2.1.2 Longevity and durability of Post-Tensioning

Experience helps to recognize PT structures have a great durability and longevity.
PT structures are often designed to limit cracking effects under service loads. When the members are uncracked, or cracked, but to a limited degree, structures become more durable, as limited cracking prevents the potential corrosion of reinforcement developeding as a result of concrete carbonation and leading to the breaking out of steel, i.e. the rebars and tendons.
The slab thus becomes virtually waterproof, i.e. crack free.

Another point is the height reduction of buildings, which impacts directly on the volumes to heat in winter or air condition in summer, which in turns improves the energy efficiency of the building.

2.2 History of post-tensioned slabs

2.2.1 Early attempts

Prestressing has long existed in many systems; most common being the wine barrel, i.e. the steel laying around the wood barrel prestresses the wood.

Even many attempts were officially made since the end of the nineteenth century, i.e. Jackson inserting rods into masonry units to stress them with a suitable device. Yet prestressed concrete would not officially arrive until the thirties, as Eugène Freyssinet publishes his first patent in 1928. The first patent for prestressed concrete, published on the 2nd of October 1928, was called “Procédé de fabrication des pieces en béton armé”.

In fact, even though the technique of prestressing concrete existed, the losses were so important due to the low strength of the steel that this steel was not strong enough to counteract the losses, thus not preventing cracking.
The arrival of high strength steel allowed Freyssinet to develop the Freyssinet system, a conical wedge anchor system for 12 wires tendons.
“At any degree, post-tensioned concrete is an improved reinforced concrete. It has with the reinforced concrete no common border. “ Eugène Freyssinet, 1946

2.2.2 Post-tensioned slabs

In the 50’s, the lift slab construction method was introduced, principally in the United States where pioneering engineers reconsidered the concept of prestressing with the principal objective to eliminate cracks and reduce slab deflection within thin flat slabs. Important to

remember is that the slab technique was quite recent when Freyssinert patented prestressing. For example, in 1913, only 1000 flat slab buildings were built around the world. As mentioned by Lin [11], post-tensioning allowed the engineer to reduce in the design the dead loads applied to a slab, through, for example, the concept of “load-balancing”.

When prestressed concrete was incorporated into the building codes in the 60’s it presented the opportunity to engineers to develop post-tensioning into building construction, primarily for slabs.

2.3 Basic principles of prestressing

2.3.1 Definition

It is interesting first to look at some of the definitions given for prestressing found through different sources. These definitions will then be discussed in order to better understand the main objective when prestressing concrete.

- Translated from Wikipedia.fr:

Prestressed concrete is a building concrete works technique, which consists of creating internal positive stresses. These are carefully adjusted to reduce the concrete weakness when it is in traction. Post-tensioning is often realized thanks to cables grouted with concrete.

- Wikipedia.en:

Prestressed concrete is a method for overcoming concrete’s natural weakness in tension. It is a material that has the characteristics of high strength concrete in compression and high ductile strength steel for tension. The bending shape should be opposite of the applied force it will service. It can be used to produce beams, floors or bridges with a longer span than is practical with ordinary reinforced concrete.

- What is post-tensioning? [14]

Post-tensioning is a method a reinforcing (strengthening) concrete or other materials with high-strength steel strands or bars typically referred to as tendons.

- ACI Committee:

Prestressed concrete: Concrete in which there have been introduced internal stresses of such magnitude and distribution that the stresses resulting from given external loadings are counteracted to a desired degree. In reinforced-concrete members the prestress is commonly introduced by tensioning the steel reinforcement.

What is mainly stated is that prestressing is a way to create internal prestresses which overcome the concrete’s natural weakness in tension. Prestressing is realized thanks to the help of post-tensioned steel tendons. The prestressing force P, which tends to satisfy the conditions of geometry and loading of a given element is determined from the principles of mechanics. Below, the case of a simply supported rectangular beam is shortly analyzed.

2.3.2 Fundamental mechanics of prestressed concrete

The first attempts of prestressing as invented by Freyssinet transformed a brittle material into an elastic one by the compression given to it. From this concept the criteria of no tensile stresses was born, according to the following steps:

1- NO TENSILE STRESSES
2- NO CRACKS
3- CONCRETE NO LONGER BRITTLE
4- CONCRETE AS AN ELASTIC MATERIAL

Considering a simple supported rectangular beam subjected to a concentric force P, the compressive stress acting on the beam is uniform. Cracking of concrete due to loads is prevented or delayed by the precompression produced by the tendons. Evidence of cracking allows one to consider the stresses, strains and deflection of the concrete separately and even to superimpose upon it.

Four different cases will be presented in order to better understand the role of prestressing and also the role of eccentricity.

1) Case 1: Without external loads, only the prestressing forces are applied

$$f = -\frac{P}{A}$$

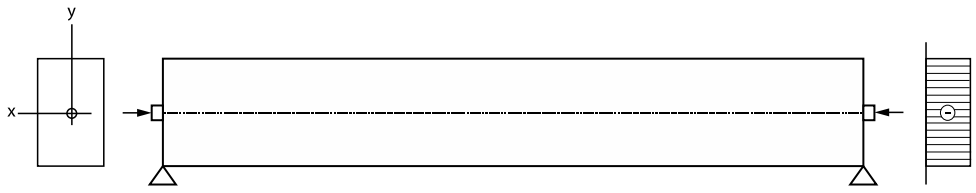

Figure 4: Concrete fiber stress distribution in a rectangular beam with straight tendon: Concentric tendon, prestress only (Source: Nawy, 2009)

A = bh, area of the beam section

2) Case 2: Application of external transverse loads added to the prestressing forces

At the top of the beam:

$$f^t = -\frac{P}{A} - \frac{M}{I_g}$$

At the bottom of the beam:

$$f^b = -\frac{P}{A} + \frac{M}{I_g}$$

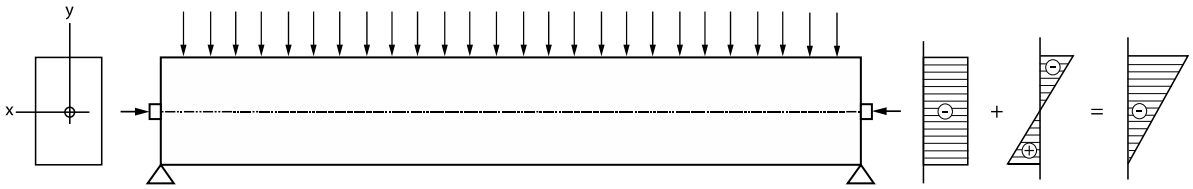

Figure 5: Concrete fiber stress distribution in a rectangular beam with straight tendon: Concentric tendon, self-weight added (Source: Nawy, 2009)

Where:

f^t = stress at the top fibers
f_b = stress at the bottom fibers
c = ½ h for the rectangular section
I_g = moment of inertia of the section = $bh^3/12$

What we observe here is that the compressive stress capacity of the beam to counteract uniformly distributed external loads is limited by the fact that the prestressing forces are placed concentrically, that is to say centered at a mid-distance of the section. Placing the tendon with an eccentricity, in the bottom part of the beam, helps the concrete beam to reduce the tensile stresses into the bottom fibers. This also creates tensile stresses at the top fibers of the beam, instead of compressive stresses, as seen before, without eccentricity into the tendons position.

3) Case 3: Case 1 considering the prestressing force applied with an eccentricity

$$f^t = -\frac{P}{A} + \frac{P_{ec}}{I_g}$$

$$f^t = -\frac{P}{A} - \frac{P_{ec}}{I_g}$$

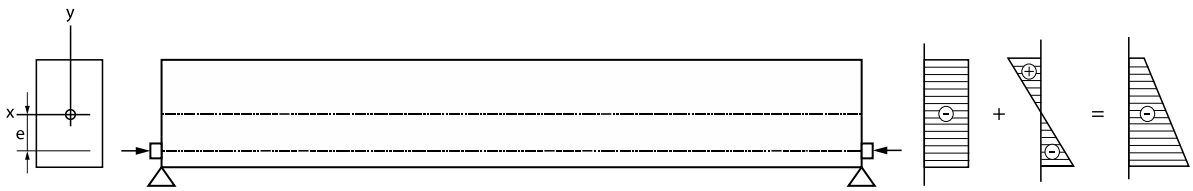

Figure 6: Concrete fiber stress distribution in a rectangular beam with straight tendon: Eccentric tendon, prestress only (Source: Nawy, 2009)

With P_{ec} generated by the tendon placed at a distance e from the center of gravity of the
Concrete beam.

4) Case 4: Case 2 considering the prestressing force applied with an eccentricity

$$f^t = -\frac{P}{A} + \frac{P_{ec}}{I_g} - \frac{M}{I_g}$$

$$f^t = -\frac{P}{A} - \frac{P_{ec}}{I_g} + \frac{M}{I_g}$$

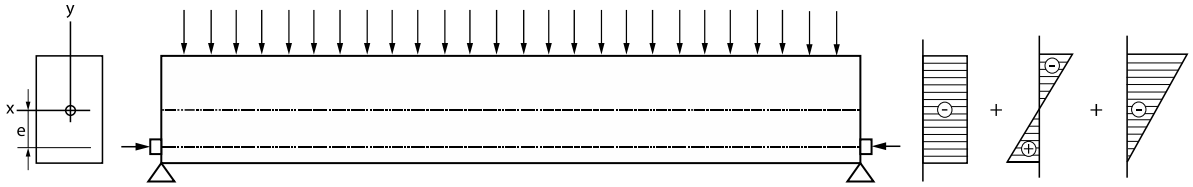

Figure 7: Concrete fiber stress distribution in a rectangular beam with straight tendon: Eccentric tendon, self-weight added (Source: Nawy, 2009)

These different studies are a valuable way to conclude that concrete stresses at a section due to prestress are dependent only on the magnitude and F location at the section, depending on how the tendon profile location could vary along the beam height [11].

2.4 Prestressed Concrete

2.4.1 Intrinsic characteristics

High strength concrete for prestressing is preferable for many reasons:

- The anchorages are mainly designed based on high-strength concrete.
  In fact, if the concrete is not strong enough, it could fail under the pressure of the anchorages when applying the prestress.

- Second, a concrete submitted to prestress is under higher stresses than a classical reinforced concrete. It is therefore interesting to increase its strength, which allows to increase the resistance in tension and shear.
- A high-strength concrete allows to avoid shrinkage cracks, principally the ones which could occur before the application of prestresses.
- It will also help through a smaller loss of prestress in the steel, i.e. a high strength concrete will have smaller creep strains, having a higher modulus of elasticity.

The short-term properties will particularly deal with:
- Strength in compression and in tension
- Stiffness

And the long term one is principally related to:
- Creep
- Shrinkage

2.4.1.1 Compressive strength

The normal production of concrete retains a compressive strength comprising between 4000 to 12000 psi, with a common concrete with an average of 6000 psi.
For prestressed concrete a compressive strength f'_c exceeding 20000 psi is recommended. When making a strength test, the ACI code specifies [13]:

To use the average of two cylinders from the same sample tested and the same age, which is usually 28 days. As for the frequency of testing, the code specifies that the strength of an individual class of concrete can be considered satisfactory if (1) the average of all sets of three consecutive strength test equals or exceeds the required f'_c and (2) no individual strength test (average of two cylinders) falls below the required f'_c.

Also, Guyon [7] specifies the required resistance depends on the class of building.
- 380 to 450 kg/cm2 after 28 days for a class 1 building (total prestressing)
- 330 to 380 kg/cm2 after 28 Days for a class 2 and 3 building (prestressed reinforced concrete)

2.4.1.2 Tensile strength

Concrete is particularly known to suffer from a low tensile strength, which is the reason it requires reinforcing or prestressing, to counteract its tensile weakness under flexure.
The tensile strength is comprised between 0,10 f'_c and 0,20 f'_c:

$$0{,}10\, f'_c < f'_{ct} < 0{,}20\, f'_c$$

2.5 Concrete strains

The initial deformation due to load is considered as the elastic strain.
When sequentially casting the prestressed concrete structures, the concrete characteristics, the exposure conditions and a chronological account of the construction steps influence the concrete creep and shrinkage behaviors. The effects of creep and shrinkage create internal stresses and additional deformations of the structure. The additional strain due to sustained load is the creep strain. And the shrinkage strain, which can be assumed to superpose the elastic strain and the creep strain, is a strain dependent on the chemical/physical behavior of the concrete.

$$Total\ strain\ \varepsilon_t = elastic\ strain\ \varepsilon_e + creep\ strain\ \varepsilon_c + shrinkage\ strain\ \varepsilon_s$$

2.5.1 Creep

The deformation due to creep causes an additional time strain contrary to the instantaneous elastic stain. This strain happens when the concrete is subjected to a constraint more or less sustained along the time.
The long-term load is significant compared to short-term loading in their effect on the behavior of a structure.
Creep deformation is proportional to applied stress, but the proportionality is valid only for low stress levels.

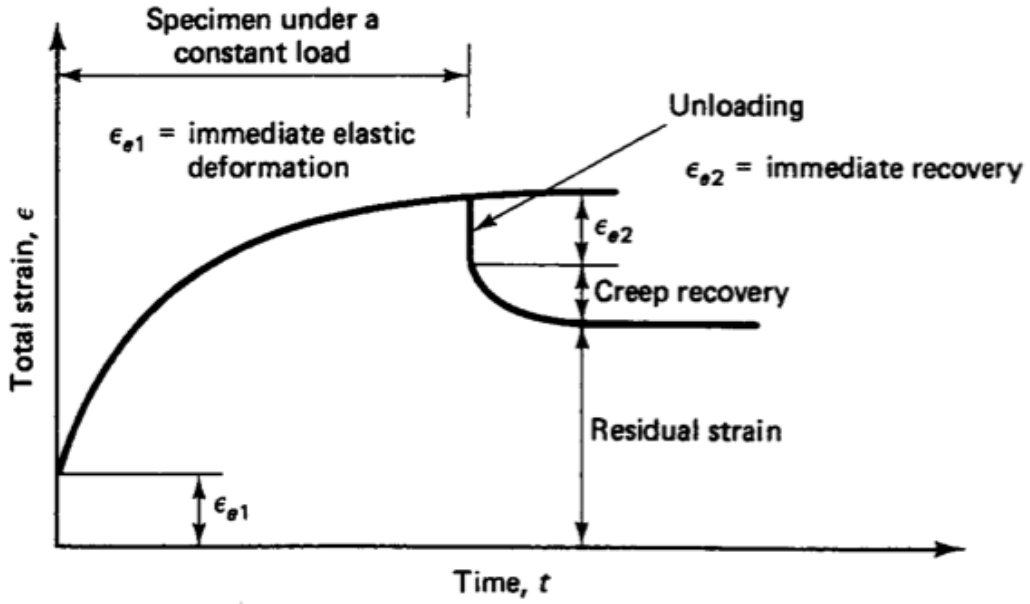

Figure 8: Graph of the delayed strain evolution in function of time (Source: Nawy, 2009)

As in shrinkage, creep increases the deflection of beams and slabs and causes losses of prestress. The initial eccentricity of a reinforced concrete column increases with time due to creep, and it results in the transfer of the compressive load from the concrete to the steel in the low part of the section.
σ being the constraint and ε_d the unitary creep, the modulous of elasticity is defined as the relationship $\frac{\sigma}{E_d}$.

Guyon [7] defines as follow the variation law of the creep delayed strain in function of time:

$$\varepsilon_d(t) = \varepsilon_d\,(1 - e^{\sqrt{\frac{t}{t_1}}})$$

It is important to precise that we should not prestress the slab too soon in order to avoid important long-term creep deformations. It is better to wait that certain shrinkage deformations happen to prestress the slab. As recommended by Guyon [7], we can prestress the component when the resistance reaches the two third of the 28 days complete resistance. The elastic modulous appears to be at 80% of the 28 days elastic modulus.

2.5.2 Shrinkage

The concrete shrinkage is mainly due to water evaporation and thanks to the moisturizing of its components over time. According to Nawy [13], shrinkage can be classified into 2 types: plastic shrinkage and drying shrinkage. Plastic shrinkage happens during the first hours after

placing fresh concrete into the forms. Slabs dry particularly easily and fast due to their large contact surface with the air. Drying shrinkage happens after concrete has attained its final strength of 28 days.

" Drying shrinkage is the decrease in the volume of a concrete element when it loses moisture by evaporation. The opposite phenomenon, that is, volume increase through water absorption, is termed swelling. In other words, shrinkage and swelling represent water movement out or into the gel structure of a concrete specimen due to the difference in humidity or saturation levels between the specimen and the surroundings irrespective of the external load."[13]

The final deformations due to shrinkage are reached after a long time – nearly two or three years if we consider elements of a classic width. In fact, the phenomenon is relatively fast at the beginning: as detailed by Guyon [7], a quarter of the shrinkage is reached after seven days, one third after fourteen days, half of the total shrinkage after one month, and three quarters after six months.

Shrinkage will evolve in time (figure) until a certain period as well defined by Guyon with the following formula:

$$\frac{\eta_t}{\eta_\infty} = \frac{(1.5 + t)\, t}{1 + 4t + t^2}$$

Where:

$\eta_\infty : final\ shrinkage$
$\eta_t : shrinkage\ varying\ with\ time$
$t : characteristic\ time\ for\ concrete\ drying$

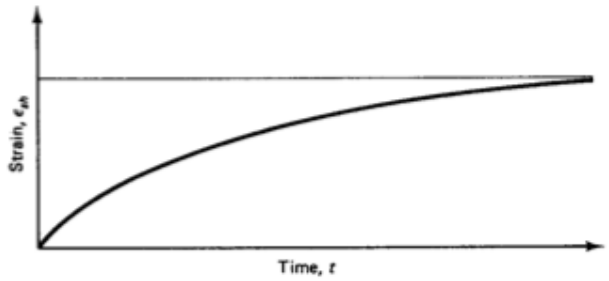

Figure 9: Shrinkage-time curve (Source: Nawy, 2009)

Also the shrinkage increases when the water quantity increases: the relationship $\frac{E}{C}$

Where:

$E : Water\ weight/m3$
$C : Cement\ weight/m3$

The shrinkage also increases when the cement grounds more finely, when the aggregates' sizes diminish, i.e. when the member compactness increases (figure). Shrinkage also increases thanks to temperature.

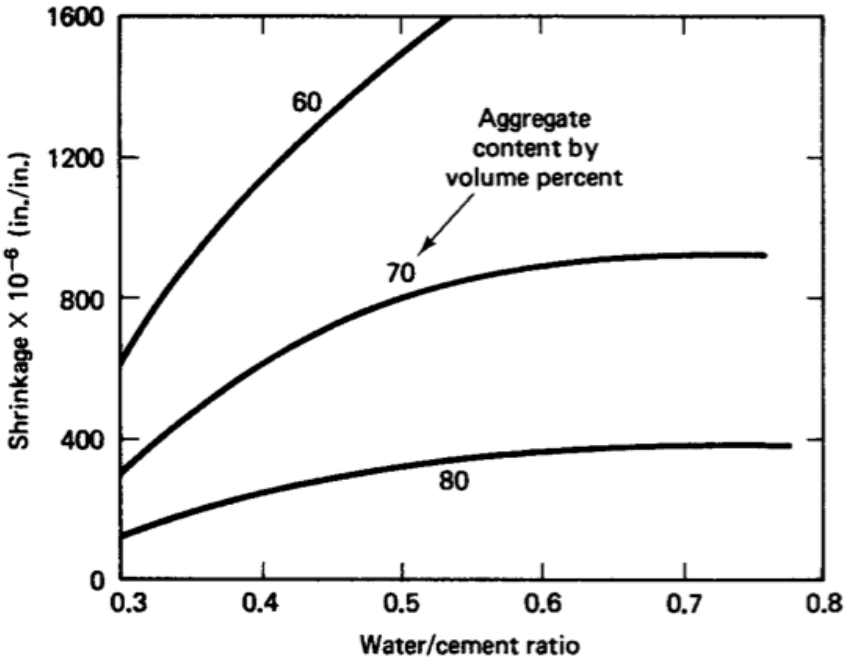

Figure 10: Water/Cement and Aggregate content effect on shrinkage (Source: Nawy, 2009)

Other factors will affect the magnitude of drying shrinkage, such as: the amount of reinforced concrete (reinforced concrete shrinks less than plain concrete), the relative humidity, the carbonation, etc

2.5.3 Importance of the surface exposure for the creep and shrinkage deformations

The study carried out by Lefebvre [10] for a prestressed bridge (Figure 11) shows the importance of the surface exposure for creep and shrinkage effects. Lefebvre studied a post-tensioned bridge (figure), but the study results could be used to provide a better understanding of the behavior of a slab, as these additional deformations will have an important impact on slab structures, due to its large surface of exposure. In fact, the study reveals the importance of the surface of exposure, thanks to two different studied exposed surfaces (Figure 12).

Figure 11: Post-tensioned precast bridge (Source: Lefebvre, 2002)

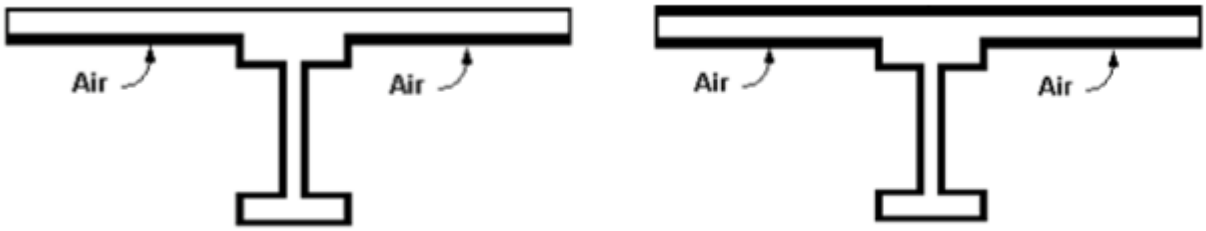

Figure 12: Surfaces under small and large exposures (Source: Lefebvre, 2002)

	Creep and Shrinkage		Only Creep	
Delay (days)	Moments under low exposure (KN.m)	Moments under high exposure (KN.m)	Moments under low exposure (KN.m)	Moments under high exposure (KN.m)
30	1876	2270	115	-203
60	1648	2040	-8	-327
100	1442	1831	-146	-465
365	802	1176	-667	-1009

Table 2: Bending moments due to creep and shrinkage (Source: Lefebvre, 2002)

Through the table, we can notice that the higher the exposure surface, the more important the delayed shrinkages. In such a case, the final moments increase during the creep and shrinkage. The effects of the shrinkage increase of the constraints on the concrete, in a similar way as post-tensioning, which increases the creep effects [10].

2.6 Post-tensioning systems for two-way slabs

Two-way systems are generally supported by columns or short walls designed to resist bending in two orthogonal directions. This study will focus on slabs with uniform thickness.

2.6.1 Prestressing reinforcement characteristics

A high-tensile steel is now the common material for prestressing in order to avoid the losses and counteract the cracking effects and shrinkage. These types of steels are in the range of 270 000 psi (1,86 MPa) or more. Prestressing steel can be accomplished through simple wires, or strands composed of multiple wires twisted in order to form a single element, or very high-strength bars. High-tensile strength steel bars are available in nominal diameters from ¾" (19 mm) to 1' 3/8" (35 mm) [13]. The ultimate tensile strength of bars does not vary appreciably with the diameter. They are called drawn in order to raise their yield strength and stress relieved (= to heat the bar at a certain temperature, technique both applied for bars and strands) in order to increase their ductility.

Figure 13: Standard and compacted 7-wire prestressing strands (Source: Nawy, 2009)

Minimum tensile strength of prestressing bars: 150 000 psi (1,034 MPa) [13].
Minimum yield strength: 85% of the ultimate strength for smooth bars and 80% for deformed bars [13].

The stress relaxation for the prestressing steel results in the loss of prestress when the wires or the strands are subjected to a constant strain, which can be compared to the concrete creep phenomena. The primary difference is that creep is a change in strain and steel relaxation is a loss in stress.
Relaxation is closely linked to the shape of the diagram $\sigma - \varepsilon$ (Figure 14). This kind of relaxation induces a loss of prestressing, i.e. the necessity to impose stronger initial tensions or to increase the steel quantity. The relaxation of the steel is much faster than the one of the concrete at the beginning.

According to Guyon [7], we assume the tension loss $\Delta\, T(h)$ after h hours to be connected to the final tension loss $\Delta\, T(\infty)$ thanks to:

$$\Delta\, T(h) = \Delta\, T(\infty)\, [1 - e^{\sqrt[4]{\frac{h}{10000}}}]$$

And the creep of the steel is expressed as:

$$\varepsilon_{c\infty} = \frac{\Delta T(\infty)}{E_T}$$

Where:

T : Initial tension
E_T : slope of the $\varepsilon - T$
$\varepsilon_{c\infty}$: creep elongation
$\Delta T(\infty)$: Final relaxation

Which give the following results for the relaxation:

1 h	100 h	1000 h (1month and a half)	10000 h (14 months)	100000 h (one year)
0.21	0.51	0.72	0.9	0.98

Table 3: Percentage of relaxation according to time (Source: Guyon,1958)

Following the previous results (Table 3), it can be observed that 72% of the relaxation would be reached after one month and a half, whereas the advancement of the delayed deformation would be reached after nearly five months.

Figure 14 shows that the prestressing steel can achieve much higher stresses for the same strain of the mild steel bars. In fact, the mild steel, which is much more ductile, has a low carbon percentage. Finally, hard steel has a smaller ultimate elongation in comparison with mild steel.

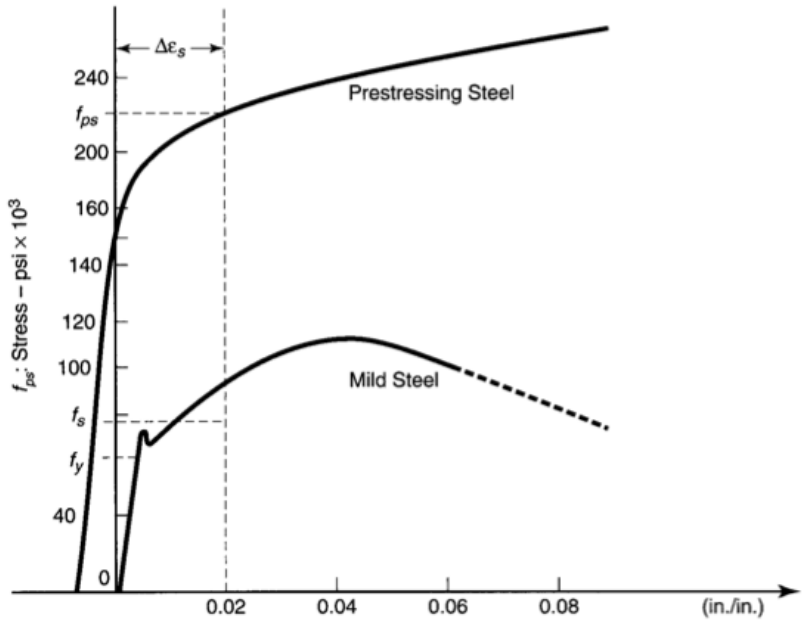

Figure 14: Stress-Strain diagram for prestressing steel strands in comparison with mild-steel bar reinforcement (Source: Nawy, 2009)

2.6.2 Bonded tendons vs unbonded tendons

Post-tensioning systems are divided into two main categories, the bonded tendons and the unbonded tendons.
The unbonded system appears to be more used in America than in Europe where the bonded one is currently the most widely applied system. In this thesis, as the technique is applied in an American office, Skidmore, Owings and Merrill LLP, a preference is made for the unbonded tendons.

2.6.2.1 Unbonded tendons

One of the advantages of unbonded tendons is that they are easier to insert than the bonded ones. They are covered with a corrosion inhibiting coating and encased in a plastic sheathing and are not bound with the concrete. For questions of durability, it may prove to be a disadvantage. In case of a building rehabilitation, if someone would like to modify the slabs by creating openings, one would have more difficulties in completing the task than with tendons bonded with concrete.
As mentioned by Bijan [4], the function of the plastic sheathing is: (1) to act as a bond breaker, (2) to provide protection from potential damage by mechanical handling, (3) to form a barrier against intrusion of moisture and mechanicals. The strand coating, commonly referred to as

grease: (1) reduces friction between the strand and the plastic sheathing, and (2) provides added protection against corrosion.

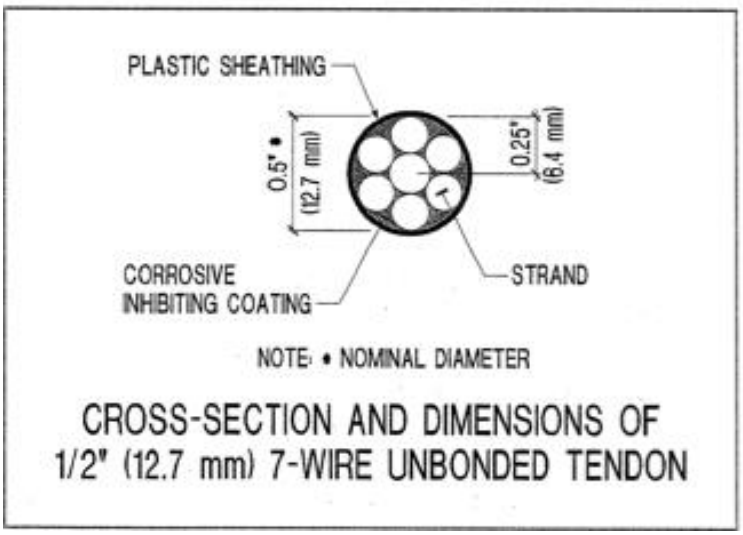

Figure 15: Cross section of unbonded tendons (Source: O. Aalami, Bijan, September 1994)

2.6.2.2 Bonded tendons

The bonded tendons have the principal characteristic to form a continuous bond along its length with the concrete around it. A duct is then installed into the slab. The strand is inserted into it and grout injected between the duct and the strand, blocking in the same time the movement of the stand into the duct. As for the unbonded tendons, Bijan [4] recalls the functions of the grout and the duct.

The function of the grout is: (1) to provide a continuous bond between the strand and the duct, (2) to increase protection against corrosion by acting as a physical barrier to moisture penetration, (3) through its alkalinity, to provide a non-conductive environment for corrosion. The function of the duct is: (1) to maintain a voided path for the strands in the concrete member during construction, (2) to transfer the bond between the grout within the duct and the concrete surrounding, (3) to act as an additional protection against penetration of moisture and chemicals into the interior of the duct.

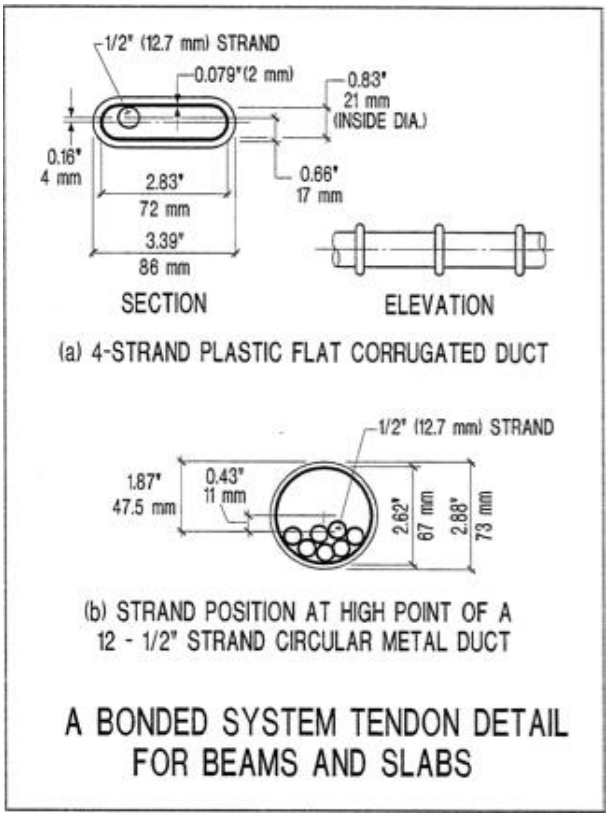

Figure 16: Cross section of unbonded tendons (Source: O. Aalami, Bijan, September 1994)

2.7 Post-tensioning unbonded slabs construction

2.7.1 Construction process

Post-tensioning is defined as prestressing with tendons after concrete hardening.

Post-tensioning is realized through applying the following steps:

- ducts are installed inside the formwork
- the tendons are thread into the ducts after concreting
- tendons are tensiled at the extremities with the help of jacks, installed onto the slab edge. The tensiled stresses provoked by tendons are applied to the concrete slab in compressing it.
- In order to control the cable's tension we measure the tendon elongation. This process must take into account the different possible losses, after friction, either instantaneous or postponed.
- The jacks are then dismantled and the supplementary tendons are cut.

- The ducts are injected/grouted with concrete (bonded tendons) or corrosion-inhibiting grease in order to protect the steel from corrosion.

This section is detailing the construction aspects required by codes specifications, practical issues or structural requirements to keep in mind in the designing phase [2] and [3].

2.7.2 Construction requirements

This section details the construction aspects required by code specifications, practical issues or structural requirements to keep in mind during the design phase [2] and [3].

2.7.3 Construction requirements

Minimum of tendons over supports

ACI 318-08, Section 18.12.6
A minimum of two tendons in each direction pass directly through the shear section as well as between the vertical bars of the columns.

Distributed tendons

The maximum spacing between any two tendons or tendon bundles is limited to less than 5 ft, or eight times the thickness of the slab.

Bundling of tendons

For ease of construction it is common practice to bundle several unbonded tendons together. Five tendons per flat bundle is the maximum recommended for floor slab construction.

Curvature in tendons

This part will be particularly dealt with in the case study.

Tendons supports

Tendon supports are used to position and secure tendons in their designated profile. The supports most commonly used are No 4 (No13) reinforcing bars or slab bolsters. For tendon heights (center of gravity) greater than 1.25 in above the soffit, the support bars are secured on chairs, whereas for heights of 1.25 in or less, slab bolsters are used. The spacing of support

bars depends on the designated profile and the type of tendon, but they generally do not exceed 4ft.

Anchorages

Large concentrated forces are introduced in the concrete at tendon anchorages. ACI 318-08 recommends determining the acceptable forces in these regions.
The first anchorage system (Figure) to be most used in construction is the so-called “button headed tendon system”. To stress the button-headed tendon a hydraulic jack is attached to the stressing washer, pulling the tendon until stressed. The button-headed tendon requires precise measurements and construction in order for the system to work properly.

(a) (b)

Figure 17: (a) Button-headed tendon system, (GTI) fixed end anchorage system (Source: Krauser, 2009)

Another methodology instead consists of a unique strand. This eliminates the need to have an exact length of the tendon (Figure).

It is also crucial that correct shop drawings are prepared to ensure the contractor understands how to properly realize the post-tensioned elements within the slab.

2.8 Design methods for flexural behavior of two-way slabs

A rectangle panel supported on the four sides by unyielding supports will be used to illustrate the principles of flexural behavior of a two-way slab system. The goal is to study how the panel will deflect when subjected to gravity loads. The two main methods for the design of post-tensioning are the load balancing method and the equivalent frame method, which can also be combined when designing a post-tensioned concrete slab.
The load balancing method, introduced by Lin [11] and explained by Nawy [13] is a well-functioning approach for indeterminate structures rather than determinate ones. In this

method, 65% to 80% of the dead load is balanced by the tendons. This helps the flexural behavior, as the flexural members are not subjected to bending stress until certain load conditions. The equivalent frame method is the most used technique for post-tensioned concrete slab as it is the one required by the ACI codes.

2.8.1 Equivalent frame method

The equivalent frame method also known as the beam method is characterized by the fact that it models the slab as a frame. According to Nawy [13], a vertical panel is cut through an entire rectangular planned building in order to create a rigid frame in the x direction; and similarly for the rigid frame in the y direction. The building becomes then divided into the middle and column strips (Figure 18).

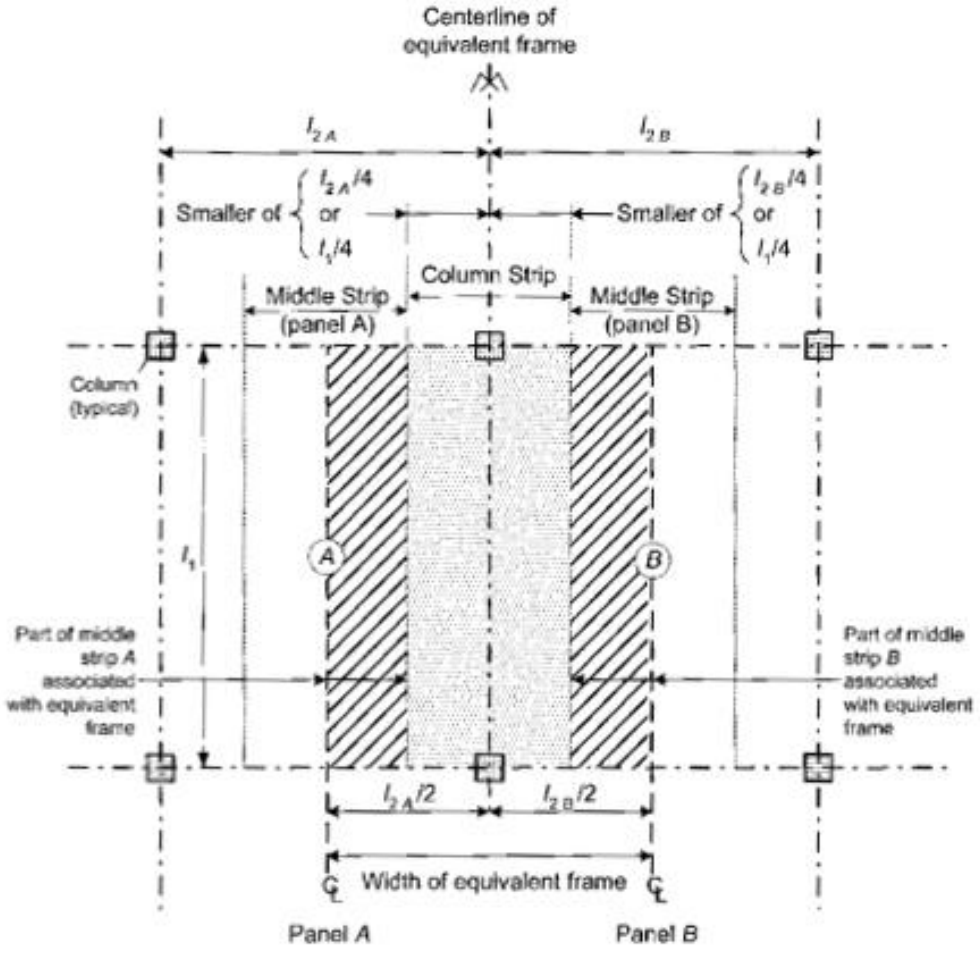

Figure 18: Cross section of unbonded tendons (Source: O. Aalami, Bijan, September 1994)

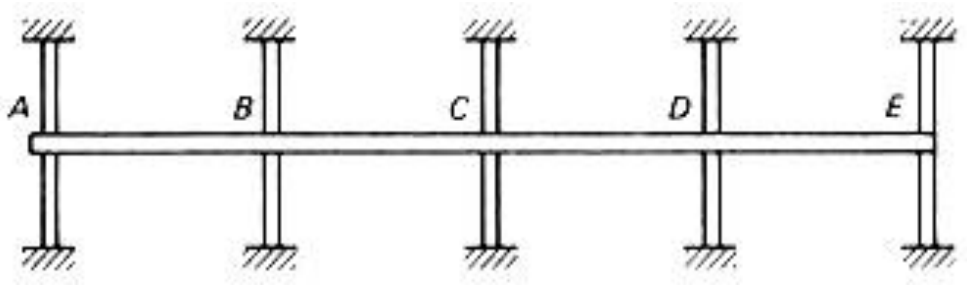

Figure 19: Cross section of unbonded tendons (Source: O. Aalami, Bijan, September 1994)

The middle strips are defined thanks to the two column strips.

$$\frac{1}{K_{ec}} = \frac{1}{\Sigma K_c} + \frac{1}{K_t}$$

K_{ec} : flexural stiffness of the equivalent column
ΣK_c : sum of flexural stiffnesses
K_t : torsional stiffness

$$K_c = \frac{EI}{l^2} \left[1 + 3 \left(l/l'\right)^2 \right.$$

I : column moment of inertia
l : centerline span
l' : clear span of the equivalent beam

$$K_t = \frac{9\, E_s C}{l_2 \left[1 - \left(\frac{c_2}{l_2}\right)\right]^3}$$

E_s : modulus of elasticity
l_2 : length of the transverse span in each side of the column
c_2 : width of the column
C : constant, approximately equal to a moment of inertia

The effect of vertical or lateral services and design loading on post-tensioned flat plates, were analyzed for rigid frames in agreement with the codes' requirements. When the columns are relatively slender or not rigidly connected to the slab, their stiffness may be neglected and a

continuous beam analysis performed. For Lin [11], the moment induced by prestressing may also be determined by a similar analysis of a rigid frame or continuous beam, using an equivalent load or load balancing concept. However, it has to be noted that the distribution of the moment's due load differs substantially between the moments due to prestressing. Service loads produce very pronounced moment peaks at the columns, whereas the moment curve produced by post-tensioning has a more gentle undulating variation of the same form as the tendon profile.

2.8.2 Load balancing method

2.8.2.1 Load balancing method for beams

The load balancing method consists of using post-tensioning to counteract gravity loads. In fact, as mentioned by Nawy: "this technique is based on utilizing the vertical force of the draped or harped prestressing tendon to balance the imposed gravity loading to which a beam is subjected" [13]. One advantage of the load-balancing method is the convenience it provides to determine the deflection, something of interest in this study. In fact, the loading value along the beam, where there is no known deflection, provides evidence to determine the deflection produced under any other conditions of loading.

In order to properly understand the load balancing method, the first step is to simplify the problem by reducing the slab problem to a beam problem, thereafter extending it for the slabs; keeping in mind that a two-dimensional load balancing differs from a linear load balancing for beams as a transverse component in one direction is closely related to the other component in the other direction. However, the main concept remains to balance a given load: that is to say that the complete structure (slab, beam, grid, etc) will deal with a uniform stress in each direction and will not suffer from camber or deflection under such a loading.

An introduction of the load-balancing method for beams problems is next required, well described by Nawy [13]. There exist two main cases: one with concentrated load and another with uniform distributed load along the beam. The study focuses on the case with distributed load.

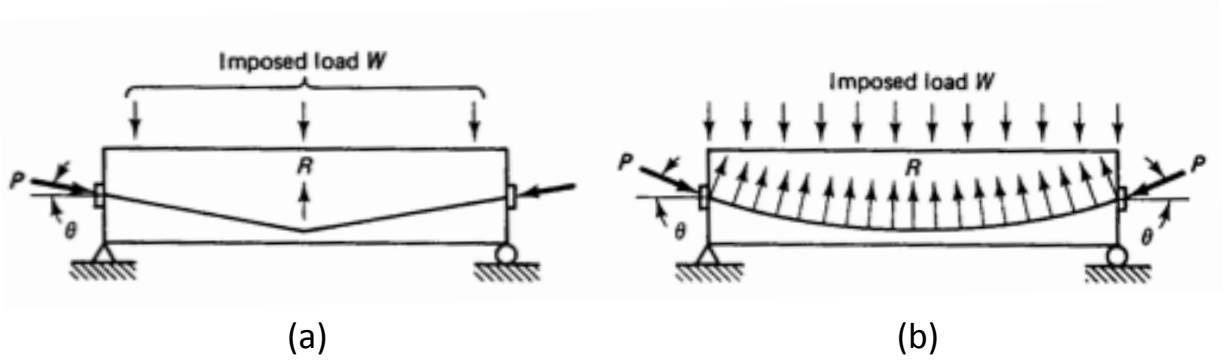

Figure 20: Load-balancing forces: (a) Harped tendon, (b) Draped tendon (Source: Nawy, 2009)

The problem is synthetized as a tendon subjected to uniform gravity load q.

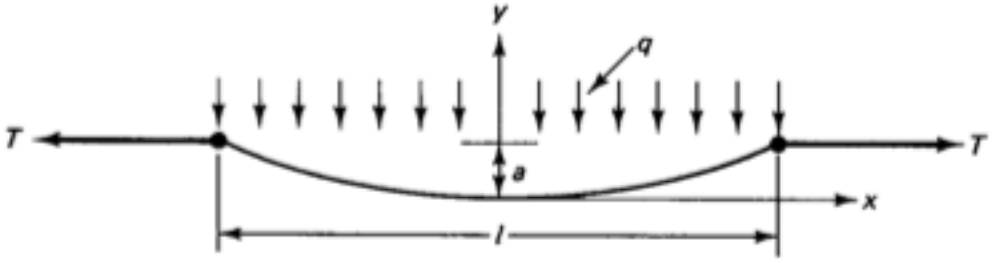

Figure 21: Sketched tendon subjected to transverse load intensity q (Source: Nawy, 2009)

The tendon drape is well described by the parabola equation, that is to say:

$$Ax^2 + Bx + C = y$$

T represents the force, which pulls the tendon, and act as a force of compression to the concrete beam.
Let find now the constant values A, B and C in resolving the parabola equation.

For x = 0:

Y = 0, $\frac{dy}{dx} = 0$, C = 0, B = 0

For x = l/2:

Y = a, A = $\frac{4a}{l^2}$

And the load intensity q is equal to: $q = T\ \frac{\partial^2 y}{\partial x^2}$

From $Ax^2 + Bx + C = y$ and $q = T\,\frac{\partial^2 y}{\partial x^2}$ we can find the value of the uniform load q:

$q = \frac{8Ta}{l^2}$??? $T = \frac{ql^2}{8a}$

So if we consider the tendon as a parabolic profile leading onto the beam profile with a prestressed force P, the balanced intensity is the following:

$$w_b = \frac{8Pa}{l^2}$$

Additionally, if the externally applied load (including the dead load) is correctly balanced by the balanced intensity w_b , there will be no bending of the beam. The beam will be subjected to a uniform compression with a stress value: $f = -\frac{P}{A_c} = \frac{F}{A_c}$

As described in the introduction, if the external load is different from w_b it will also be necessary to compute the moment produced by the load differential and therefore to obtain the following stresses: $f = \frac{M_c}{I}$

The fiber stresses value become:

$$f = \frac{F}{A_c} \pm \frac{M_c}{I} = -\frac{P}{A_c} \pm \frac{M_c}{I}$$

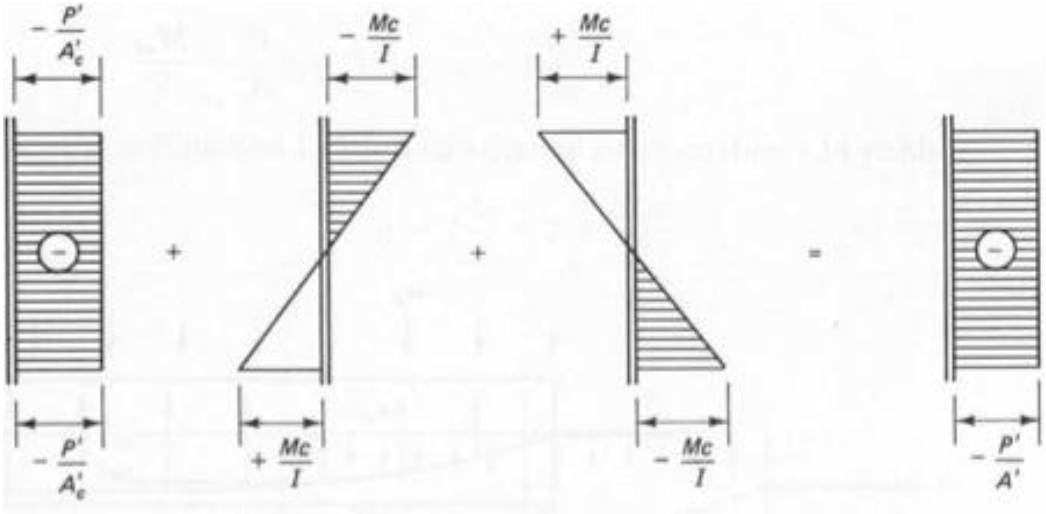

Figure 22: Load-balancing stresses: (a) Prestress stress, (b) Imposed-load stresses, (c) Balanced-load stresses, (d) Net stress (Source: Nawy, 2009)

2.8.2.2 Load balancing method applied to two-dimensional elements

Applying the load balancing method is resolved by computing directly the load-balancing approach for a beam to each direction of the slab. In this case a two-way simply supported slab with the cables in both directions will be considered.

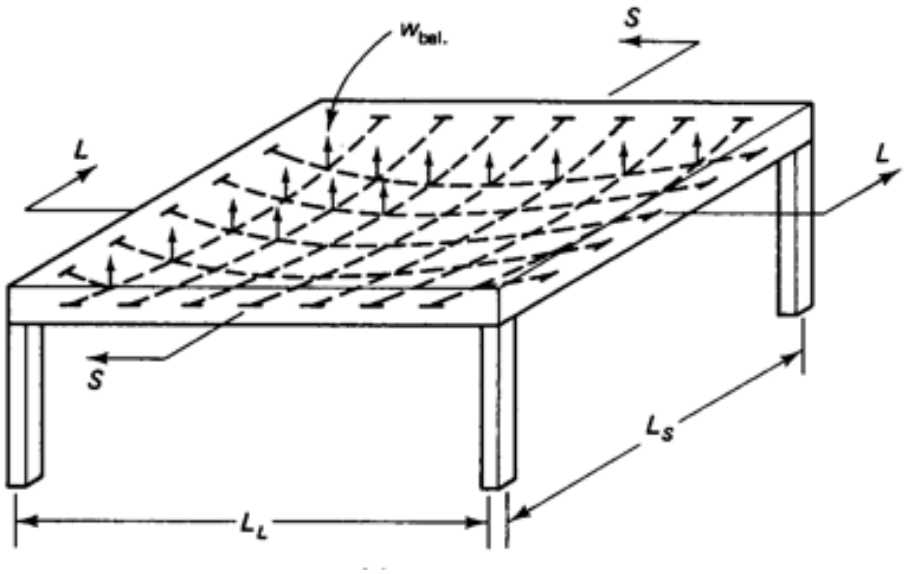

Figure 23: Balancing loads in two-way prestressed panel: Three-dimensional view (Source: Nawy, 2009)

The balanced design approach w is equal to:

$$\frac{8P_1a_1}{{l_1}^2} + \frac{8P_2a_2}{{l_2}^2} = w$$

The two options are or to carry the load in the shortest direction/span or to apply a $0,50\ w$ coefficient in each direction.

It must be remarked that, if uniform stress distribution and/or zero deflection are not essential, balanced load design may not be the most economical approach. For example, a cable placed along the middle strip is more effective than one placed along the wall.

2.8.3 FEM Method

As recalled by Bijan in the pti Techncal Notes [2], " if either the simple frame or the EFM is used, each design strip must be extracted from the floor system and analyzed as a plane frame. With the FEM, the entire floor can be analyzed at one time".

The objective of an FEM analysis is, like the Frame method, to provide information for a safe and serviceable design in agreement with the prevailing codes. The Finite Elements Method begins by defining design strips and design sections. These design strips follow the path of the load, just as in the frame method. The flow of the loading is represented as below (Figure 24), with arrows which are normal to the planes of maximum vertical shear. The arrows' length express the magnitude of the shear.

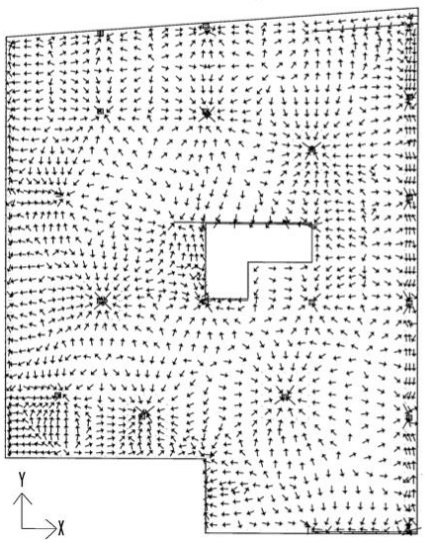

Figure 24: Diagram of load flow under service condition (Source: O. Aalami, Bijan, January 2001)

The advantage of FEM compared to the equivalent frame method is the possibility to define the design strips after processing the analysis. This flexibility allows the selection of the strip which is the closest as possible to the elastic response of the slab. In the following figure, the alternate hatched and clear regions indicate the natural load tributaries for the support lines A to G.

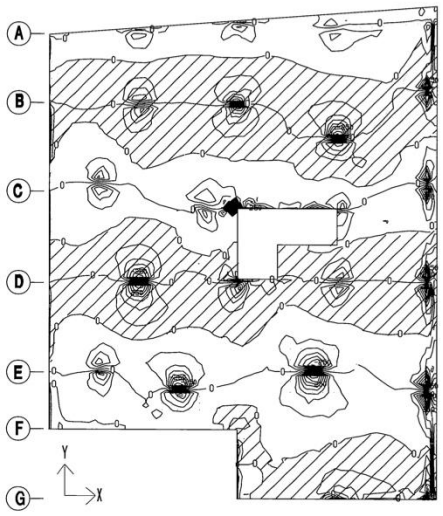

Figure 25: Zero line of shear transfer in Y-direction (Source: O. Aalami, Bijan, January 2001)

Design strips are based on the standard line supports and on the natural tributaries as shown before (Figure 25). The last step for strip design is to superimpose the design strips onto the natural tributaries (Figure 26).

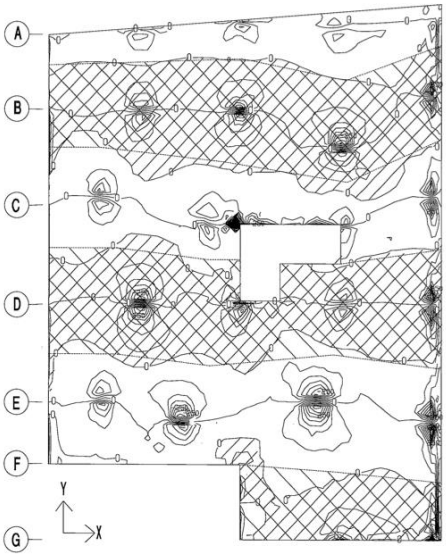

Figure 26: Assumed design strips superimposed on natural tributaries in x-diretion (Source: O. Aalami, Bijan, January 2001)

The amount of information obtained through FEM is far more than what codes require for serviceability and safety checks. FEM therefore represents a more accurate response to an applied load.

2.9 Conventional Post-Tensioning for a typical flat plate slab

This section presents an overview of the design of post-tensioned floor systems. As a conventional structural post-tensioning system, the example of the project designed by SOM in Sunset La Cienega, will be of great help to introduce the post-tensioning design procedure.

2.9.1 Principal characteristics of the conventional approach

The preferred approach for a typical slab is to have banded tendons in one direction and distributed/uniform tendons in the other. The advantage of this solution is that both directions can be designed with a maximum permissible drape.
Below is the example of the project in Los Angeles, a typical flat slab with columns at the edges with regular column position. The banded tendons pass through the columns and the uniform tendons are positioned perpendicularly (Figure 27).

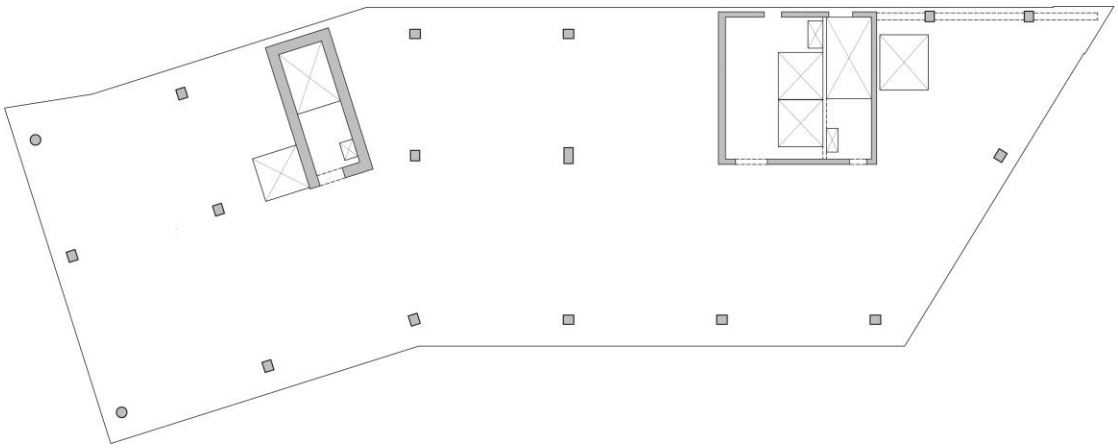

(a)

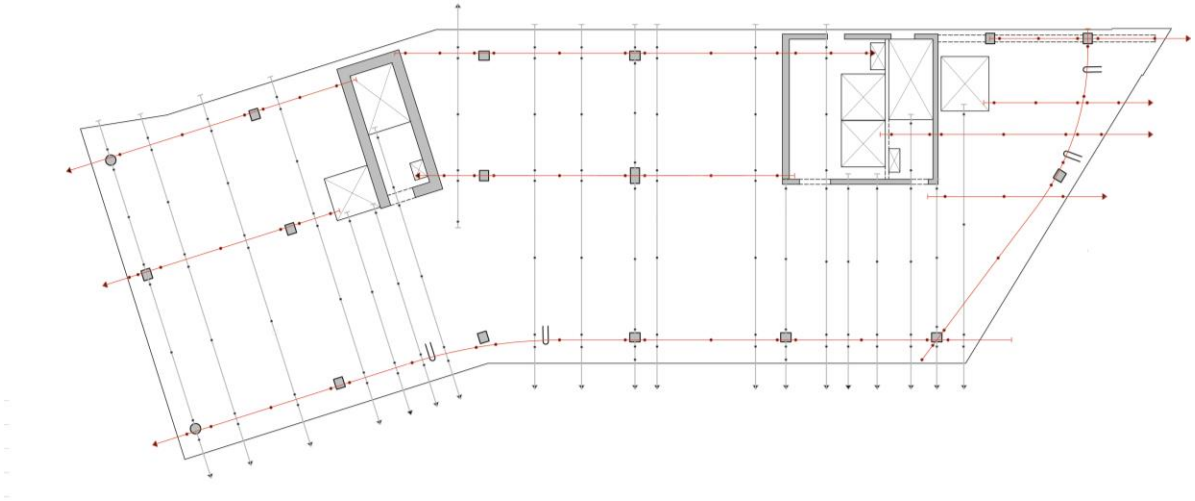

(b)

Figure 27: Sunset La Cienega: (a) Structural Plan, (b) tendons Layout (Source: Courtesy of SOM, 2015)

The conventional tendon profile will have maximum eccentricities to counteract the negative moments and maximum sags and at the mid-span to counteract the positive moments.
In fact, the cross sections have to be designed such that the internal component stresses are in equilibrium with the external loads applied from the adequate load combination into the global analysis [2].

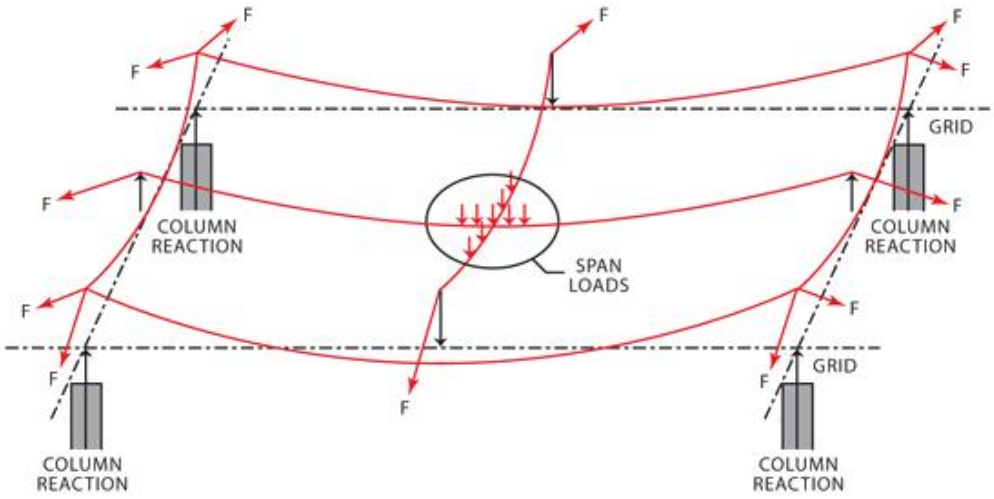

Figure 28: Two-way load balancing (Source: New York Post-Tension systems website)

2.9.2 Design Criteria

The principal criteria to study the accuracy of optimizing post-tensioning first requires considering the long-term deflection, as a max acceptable deflection.

2.9.2.1 Cover to reinforcement

The cover distances will follow the distances applied for two-way slabs general cases.
Prestressing tendon (CGS)
At top = 1.00 inch
At bottom = 1.00 inch

Mild steel reinforcement
At top = 1 ½ inch
At bottom = ¼ inch

2.9.2.2 Serviceability criteria

A- Deflection control

A very important control is that of deflection. In the latest projects by the SOM structural group the proper parameters have been applied thanks to their long and practiced design experience.

Deflection control is in fact a central consideration in serviceability of floor systems. The concrete floor plate is designed as such to have adequate stiffness to prevent changes in deflection, which might damage the attached partitions or other construction elements that are sensitive to large deflections. ACI's recommendations address the amount of deflection subsequent to the installation of non-structural elements likely to be damaged. The table below lists the ACI's stipulation on deflections.

Type of member	Deflection to be considered	Deflection limitation
Flat roofs not supporting or attached to nonstructural elements likely to be damaged by large deflections	Immediate deflection due to live load *L*	$\ell/180^{*}$
Floors not supporting or attached to nonstructural elements likely to be damaged by large deflections	Immediate deflection due to live load *L*	$\ell/360$
Roof or floor construction supporting or attached to nonstructural elements likely to be damaged by large deflections	That part of the total deflection occurring after attachment of nonstructural elements (sum of the long-term deflection due to all sustained loads and the immediate deflection due to any additional live load)[†]	$\ell/480^{\ddagger}$
Roof or floor construction supporting or attached to nonstructural elements not likely to be damaged by large deflections		$\ell/240^{\S}$

*Limit not intended to safeguard against ponding. Ponding should be checked by suitable calculations of deflection, including added deflections due to ponded water, and considering long-term effects of all sustained loads, camber, construction tolerances, and reliability of provisions for drainage.
[†]Long-term deflection shall be determined in accordance with 9.5.2.5 or 9.5.4.3, but may be reduced by amount of deflection calculated to occur before attachment of nonstructural elements. This amount shall be determined on basis of accepted engineering data relating to time-deflection characteristics of members similar to those being considered.
[‡]Limit may be exceeded if adequate measures are taken to prevent damage to supported or attached elements.
[§]Limit shall not be greater than tolerance provided for nonstructural elements. Limit may be exceeded if camber is provided so that total deflection minus camber does not exceed limit.

Table 4: ACI 318-08, Maximum permissible deflection

The ACI criterion for deflection is a length/ratio criteria, which is not entirely accurate, particularly in the case of heavy curtain loads. The codes require a live load deflection of L/360 and a deflection after installation of non-structural components with a live load of L/240.
In order to maintain a practical margin for sensitive partitions and facade, the criteria used will be the one developed by SOM as the deflection is limited to maximum **0.75 inch** on the edges. This point insists on the importance of the collaboration between architects and engineers, for example: when installing a heavy curtain wall on a long span slab. This coefficient will provide positive concrete slab behavior even in this case.

Other criteria have been personalized by the SOM structural team, such as a modulus of rupture of 4(f'c)^1/2 is used as the maximum allowable tension stresses in the design of floor deflections. This modulus of rupture value is also more conservative than the value 7.5(f'c)^1/2 required by ACI318-08 Section 9.5.2.3.

B- Limit of stresses

When the deflection is verified, the stresses can be checked. It is quite always found that when the deflection is verified, the stresses should be also verified.

Also according to ACI 318-08, part 18.4, the post-tensioned slab should meet the stress limits as follows, which correspond to the prestressed concrete of Class U, i.e. un-cracked section:

f'c = 5000 psi = 35 Mpa
f'ci = 3750 psi = 26.25 Mpa

At initial limit state:
Top and Bottom fiber tensile stresses $\leq 3\sqrt{f_{ci}'}$
Extreme fiber compressive stress $\leq 0.6\sqrt{f_{ci}'}$

At sustained state:
Top and Bottom fiber tensile stresses $\leq 6\sqrt{f_{ci}'}$
Extreme fiber compressive stress $\leq 0.5\sqrt{f_{ci}'}$

At Total service limit state:
Top and Bottom fiber tensile stresses $\leq 6\sqrt{f_{ci}'}$
Extreme fiber compressive stress $\leq 0.6\sqrt{f_{ci}'}$

2.9.2.3 Finite Element Study with SAFE

In order to study the post-tensioned effect on the concrete and also investigate the two-way action more precisely, the floor area will be parceled into smaller elements, allowing a more accurate prediction of the slab behavior. Therefore, the model will be studied using the SAFE software, a finite element software specialized to analyze the concrete floors behaviors, with ADAPT as its direct concurrent, also a structural concrete software.
SAFE is in fact a performing tool for designing concrete floor and foundation systems. Comprehensive and customizable reports are available for all analyses. Sections, elevations, and tables may be generated, and printed from within SAFE or exported to a CAD software.

C- Geometry

The main drawing is imported from CAD, as SAFE is not particularly recognized to be the most adaptable software to produce drawings. Height values are affected to the cores and the columns with an adequate thickness to the slab (Figure 29).
Material properties are assigned to the different elements.

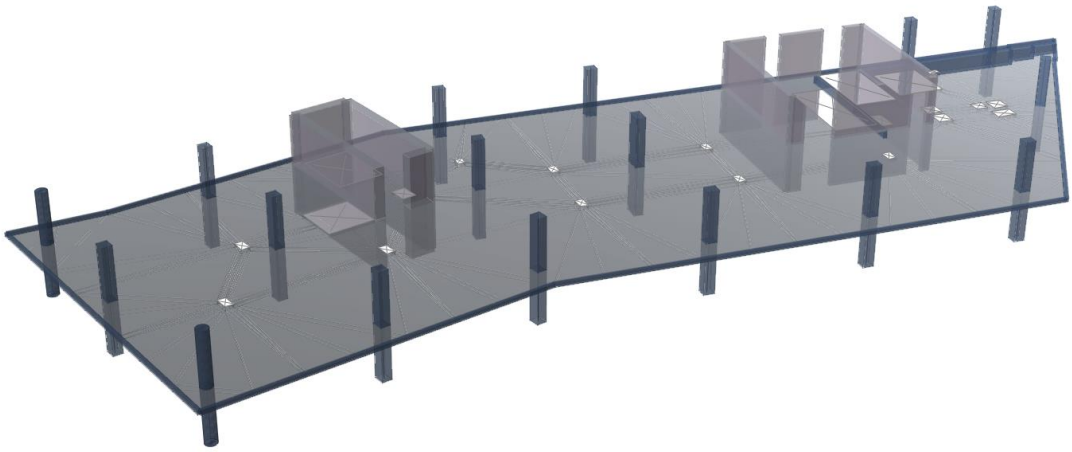

Figure 29: 3D Model set up in SAFE (Source: Courtesy of SOM, 2015)

D- Finite Element Model

A mesh is then applied to the slab (Figure). The more precise the mesh, the better the results will be. However, a compromise has to be found between accuracy of the results and the time required to run the analysis.
Openings are also highlighted and load cases are created along with load combinations. Finally, the gravitational loads can be applied to the slab.

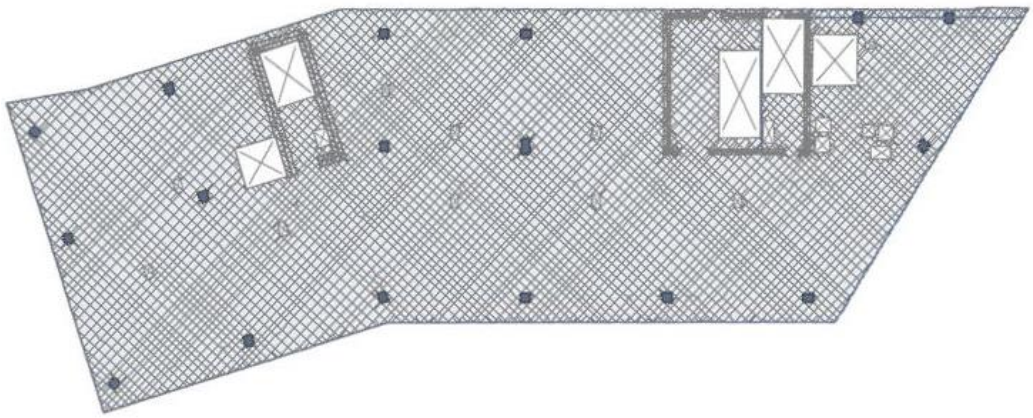

Figure 30: Floor plate 'finite element mesh (Source: Courtesy of SOM, 2015)

E- Design Strips

The strips design has two roles under SAFE:

- To activate the supports in order to adjust the tendons profiles
- To evaluate the stresses magnitudes even a color plot of the stresses will be preferred

When used to measure the stresses the design strips are idealized to establish an *Equivalent Frame Method* approach.

The strips will so principally help to regulate the profiles.

The slab is then split into X and Y design strips as observed in the figure above, with the X-direction strips.

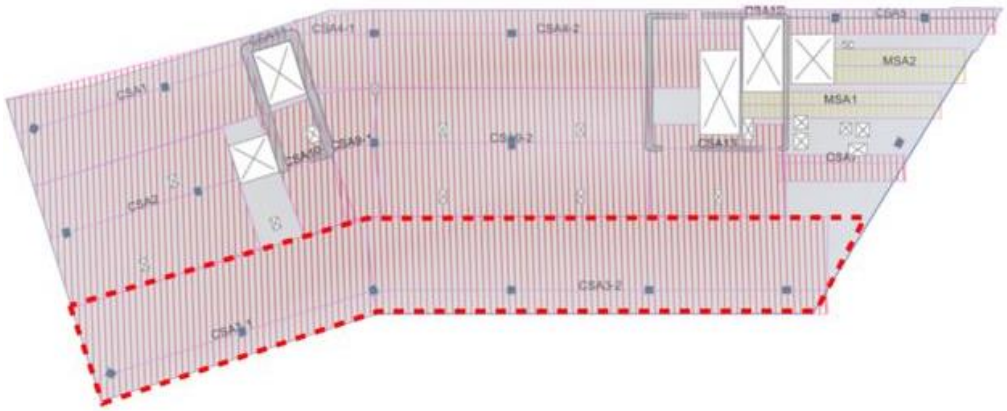

Figure 31: Model set up in SAFE (Source: Courtesy of SOM, 2015)

F- Unbounded Tendons Layout

Figure 32 shows the final configuration of the tendon layout. As can be observed, the spacing between tendons is congested in the large spans while it becomes sparser for the others. The main banded groups of tendons are oriented parallel to the longer direction of the floor plate. Nevertheless, in order to control the stringent long-term deflection criteria of 0.75 inches, the shorter direction of the floor plate has banded groups of tendons passing through the column lines to stiffen the column strips as much as possible.

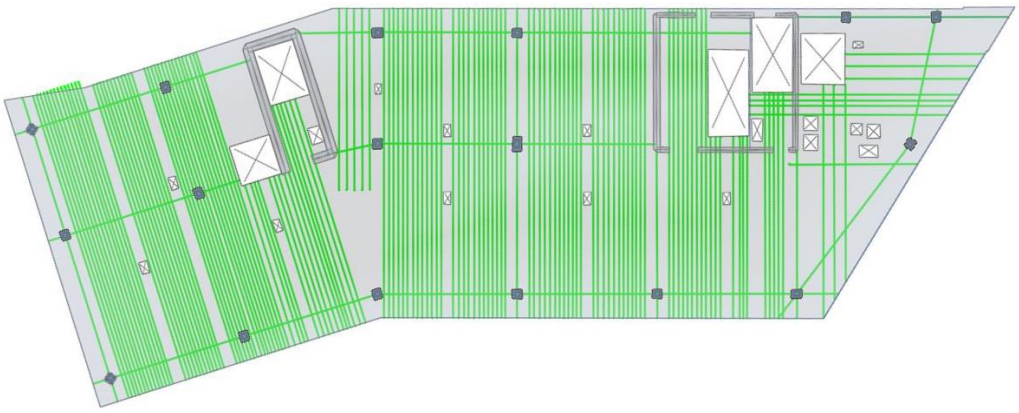

Figure 32: 3D Model set up in SAFE (Source: Courtesy of SOM, 2015)

Thanks to the strip design and the tendons placement onto the slab, the profiles can be adjusted as necessary (Figure 33). Between two supports the profiles follow the moment curvature with a maximum eccentricity at the supports. In the SAFE profiles interface the drapes of the curve can be set part by part, keeping a limit of 1 for the cover. The height at the edges is 4 inches, being at mid-height of the slab thickness and corresponding to a practical point when it is to build it.

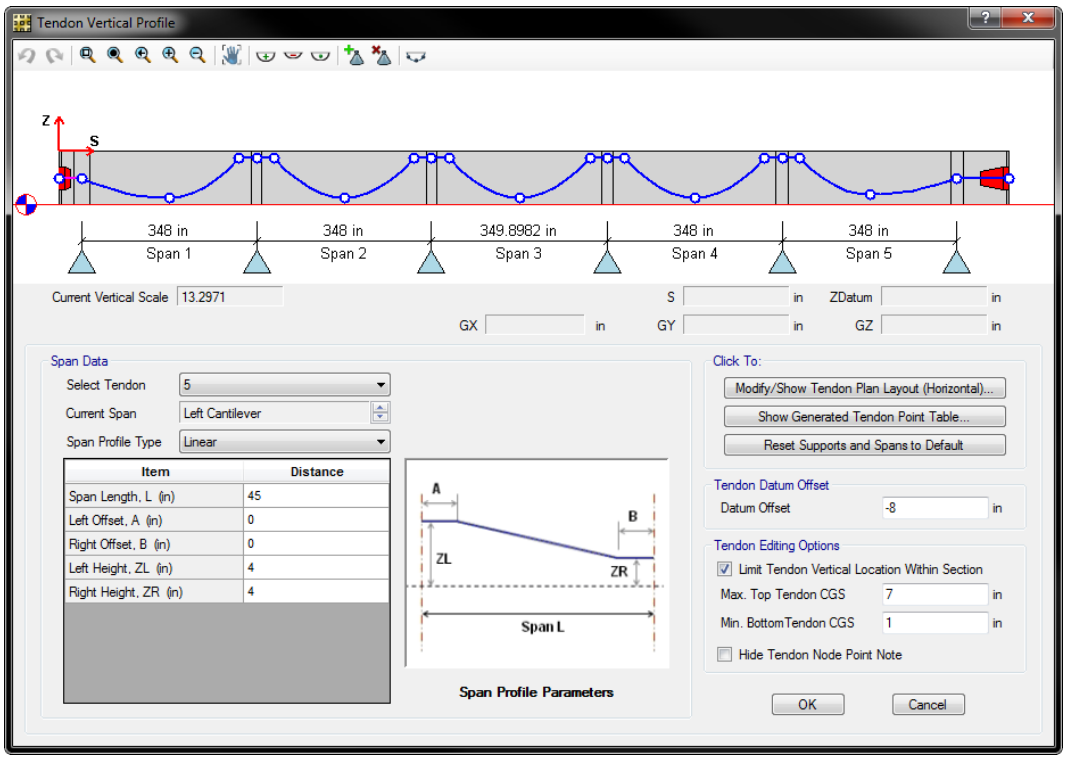

Figure 33: 3D Model set up in SAFE (Source: Courtesy of SOM, 2015)

G- Deflection study

Next comes the deflection over the long-term and one at the initial stage (Self-Weight + PT), as it provides a good and first approximation of the required results.

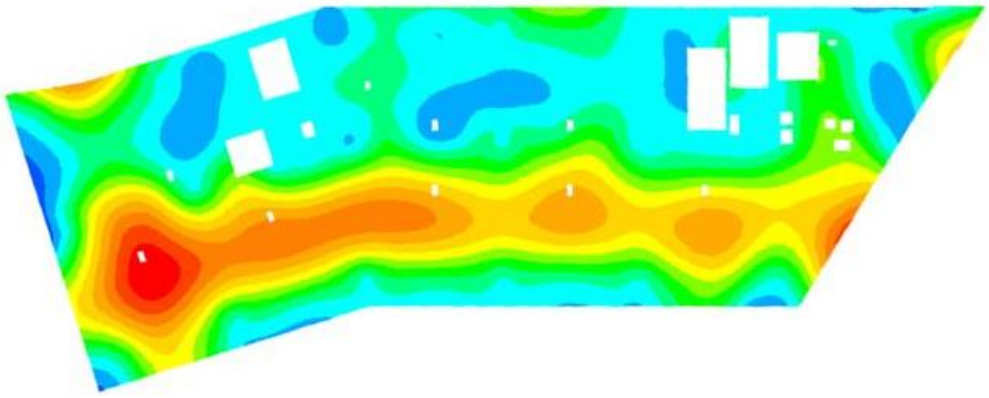

Figure 34: Long-term deflection (Source: Courtesy of SOM, 2015)

The tendons have been laid out to have as few deflections as possible for the load case attributed to the initial stage (figure), and defined as follow:

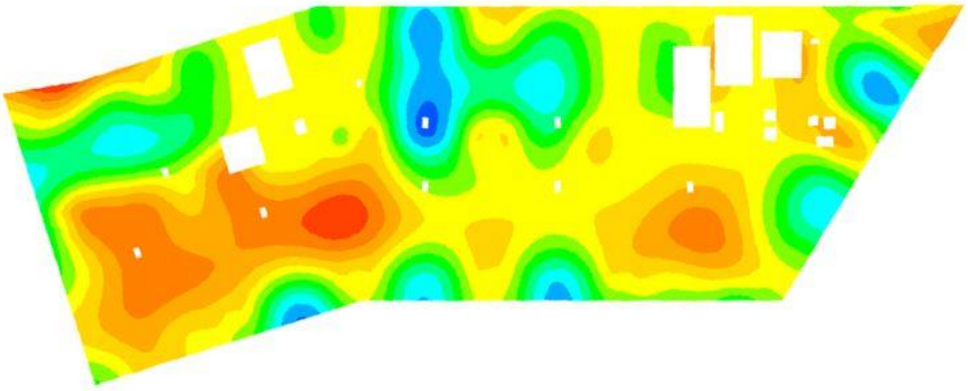

Figure 35: Initial deflection (Source: Courtesy of SOM, 2015)

Load combinations

1) Strength: Initial (or transfer) limit state

Stresses are major concerns

SW + 1.15 PT

2) Service limit state

Both stresses and deflection are the main criteria

PT + SW + SDL 0.3 LL

H- Stresses Verifications

Stresses can be then verified following the values introduced into the design criteria chapter previously.

In order to ensure the punching shear strength of the slab under both gravity and seismic forces, the reactions from load combinations are super imposed. However, the punching shear will not be checked into this study as the choice has been made to concentrate solely on the bending deformations.

2.10 Conclusions and Objectives

The conventional approach is currently developed as a trial and error process (Figure 36) and time consuming. This requires an iterative process, the right intuition from the engineer, and takes into account the architectural modifications all along the design phase.

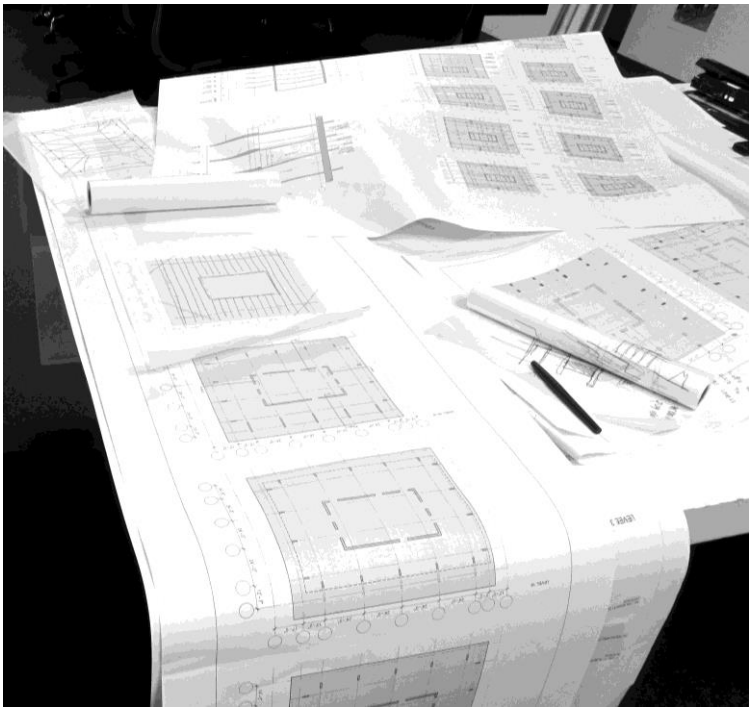

Figure 36: Trial and error procedure: The engineer follows the classical rules, his intuition to find the appropriate post-tensioning layout (Source: me, 2015)

Moreover, thanks to computer possibilities, design procedures have undergone a radical evolution in the past several decades. Each building can now maintain its own unique shape. For example, the structure found at 1111 Lincoln road in Miami beach by Herzog et de Meuron, has slabs standing over a set of irregular columns. The Park Merced project, designed by SOM, provides another example where the columns have an irregular layout . The question becomes How to apply conventional post tensioning in the ever-more-common uniquely shaped structure? Can there be a better way to do Post-Tensioning?

Figure 37: 1111 Lincoln road in Miami beach, Herzog et De Meuron (Source: me, 2015)

Optimization methodologies will be investigated in order to better understand which ones could help the engineer define new rules when designing a post-tensioning concrete flat slab, whatever the architectural form to be built.

3 Global aspects of Structural Optimization

The efficient use of materials is important in many fields from the aerospace industry to building construction it is now more a necessity to reduce than ever, especially in consideration of the carbon footprint. This chapter covers some of the optimization techniques developed in the field of structural engineering. Topology optimization and the Force Density Method are briefly illustrated with their advantages and disadvantages. The aim is to show the large applicability of optimization methods in the structural design world. The principal objective of structural optimization is to maximize the performance of structural component in minimizing the materials use. Computers and software are powerful tools able to achieve structural optimization which can become a important new design and automation tool for engineers. The key point is to choose the most efficient optimization procedure and software that can best solve the problem at hand.

3.1 Topology Optimization

3.1.1 Introduction

Topology Optimization is well known within the industry field, primarily in aeronautical and mechanical engineering. These are industries where reducing weight in the structure is a necessity, in part an issue of savings but also for the overall performance of the end product. “For example, in the design of the A380 aircraft, topology optimization was used to significantly reduce the weight of the several components, among those, the outboard and inboard inner fixed leading edge ribs and the fuselage door intercostal. The contributed weight savings was in the neighborhood of 1000 kg per aircraft” [23].
The main wing box rib below (Figure 38) has been optimized, removing the stiff non-designable upper and lower channel sections. Load cases include both local air pressure loads and running loads from several wind-bending cases.

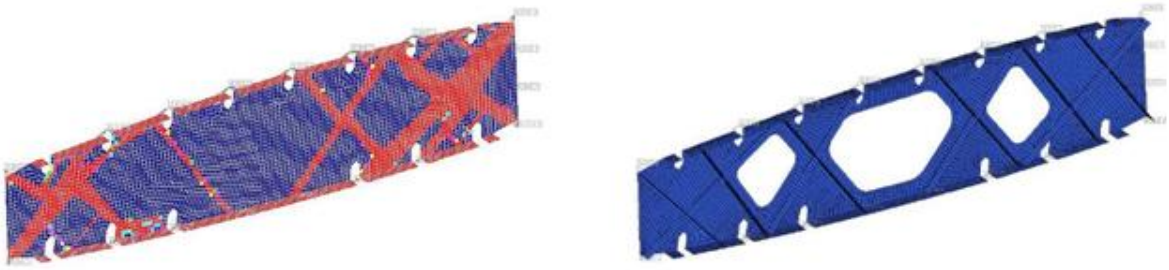

(a) (b)

Figure 38: Topology optimization applied to an A380 main box rib: (a) Rib where the formation of intermediate densities have been penalized, (b) Initial design for sizing/shape optimization, obtained by engineering the solution from a Topology Optimization (Sourc

Topology Optimization has begun to be imported to civil engineering practice recently, principally into the design of high-rise buildings, which also enhance the development of a new architectural aesthetic. This results in improved collaboration between architects and engineers as the architects are not focused solely with the “form” and engineers not only by “function”, but they can work together focusing both on form and function.

A number of examples designed through a Topology optimization procedure exist for bracing systems or skin of high-rise buildings structures. Topology Optimization has in fact been principally applied to the definition of global structural systems up till now. These have dealt with overall gravitational loads and sometimes also horizontal or seismic; but never applied to local structural systems as post-tensioned slabs, as is the main purpose of this thesis.

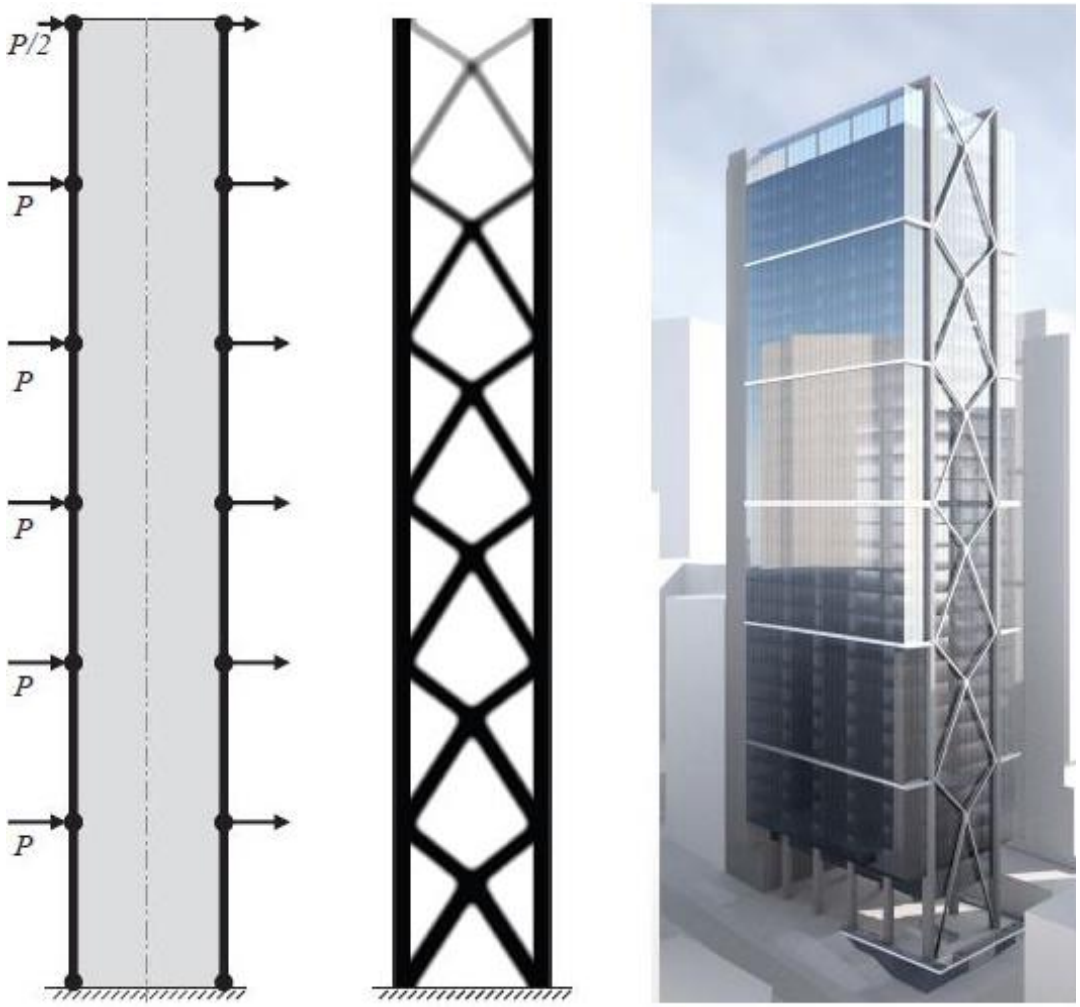

Figure 39: Illustration for the concept design of a 288 m tall high-rise building in Australia, which shows the engineering and architecture expressed together: (a) problem statement, (b) results of the topology optimization, (c) renderings of the design (Source: Courtesy of SOM 2016)

Figure 39 shows a bracing system in which the densities increase as the load increases throughout the height of the structure, which gives also an aesthetic value to the design of the façade.

3.1.2 Topology Optimization overview

Topology optimization is in fact a "material distribution method" [30] in which the goal is mainly to find the most optimal layout for a linear elastic structure.
Topology optimization allows one to determine:

- The number, the location and the shape of the holes

- The connectivity of the domain

Or as strictly defined by Sigmund [30]: “Topology Optimization is a way to find the optimal lay-out of the structure within a specified region”.

Having as known quantities:

- The applied loads
- The possible support conditions
- The volume of the structure to be built
- Some additional design restrictions, such as the location and size of holes or solid areas

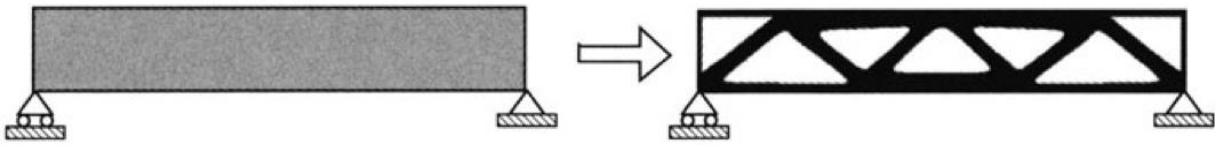

Figure 40: Topology Optimization: The initial problems are shown at the left hand side and the optimal solutions at the right (Source: Sigmund,2004)

3.1.3 Mathematical approach

In this section we will discuss the parametrization of the design following the mathematical approach and summarizing the detailed method explained by Sigmund and Bendsoe [30].

3.1.3.1 Minimum compliance design

A structural optimization problem can be treated as a compliance minimization problem. The compliance minimization problem is considered as the simplest type of design problem formulation. As the compliance is the inverse function of the stiffness, this problem can be formulated as the maximization of the stiffness.

The problems takes into account a physical element which behaves to a reference domain Ω in R^2 or R^3.
The reference domain Ω is the point of departure for defining the optimal design problem which consists in finding the optimal choice of stiffness tensor $E_{ijkl}\ (x)$.
X is the density of the domain.

Next it necessary to define the energy bilinear form:

$$a\ (u, v) = \int_{\Omega} E_{ijkl}\ (x)\mathcal{E}_{ij}\ (u)\mathcal{E}_{kl}\ (v)d\Omega$$

Where:

u : is the equilibrium
v : is arbitrary virtual displacement
$\mathcal{E}_{ij}$: is the strain linearized $\mathcal{E}_{ij}(u) = \frac{1}{2} . (\frac{du_i}{du_j} + \frac{du_j}{du_i})$

And the linear load:

$$l(u) = \int_{\Omega} fu \, d\Omega + \int_{\Gamma_T} tu \, ds$$

Subsequently the minimum compliance problem is written as:

$$\begin{gathered} min\ l(u) \\ u \in U, E \\ a_E(u, v) = l(v), for\ all\ v \in U \\ E \in E_{ad} \end{gathered}$$

Where:

U : is the space of kinematically admissible displacement fields
f : are the body forces
t : are the boundary tractions on the traction part $\Gamma_T \subset \Gamma \equiv \partial\Omega$ on the boundary
E_{ad} : is containing all the admissible stiffness tensor reaching the isotropic material properties

$$E(x) = \rho(x)^p E_0$$

3.1.3.2 Topology Optimization numerical functioning

Topology Optimization focuses on the optimal placement of an isotropic material in space, i.e. to understand the points of space that are material and those that are void (no material). It can be compared to a geometric representation of a structure as a black-white rendering of a jpeg image. The image is defined as a black-white representation, with pixels or voxels. Theses pixels are determined by the discretization of the image into finite elements.
The objective is to find the optimal Ω_{mat} of material elements.

$$E_{ijkl} = l_{\Omega^{mat}} {E_{ijkl}}^0 , l_{\Omega^{mat}} = \begin{cases} 1\ if\ x \in \Omega^{mat} \\ 0\ if\ x \in \Omega / \Omega^{mat} \end{cases}$$

$$\int_{\Omega} l_{\Omega^{mat}}\, d\Omega \; = Vol\,(\Omega^{mat}) \leq V$$

The interesting point of the previous equation is the volume to be limited by an idealized volume V, i.e. the volume imposed by the amount of material available. Topology optimization has only one variable. This variable is the density and related stiffness of each element.
${E_{ijkl}}^{0}$ depends on the function of the density of the material, the density becomes the design variable. This implies that when the density varies it will strongly influence the stiffness tensor of the concerned elementE_e, which will affect the total material distribution within the optimized structure. This is in fact the desired goal when using topology optimization.
As explained in the equation below, the defining a black-white model implies that all possibilities should be either 0 or 1.
Different algorithms are not comprised (they are comprised between 0 and${E_{ijkl}}^{0}$) as mentioned and do not define a black-white affiliation as expressed by the following equation:

$$E_{ijkl}\,(\rho = 0)$$
$$E_{ijkl}\,(\rho = 1) = 1 = {E_{ijkl}}^{0}$$

In such cases, i.e. for regions of grey material, or intermediate densities, the commonly used SIMP model is employed [22].

3.1.3.3 SIMP Model

In order to obtain a non-discrete solution that approximates a discrete solution, the mathematical model used to perform the analysis of the structure is changed to reduce the influence of intermediate values of the variables.
This type of scheme is known as *Solid Isotropic Material With Penalization*, also referred to as the *penalized, proportional stiffness model*, is a gradient-based model.

$$E_{ijkl\,(x)} = \; \rho\,(x)^{p}\, {E_{ijkl}}^{0}\,, p > 1$$

$$\int_{\Omega} \rho\,(x) d\Omega \; \leq V\;;\;\; 0 \; \leq \; \rho\,(x) \leq 1, x \, \epsilon \, \Omega$$

The equation shows how Young's Modulus of solid material E_0 with the penalization factor $p \geq 1$ can be utilized in order to force the material to tends toward 0 or 1, i.e. void or solid, i.e. thus removing the grey areas.
The penalization factor penalizes the density values and are range between 1 to 4 during the procedure of optimization, in steps of 0.5.

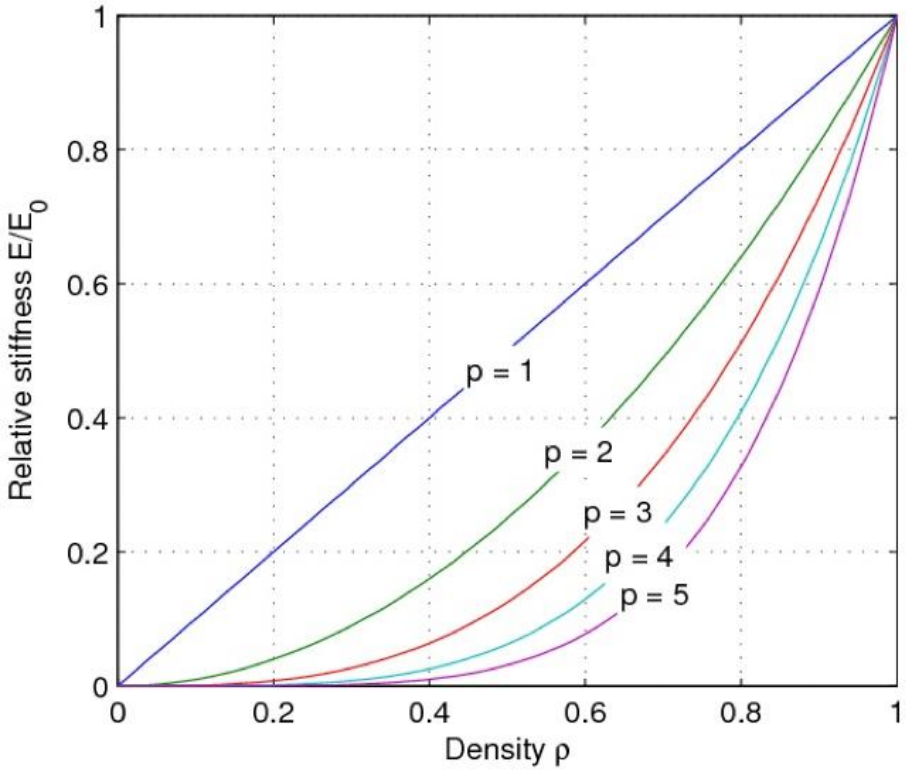

Figure 41: Relative stiffness as a function of density with different penalization factors (Source: Olason, Anton, 2010)

In fact, as can be noticed in the previous graph (Figure 41), increasing the value of p allows to rapidly increase the slope of the curve, which represents cost saving, as it is more economical to penalize the stiffness of the material through its density than increasing the volume of the element. This is called the 'density method'.

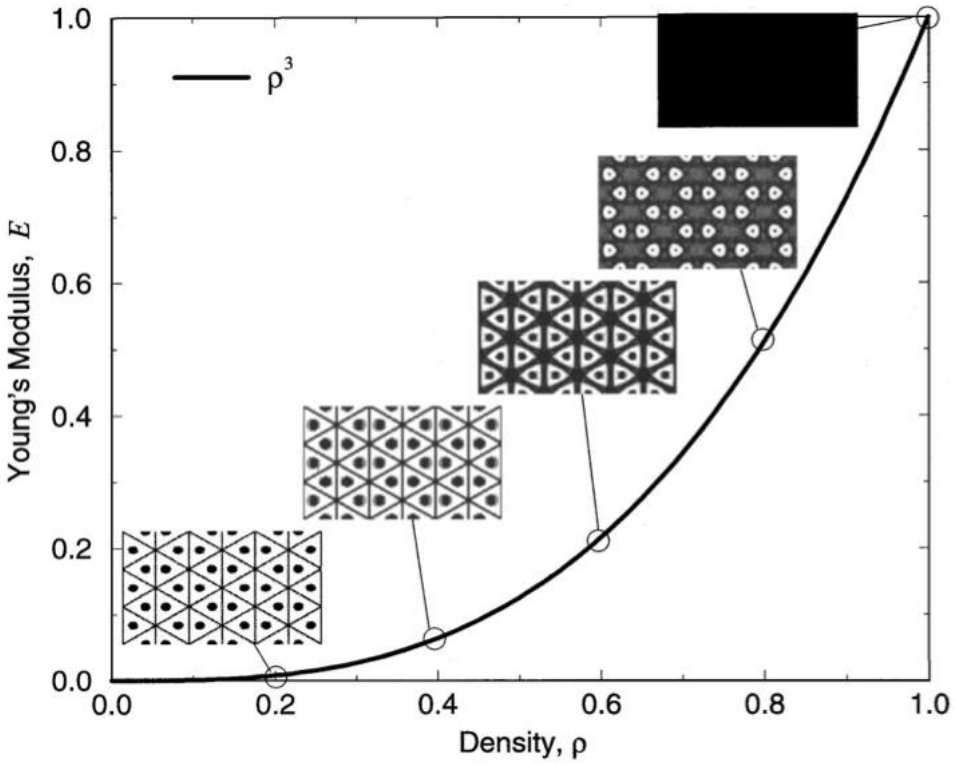

Figure 42: Microstructures realizing the material properties with p=3 and v=1/3 (Source: Olason, Anton, 2010)

The workflow of the SIMP-algorithm is seen in the following figure. SIMP often begins to uniformly distribute densities in the elements of the design domain and a volume fraction equal to the one specified.

3.1.4 Overview of the tools used

Continuum structural Topology Optimization is now available in a number of commercial finite element analysis codes, such as Abaqus/ATOM, Ansys, Altair HyperMesh/Optistruct.
The analysis will be performed with the software in the Altair suite: HyperMesh. HyperMesh is well known as an excellent mesh generator as it transforms the proposed geometry into a mesh of very small elements (principally triangles with tetrahedras and quadrilaterals).

Three parameters are taking into account (the design variables, the design space and the response) to conduct the optimization study. The objective of topology optimization is in fact to obtain the most optimal layout of a structure, within a specific domain and for a specific target: deflection, stiffness, compliance, etc. The only known quantities are the:

- geometry including openings, solid areas not be optimized
- whole volume of the structure

- material properties (concrete strength f_{ck}, modulus of young E, etc)
- constraints
- applied loads

Then the analysis is performed, that is to say the Finite Element Method is applied by dividing a design domain into finite elements, as the objective is that each element comes to represent an ideal design. These components can then be compared, as mentioned before, as an image with pixels or voxels, in containing a density that is either solid (black) or empty (white). In fact, in topology optimization it is interesting to understand the optimal placement of a given isotropic material. What pixels should remain empty and which ones should remain solids.
The new layout resulting from topology optimization is relevant for engineers in order to verify the physical behavior expected of the geometry under fixed constraints and loads, as topology optimization is a tool which allows for the principal path of forces inside the structure to be observed.
It is a way to verify the intuition of the engineer as to precisely understand the behavior of the optimized element.

3.1.5 Optimization procedure

The optimization problem proceeds with the following step

As described in the master thesis of Steffen Johnsen [33]:

- The first step in the iterative analysis is to solve the equilibrium equations
- Establish a sensitivity analysis calculating the derivatives of the design variables
- Run a simulation to limit the magnitude of the density updates
- Ensure numerical stability, filtering techniques are applied before the densities are updated using the minimum compliance criteria
- A new finite element analysis is run
- Repeat the procedure until convergence has been achieved

The whole procedure is depicted in Figure 43.

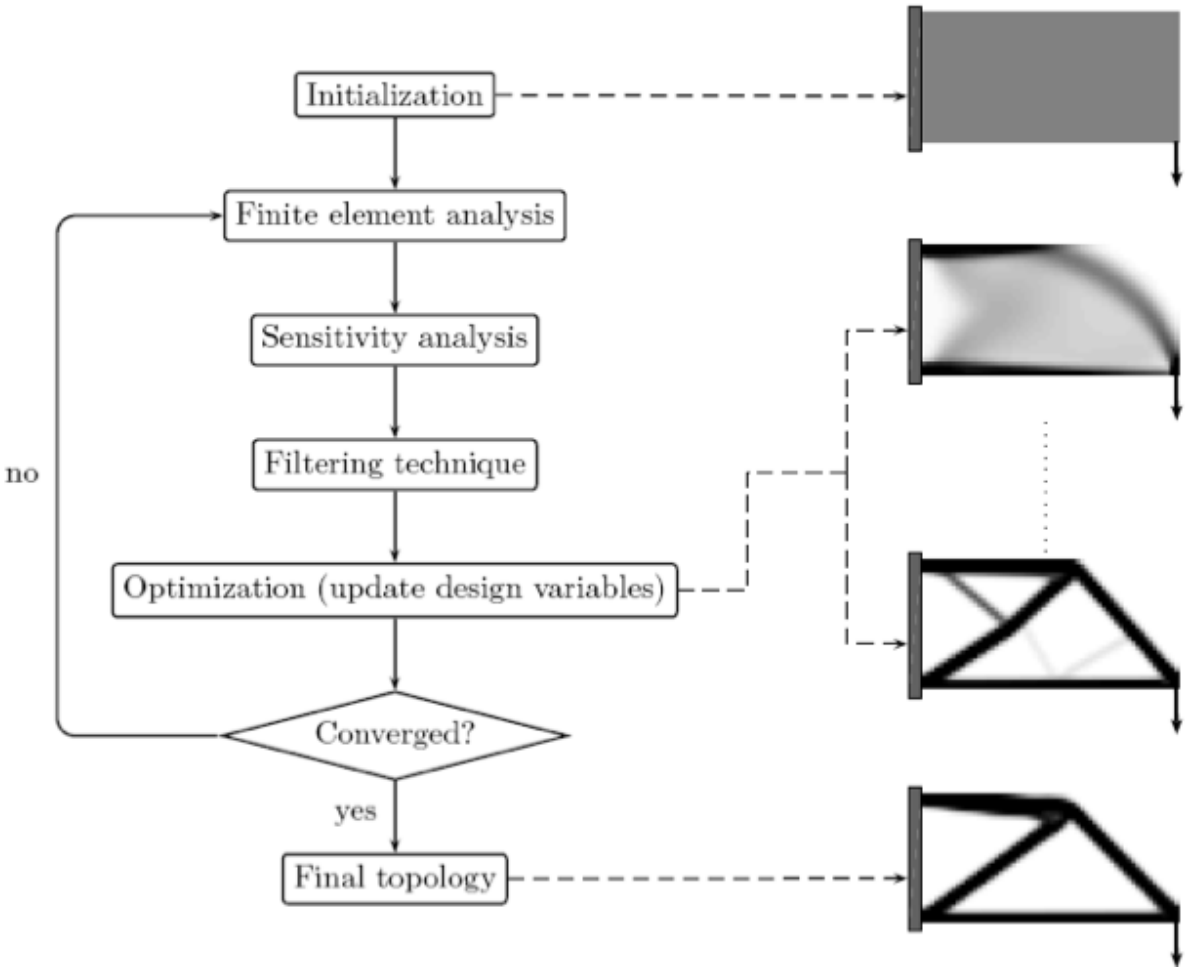

Figure 43: Work scheme of topology optimization using the SIMP-algorithm (Source: Johnsen, Steffen, 2013)

An example of this procedure was the conceptual design pursued by the SOM team for the Zendai competition.

The goal of the Topology Optimization was to assist in creating a unique and innovative design for the upper “bridge” structure spanning several towers. The gravity loads were applied onto the mesh as a series of equal point loads at nodal locations. The mesh was constrained with pin supports at the nodes corresponding to the emplacements where the towers would have to support the bridge.

The (h) results of Figure 44 show member lines which intersect at 90 degree angles reminiscent of the geometries of Michell frames [22].

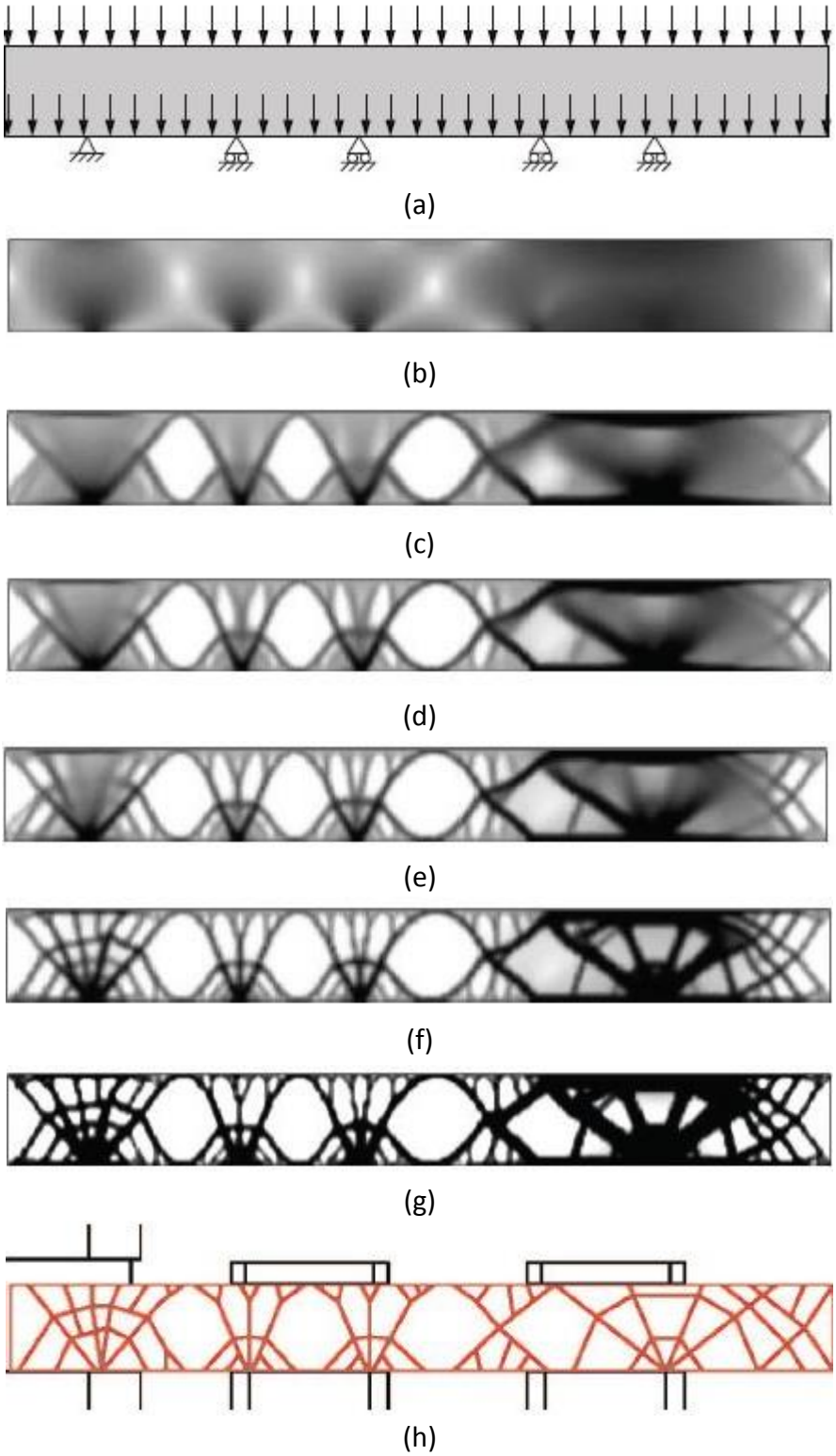

Figure 44: Topology Optimization for design of the upper “beam” spanning several towers: Iterations (a), (b) 1, (c) 10, (d) 15, (e) 20, (f) 40, (g) 100 (final design), (h) results engineering interpretation (Source: Beghini, 2013)

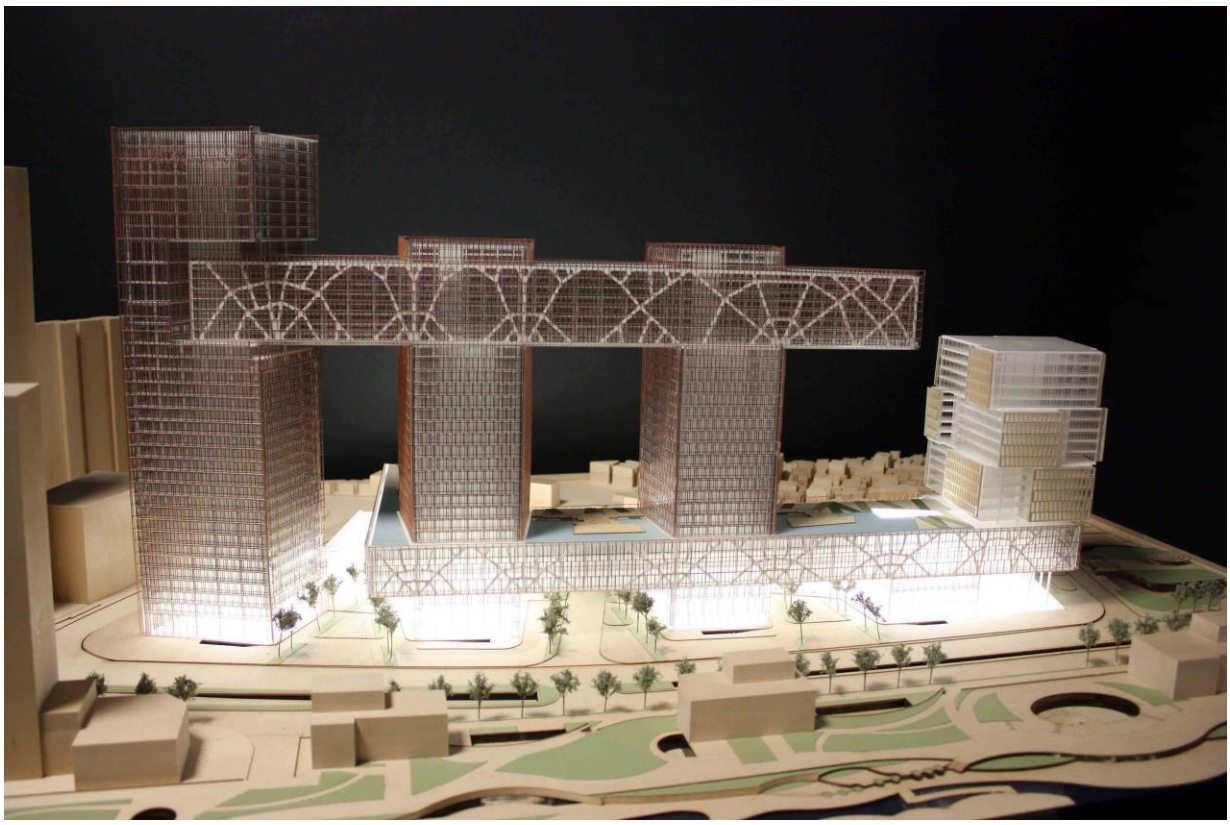

Figure 45: Picture of the physical model for the concept design competition using the previous topology optimization results (Source: Beghini, 2013)

3.2 Force Density Method

3.2.1 Introduction to form finding

Membrane structures have a particular appearance, which directly reflect their structural behavior. Finding the equilibrium shape of these pure tension or compression structures consists of determining the membrane geometry, which is compatible with a set of prestress conditions and boundary conditions beginning with an initial geometry.
The procedure of finding the equilibrium shape is known as form finding.
The first form finding techniques were based on building physical models based on, for example, chain models, soap bubbles, hanging fabric and air inflated elastic membranes. The German pavilion for the Montreal EXPO in 1967 was built along these principles despite no analytical solution existing nor computer or powerful software to define the cable-net form. The only way to proceed with the design of these forms at this point in time was to use physical models.

When Frei Otto had to inform the net structure of the Olympic stadium in Munich, he built precise physical models. While these experimental methods helped greatly in visualizing and understanding the structural behavior of tensile structures, it was nevertheless clear that these models lacked the necessary precision and were considerably time consuming to create.

(a) (b)

Figure 46: Experimental method to find the optimal structural curvature: (a) Soap buble model, (b) Munich stadium chain model (Source: Gründig, 2000)

In 1971, Linkwitz and Schek discovered a new way to formulate the figure for the equilibrium of forces, that is to say the force density formulation. The form finding technique relied by Schek,i.e. the Force Density Method, provided a more flexible approach to form finding and used different mathematical techniques leading to the equilibrium geometry of a prestressed membrane subjected to a certain load case and a set of predefined boundary conditions. Force Density Method, thanks to new computer tools, could allow in depth analysis of tensile structures.

For example, the Force Density Method has been explored for the project of a large scale "dreamcatcher" structure to be installed between two buildings in Los Angeles.
The optimization tool has been employed by the engineers in order to achieve as much as possible the form required by the artist (Figure 47).

Figure 47: “Dreamcatcher” atist structure in Los Angeles (Source: Courtesy of SOM, 2016)

FDM has in fact been developed to optimize the quantity of rope used, so that the correct amount of rope may be determined.
The objective was to devise as few junctions as possible to attach the ropes between themselves, as the cost of the structure does not result as much from the price of rope, but from the labor required to construct it. The more junctions there are, the more time would be required to build the structure. FDM helped in testing many different forms and possible evaluative results (Figure 48).

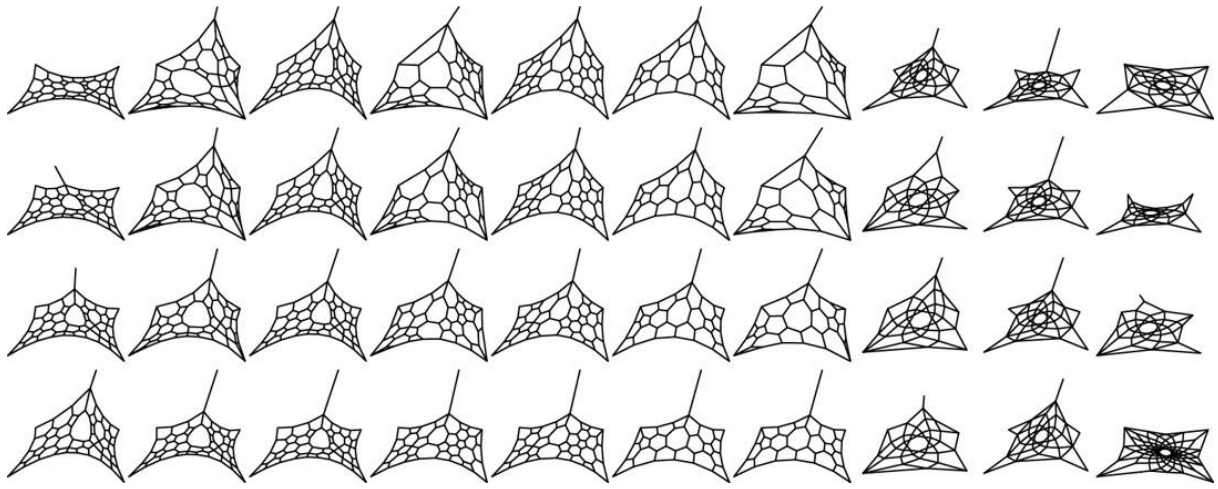

Figure 48: Changing boundary conditions and loads conditions make possible different structures developments (Source: Courtesy of SOM, 2016)

3.2.2 Mathematical approach

The fundamental principle of force density method is to transform a system with non-linear equilibrium equations into a system of linear equations when prescribing a constant force-density value.
The force density method then calculates the equilibrium state of predefined net structures.

The membrane is transformed into a discrete cable net system where the cable elements represent part of the membrane.
The force density method is based on the idea that the ratio between the length and the tension measured into the cable element is a constant value.

Method:

An initial mesh (net structure) is modeled. This net structure consists of a series of points/nodes connected by lines/branches. The mesh is described with the use of a branch node matrix by setting the connectivity between the points and the branches. All the points n are numbered from 1 to n and the branches from 1 to m. The branch node matrix C_S contains m rows and n columns. There are both fixed points and free points. It also becomes necessary to subdivide the matrix into two sub matrixes C and C_f:

$$C_s = C + C_f$$

On a branch node matrix of this assembly, the free points are designed as dashed molecules and the fixed points with a continuous line.

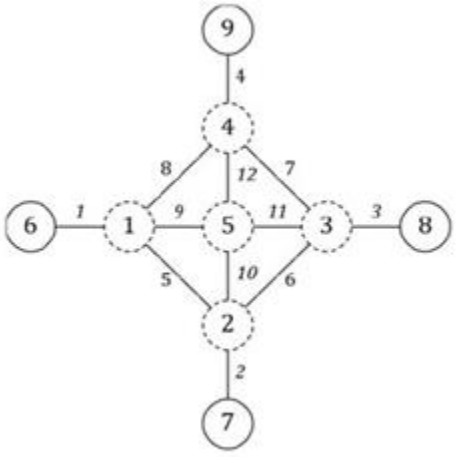

$C_s =$

	1	2	3	4	5	6	7	8	9
1	1	·	·	·	·	−1	·	·	·
2	·	1	·	·	·	·	−1	·	·
3	·	·	1	·	·	·	·	−1	·
4	·	·	·	1	·	·	·	·	−1
5	1	·	·	−1	·	·	·	·	·
6	1	−1	·	·	·	·	·	·	·
7	·	1	−1	·	·	·	·	·	·
8	·	·	1	−1	·	·	·	·	·
9	·	·	·	1	−1	·	·	·	·
10	1	·	·	·	−1	·	·	·	·
11	·	1	·	·	−1	·	·	·	·
12	·	·	1	·	−1	·	·	·	·
			C				C_f		

(a) (b)

Figure 49: Picture from H.Schek: (a) Branch-node matrix, (b) Graph (Source: Liang, 2012)

Different matrixes which contain force-density values must then be created consisting of point coordinates and loads, which are necessary for the assembly of the system made with equilibrium equations.

- There are three coordinate matrixes of dimension n:

$$x_f = \begin{bmatrix} x_{f1} \\ x_{fn} \end{bmatrix}$$

- Then the loads in the x, y and z directions and specifies the matrixes of dimension n:

$$P_x = \begin{bmatrix} P_{x1} \\ P_{xn} \end{bmatrix} \quad P_y = \begin{bmatrix} P_{x1} \\ P_{xn} \end{bmatrix} \quad P_z = \begin{bmatrix} P_{z1} \\ P_{zn} \end{bmatrix}$$

- Finally the diagonal force density matrix Q of dimension m x m is described:

$$Q = \begin{bmatrix} q_{11} & 0 \\ 0 & q_{mn} \end{bmatrix}$$

As soon as the 3 matrixes are correctly determined, the equilibrium in the 3 directions x, y, and z can be applied:

$$C^t Q\ C\, x + C^t Q\ C_f x_f = P_x$$
$$C^t Q\ C\, y + C^t Q\ C_f y_f = P_y$$
$$C^t Q\ C\, z + C^t Q\ C_f z_f = P_z$$

These equations can be simplified imposing:

$$C^t Q\ C = D$$
$$C^t Q\ C_f = D_f$$

Which obtains:

$$D\, x + D_f x_f = P_x$$
$$D\, y + D_f y_f = P_y$$
$$D\, z + D_f z_f = P_z$$

The new coordinates of the points can be easily written, as a part of the equilibrium mesh:

$$x = D^{-1}\,(P_x - D_f x_f)$$
$$y = D^{-1}(P_y - D_f y_f)$$
$$z = D^{-1}(P_z - D_f z_f)$$

By solving the three systems of linear equilibrium equations, the new coordinates of the free points are obtained. Thanks to the use of the branch node matrix the deformed mesh can be built putting in evidence the membrane shape (Figure 50) as follow:

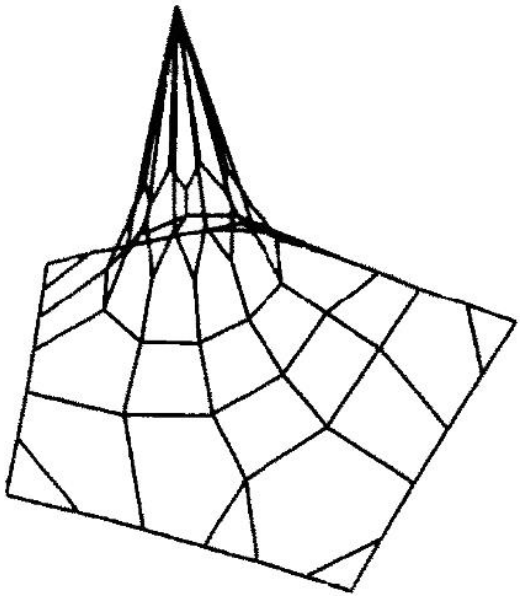

Figure 50: Picture fron H.Schek: Membrane shape (Source: Liang, 2012)

3.2.3 Overview of the tools used

Numerous form-finding methods have been developed in recent decades, closely related to the development of computer-based structural software.

The starting point is a pin-joint network consisting of cables or bar elements, in which some of the points are fixed while the others remain free. The free points will have to find a position in the equilibrium configuration and the constrained points are the input data for the initial configuration problem.

Pin-jointed network structures assume the state of equilibrium while internal forces s and external forces p are balanced (Figure 51).

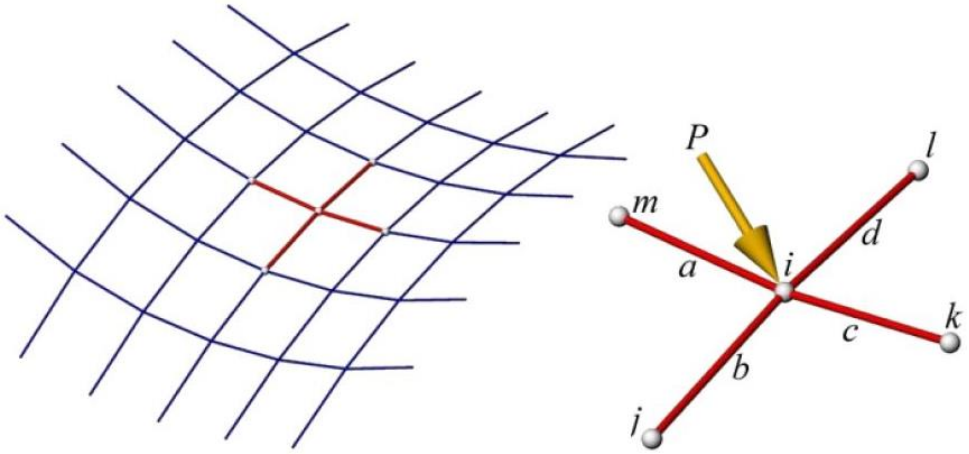

Figure 51: Part of a cable network (Source: Basso, September 2009)

In the end, the optimization force density method tends to solve an algorithm describing the previous explanation. One of the possible methodologies, which is developed by the SOM structural group in San Francisco could result in the use of combined softwares, i.e. S-FRAME to model the object to optimize, combined with a home-made MatLab code to run the Force Density method. This methodology will be first applied as precisely described in the following chapter.

3.2.4 Optimization procedure

The force density method is based on the mathematical assumption that the ratio between the length and tension within each cable element is a constant value (Lewis 2003).
Figure 52 shows the simplest application of an FDM procedure. A square surface is defined as a homogeneous mesh, i.e. divided in n number of bars and nodes. Uniform gravitational loads are applied and the corners are fixed on the z direction. Which results in a pure symmetric membrane shape under Force Density.

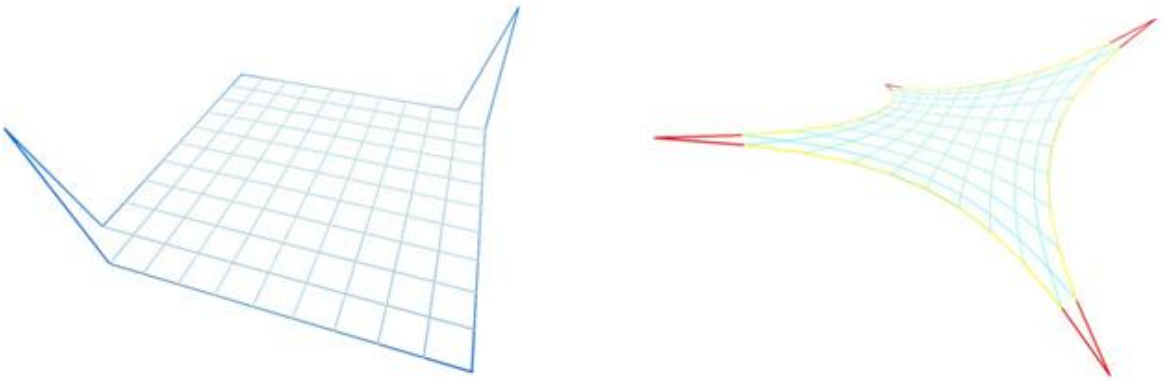

Figure 52: Membrane Shape (Source: Courtesy of SOM, 2016)

The same ideology will be used to proceed with an initial experimental model obtained through the Force Density Method. The following workflow (Figure 53) is applied, using a procedure developed by the SOM structural group in San Francisco by Alessandro Beghini.
This first trial example is a building slab case study with columns, core and distributed gravity loads. A very simple geometry in order to display the accuracy of the procedure.

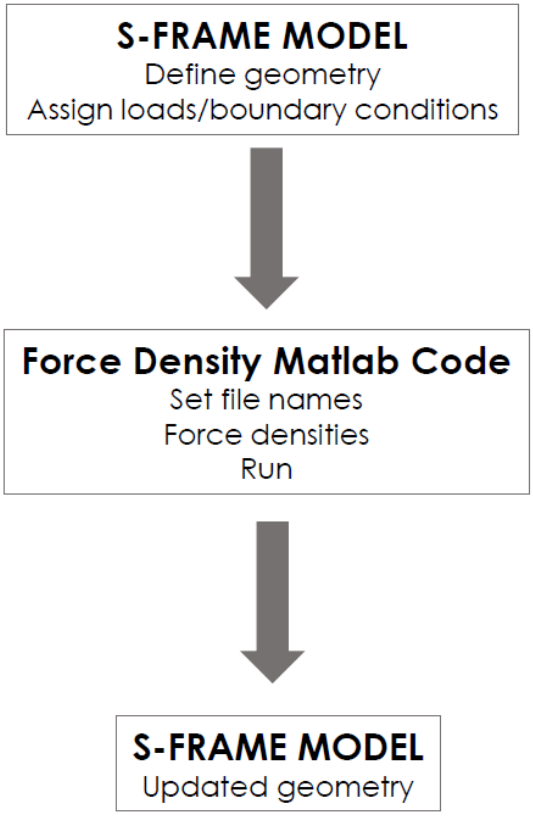

Figure 53: Work scheme of Topology optimization (Source: auhtor, 2015)

A square surface is first drawn on CAD, paying attention that the element is composed of multiple elements linked together to form the plate.

The drawing is imported into the S- FRAME software, where the gravitational loads and the boundary conditions can be assigned. The loads have a value of -10 kips, which allow it to give way to the application of loads, the amplitude of the load value having no meaning in this study. The core and the edges are blocked in the three directions.

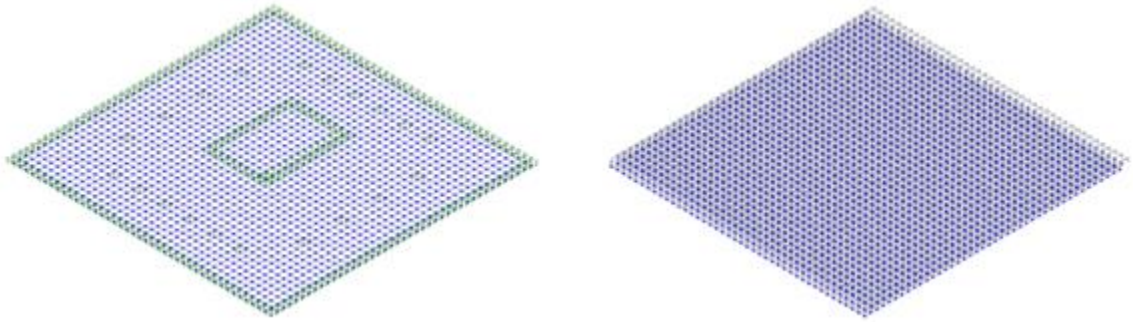

(a) (b)

Figure 54: S-FRAME model: (a) supports, (b) loads (Source: author, 2016)

The deformed final shape is obtained through the use of MatLab. The new coordinates are updated into the S-Frame model. This cable net, on Figure 55 is consistent with the global response we would expect to find with the Force Density Method. Increasing the load values would curve the cable net more dramatically.

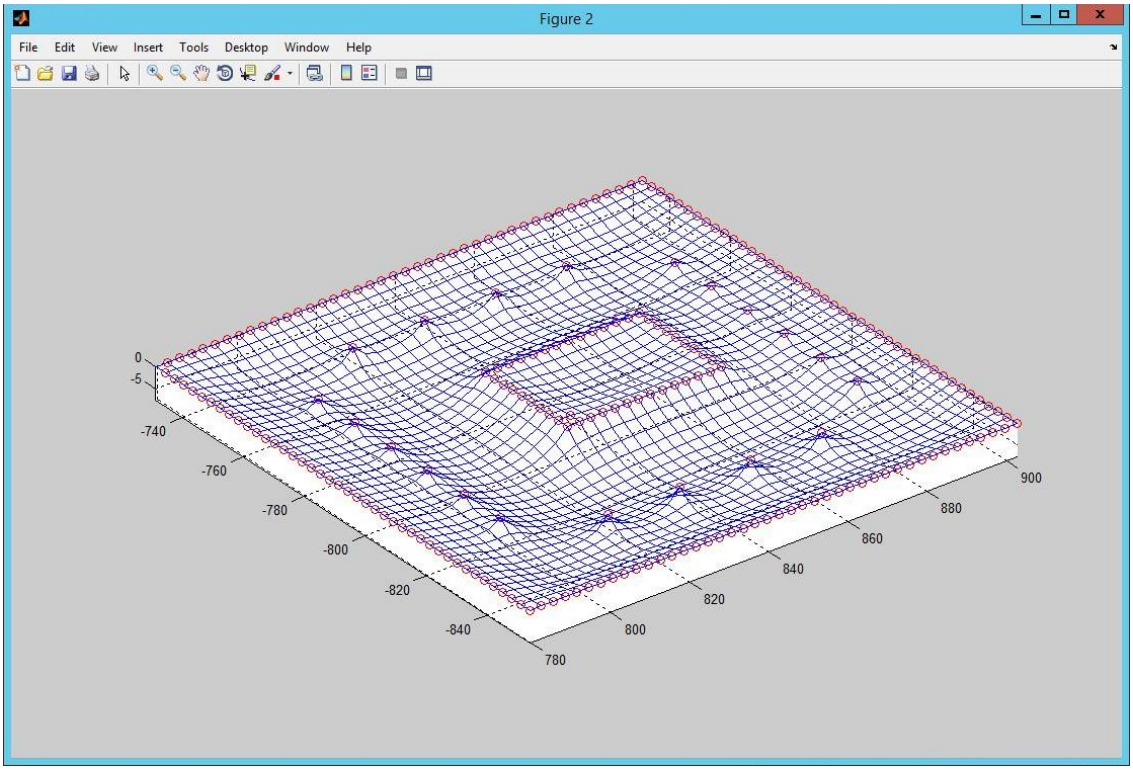

Figure 55: S-FRAME model: deformed shape (Source: me, 2016)

4 Case study: Conventional Approach

4.1 Project overview

4.1.1 Site conditions and architectural presentation

The study will focus on a building situated in the south of market area of San Francisco that benefits from a great location, facing the bay. The project consists of the transformation of an 8 story-parking garage into a 20-story, 220 foot tall mixed-used building.

Figure 56: View from the bay bridge (Source: Courtesy of SOM, 2015)

The great location of the project strongly influenced the architectural design. In fact, the main architectural goal is to take advantage of the bay view, which is expressed by a number of

features: large openings, no corner columns in order to increase the view from the living rooms in the future apartments as well as many outside spaces including terraces and balconies.
In order to achieve these conceptual intentions, the architectural design of the building makes use of shifted plans. The building is divided into five blocks with each one composed of a number of floors. Each of these blocks is shifted from the other, creating terraces and balconies that take advantage of the bay view and receive the best sun exposure. The view from the street reveals the main architectural feature of the façade: no columns can be seen.

Figure 57: View from embarcadero (Source: Courtesy of SOM, 2015)

The prime location of the future building demands high quality architecture. In order to achieve the best exterior appearance for the building, a special facade was designed: all the window frames are covered with stone, providing an architecturally stunning façade finish, but also functions to add some important gravity loads acting on the slabs.

Figure 58: View from the building entrance (Source: Courtesy of SOM, 2015)

4.1.2 Structural description

The design of the structural system must first take into account all of the architectural constraints, most significantly in this case, a pre-required thickness of 8” for each slabs with some large cantilevered spans at the corners and on the sides.

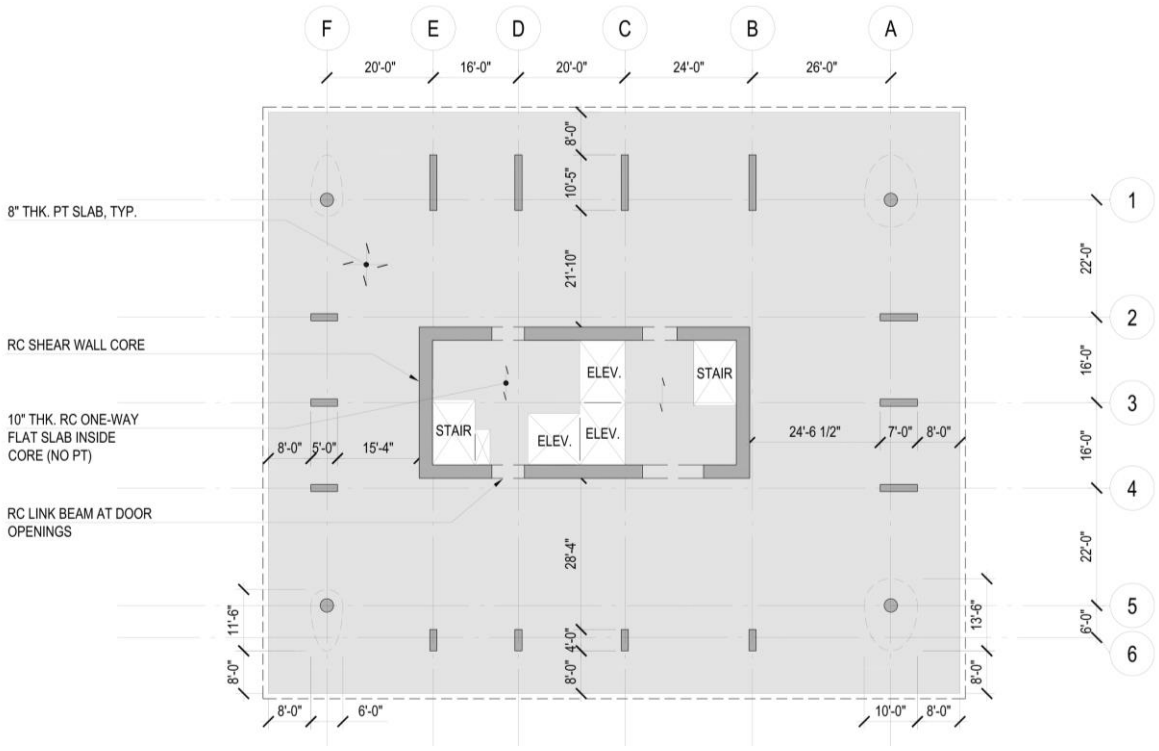

Figure 59: Structural plan (Source: Courtesy of SOM, 2015)

A steel frame supported by the slabs carries the glass and stone façade. A heavy façade plus a super high dead load imposed by a high quality floor finish creates a truly luxury program. These important architectural constraints (dead loads + the important cantilevers + 8” slab) will demand a particular attention dedicated to the slab structure. In fact, the more floors to be built, the more the building will be financially feasible and interesting for investors. The slabs will of course be post-tensioned as it is the best manner to achieve these desired spans with relatively thin slabs.

Figure 60: View onto the face, where the column distribution is not visible from the outside (Source: Courtesy of SOM, 2015)

Even when using post-tensioning, it has been challenging to find the best position to locate the columns in order to first keep the 8 inch slab, and second, to always keep the columns before the windows from the inside while also preventing a view of the columns from the street.

In fact, one of the strongest architectural choices was to design balconies without columns, i.e. the columns would be always placed inside the building just behind the glass. As mentioned before, the floors are shifted, which makes it impossible to align the columns with the building full height. The solution found by the structural team was to design a system of flags' columns, i.e. an evolving column system where columns pass from a classical column shape to a wall in some floors (figure). This design will not interrupt the load lowering and at the same time keeps a maximum of an 8 ft cantilever between the wallumn (wall + column) and the slab edge. The 8 ft distance corresponds to an acceptable cantilever for an 8 in thick post-tensioned slab.

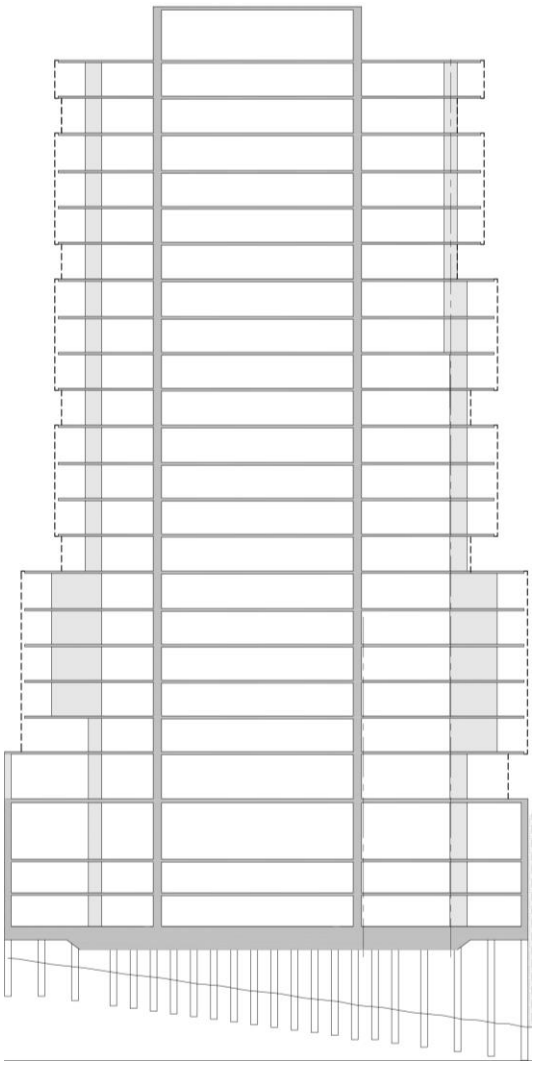

Figure 61: East-West section of the building. The flags columns are clearly represented (Source: Courtesy of SOM, 2015)

Nevertheless, this system also creates in some cases architectural constraints, particularly at the corners. In such a case, the wallumns would have to be placed diagonally, but this choice would dramatically affect the architectural spaces. These diagonals would have been located within the living rooms of the future apartments, which on one hand would make everyday life more difficult, and on the other hand would interfere with the view onto the bay.

Therefore, a special treatment for the corner columns had to be devised besides the flags' system.

Aligned columns at the corners were selected as the solution. The constant evolution of the cantilever, which reaches 15 feet on some floors, will be solved by an excrescence at the top of these columns to carry the loads coming from the extra cantilevers.

These excrescences take the shape of an oval and are not circular as in this case it allowed to orient towards the slab's edge corners. These systems were quickly designated as "avocados".

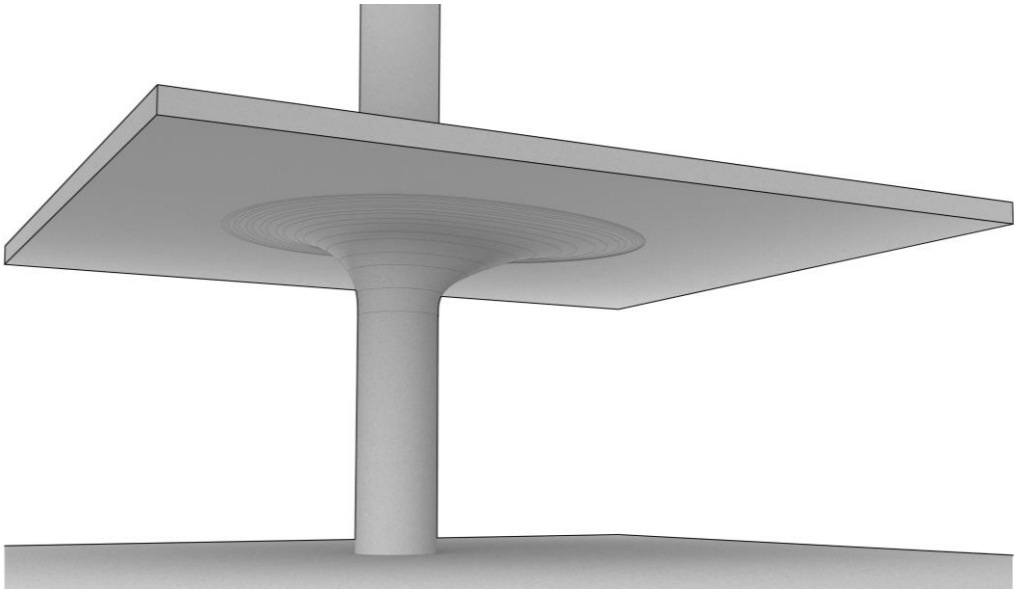

Figure 62: Tappered-column (Source: Courtesy of SOM, 2015)

With the aim of saving material, it also became necessary to understand how much material would be required to create the "avocados". As the behaviors of the slab and columns are intimately correlated, the number of tendons in this case could be used for a first approximation of the avocado shape.
Therefore, as the number and layout of tendons are evaluated and may change, the avocado shape could be updated as well.

Finding the optimal curve returns to evaluate the height of the concrete slab at the avocado location, in the three directions: x y and z, for the corner direction.

Let us return to the basic formula of the demand moment:

$$M_n = A_s * f_y * (d - \frac{a}{2})$$

With:

$$a = \frac{A_s * f_y}{0.85 * f_c' * b}$$

So:

$$M_n = A_s * f_y * (d - 0.57 * (\frac{A_s * f_y}{f_c' * b})$$

As Mx values can be extracted from an ETABS model, it is then easy to equalize Mn and Mx (Figure 63) in order to plot only the unknown value, i.e. h (see all the details in Appendix 1):

$$M_n = M_x$$

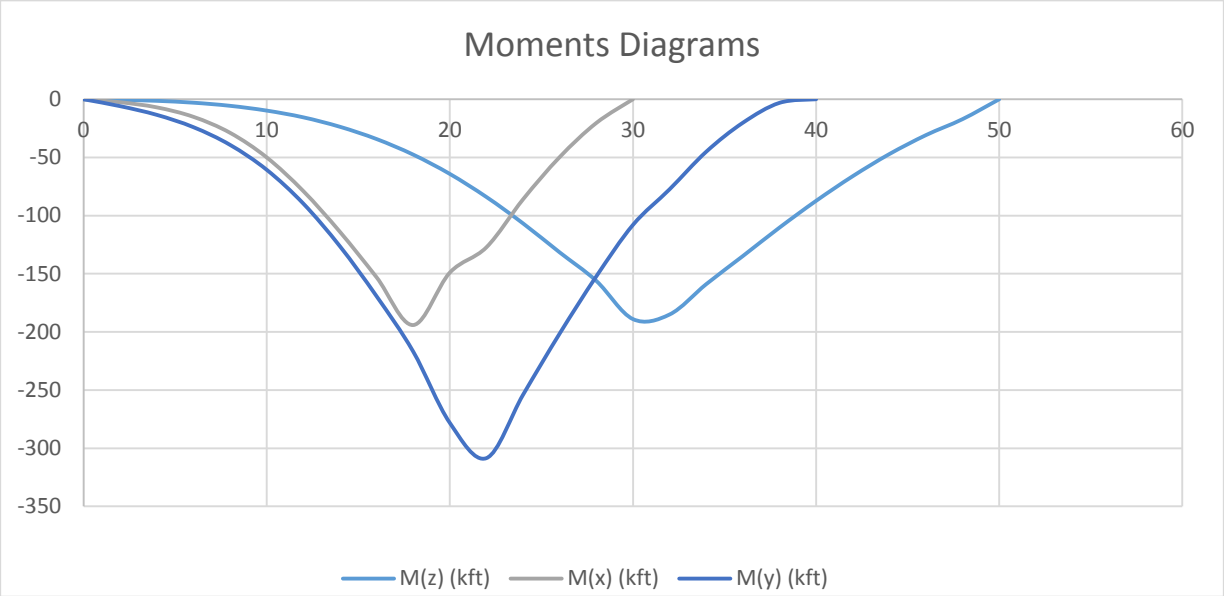

Figure 63: Moments diagrams in the three directions: x, y and z (Source: author, 2015)

Which allows the approximate shape of the avocados to be found.

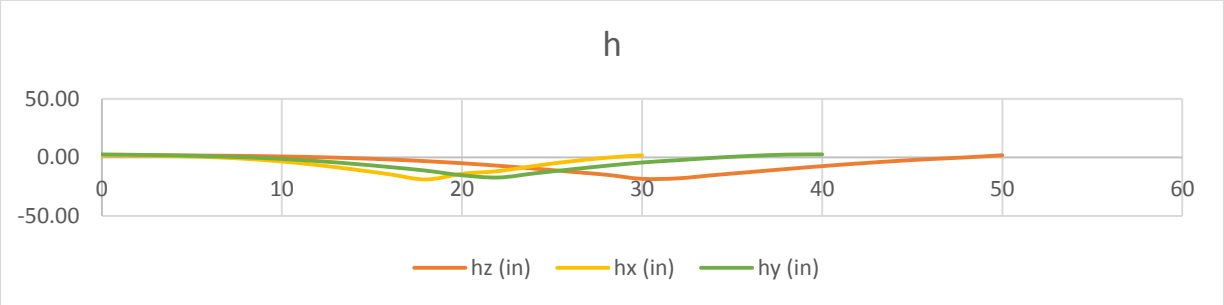

Figure 64: Avocado Curves' profiles in the three directions: x, y and z (Source: author, 2015)

4.2 Design phase

4.2.1 Materials

Concrete Properties:
f'c = 5000 psi cylindrical strength at 28 days
f'ci = 3750 psi concrete strength at stressing (initial/PT transfer)
Ec = 4287 ksi modulus of elasticity at 28 days
Creep coefficient = 2.0

Prestressing cable properties:
f_{pu} = 270 ksi ultimate stress
f_{py} = 245 ksi yield stress
Eps = 29000 ksi modulus of elasticity
Typical diameter = 0.50 "
Typical Area = 0.153 in^2

Estimated prestress losses:
f_{se} = 0.7 (270 ksi) – 15 ksi = 174 ksi (ACI 18.6)
$P_{eff} = A*f_{se}$ = (0,153) (174 ksi) = 26,6 kips/tendon

4.2.2 Loadings

Static load case

The floor plate actions are studied under two main gravity loads, i.e dead and live loads.

SDL	45	Psf (2.15 KPa)
Live Load	40	Psf (2.15 KPa)
Curtain distributed Load	35	Psf → 35 x 11' =385 p/ft (3.67 k/m)

Load combinations

The floor plates are designed under 3 major limit states:

3) Strength: Initial (or transfer) limit state

Stresses are major concerns

SW + 1.15 PT

4) Service limit state

Both stresses and deflection are the main criteria

PT + SW + SDL 0.3 LL

4.2.3 Design criteria

The Design Criteria to be applied will be the one described in chapter 2.9.2, following the ACI codes and SOM methodologies.

4.3 Strategy

Post-tensioning design for concrete flat slabs shows the limit of the classical procedure when the engineer must apply a conventional approach to design a non-conventional shape, observing that such a trial and error process leads to a time consuming practice along with wasting materials at the same time. This argument holds true in the cases of classical shapes as well where the post-tensioning layout has to be modified as many times as the architects change the design.
It therefore becomes crucial to find the most efficient way to post-tension a regular or complex shaped flat slab. Investigation of topology optimization and the force density method can be used in order to discover new ways of post-tensioning.

The strategy will proceed through the analysis of three different tendon layouts and then to compare them in terms of deflections, post-tensioning weight, stresses and rebar quantity.
Comparing three layouts makes the most sense because:

- The first layout is the current scheme, the one which has been designed using existing everyday practice and obtained without pursuing any optimization procedure
- The second scheme will be an optimized current scheme, i.e. an optimal scheme but realistic and buildable by simplifying the current model obtained. This approach will focus on optimizing the banded tendons only, keeping between the first and the second scheme the same amount of tendons. Banded tendons appear to be in less quantity, and have a strong effect on the global structural slab behavior.
- The third scheme will try to develop the greatest possible optimized layout, without taking into account too many constraints such as cable curvature. The aim is to be strongly experimental and innovative. The buildable aspect is not take into account as strongly.

The following Figure shows synthetizing the optimization procedure (Figure 65).

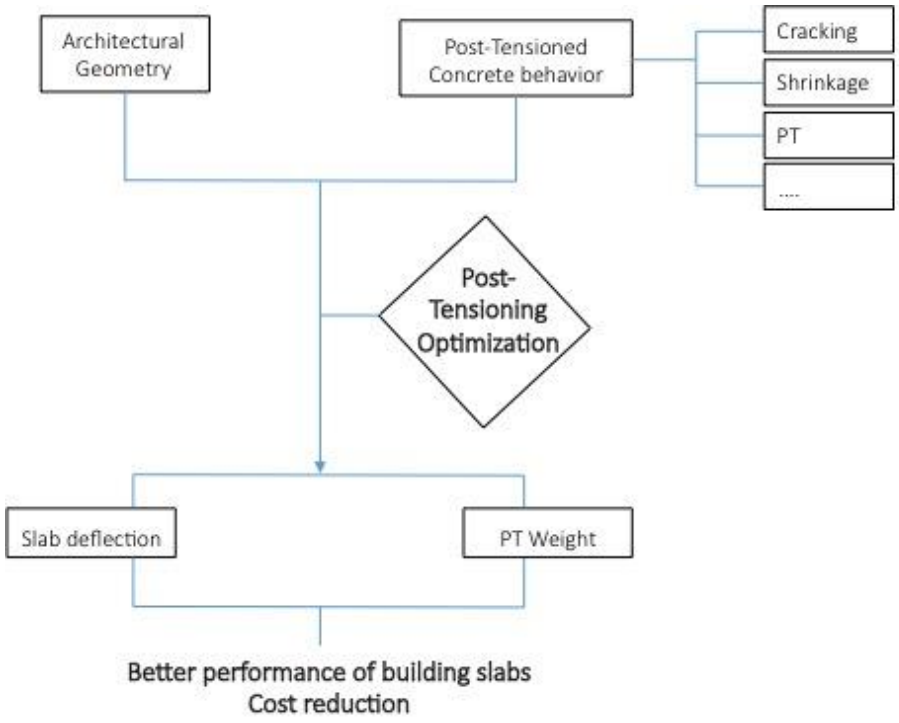

Figure 65: Flowchart of the optimization procedure (Source: author, 2015)

4.4 Conventional approach for post-tensioning design

The model will be designed in SAFE, a specific finite element software, currently used to analyze post-tensioned concrete slabs, and introduced in-depth in chapter 2.9.2.3. (Finite Element study with SAFE). It will allow, amongst other things, to check the long-term deflection of the slab.
The finite element analysis will consider the specific load cases, load combinations, prestressing cable properties and estimated prestress losses previously described in the chapter 4.2: Design Phase.

Conventional post-tensioning is made with banded and uniform tendons. Banded tendons pass through the columns and are also laid in diagonal directions to reach the corners as well as to counteract the cantilevers.

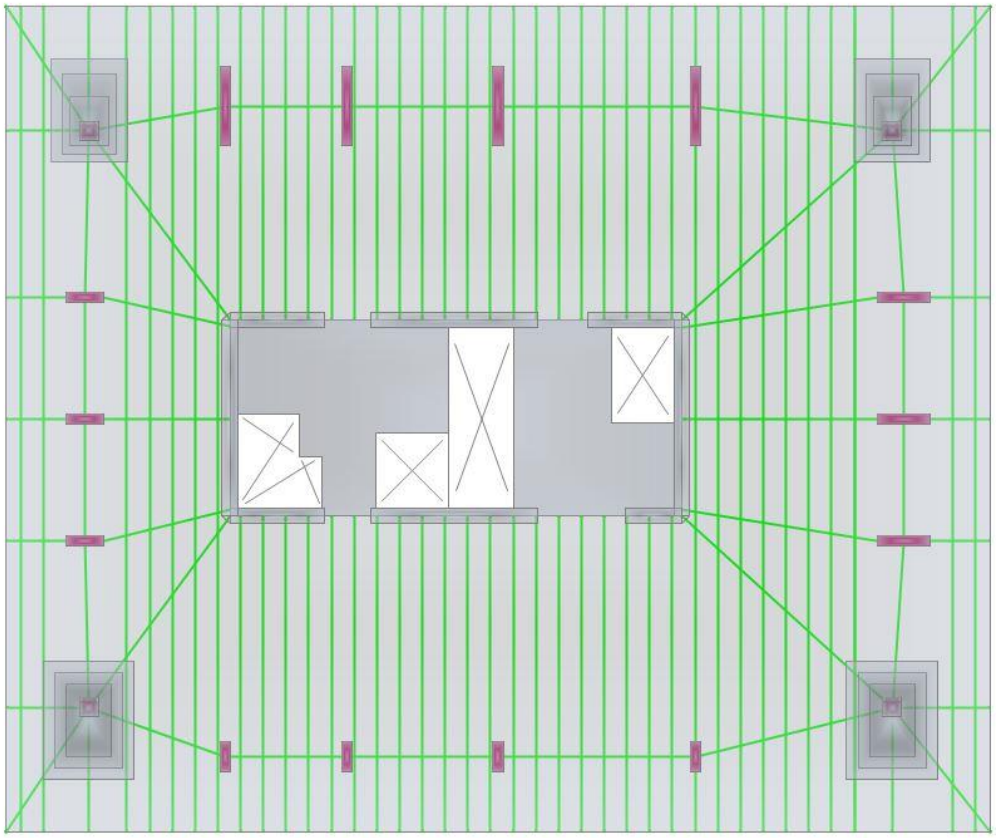

Figure 66: Tendons layout: current scheme (Source: author, 2015)

The profiles of the tendons have a real impact on the control of the deflection and affect significantly the design procedure.
The traditional profile follows the moment diagram, as in the Figure, “Mid-High-Low-High-Low-High-Mid”, for a typical uniform tendon profile, for example (Figure), which corresponds for an 8” slab (taking as the reference coordinate for the underside of the slab):

- Mid at the edges for technical reasons, i.e. placing the anchorages to satisfy the cover: z = 4 in
- High at the supports, with max eccentricity: z = 7 in
- Low at the mid span between two supports, corresponding to the max slab deflection: z = 1 in

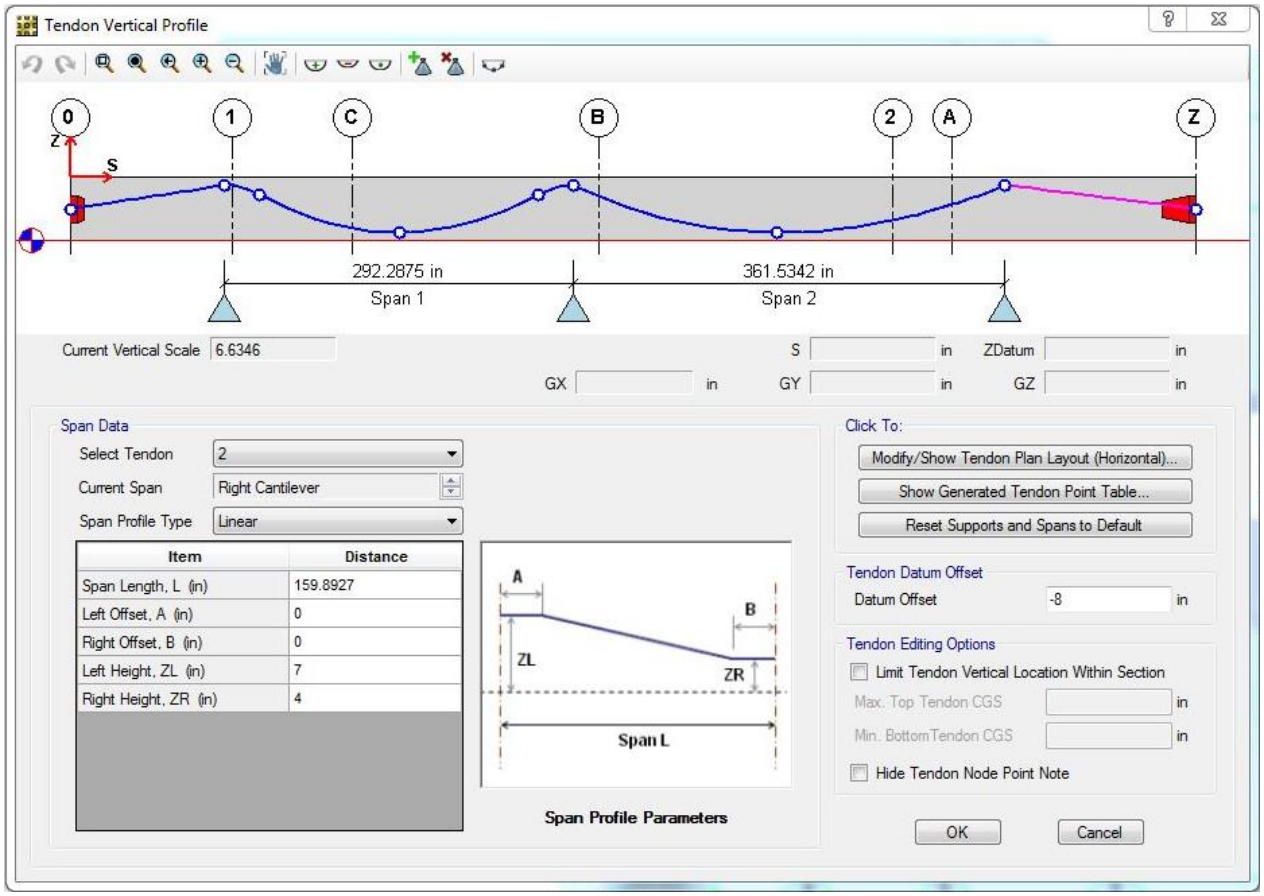

Figure 67: Uniform tendon‘s profile (Source: author, 2015)

The same logic that adjusts the tendon profiles is then applied to the uniform tendons as well as for the banded tendons.

The design criteria will be to not overtake the deflection values of 0.75 in at the edges.

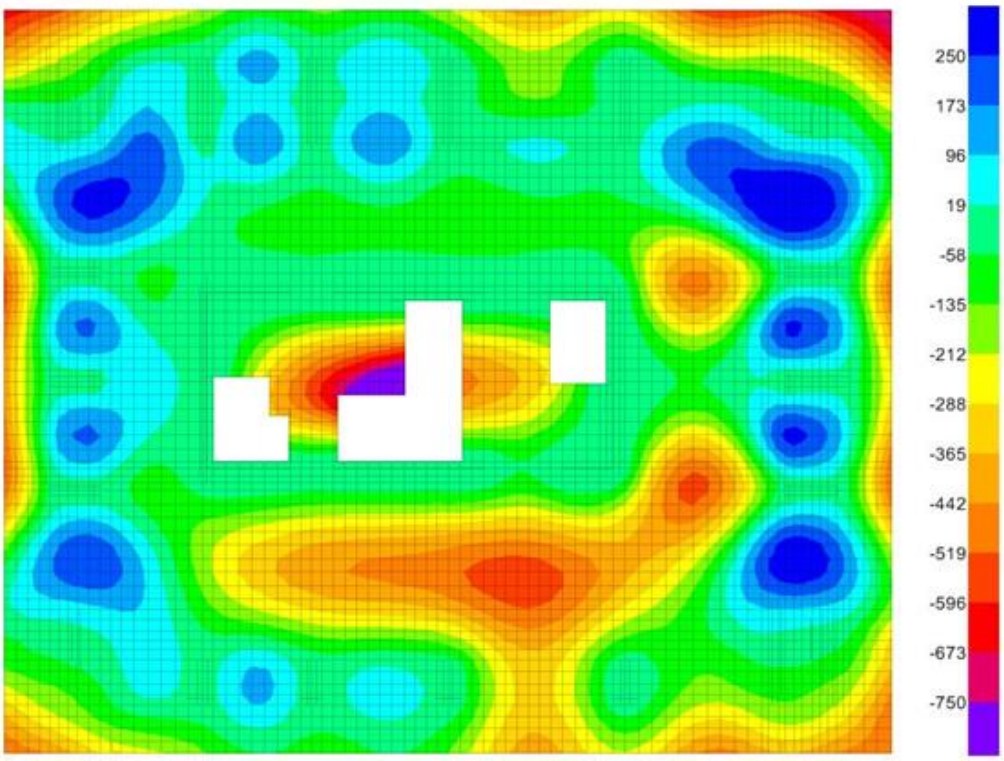

Figure 68: Long-term deflection: the blue color corresponds to the max uplift and the purple color to the max deflection (Source: author, 2015)

What can be observed is an irregular deflection profile. What would be expected is a light red shade at the edges and a light blue at mid span. A huge uplift appears at the placement of the diagonal tendons. A higher amount of tensile forces is required for the cantilevers, especially for the corners. But these tendons are not necessary for the areas between the core and the corner columns, due to the large amount of uniform tendons in this zone. This is a way to explain why the admissible uplift values greatly overtake the code requirements.

5 Case Study: Structural Optimization

The main performance standard used to gauge the effectiveness of the optimized post-tensioning layout is the maximum acceptable long-term deflection, as compared to that of the traditional solution.

As mentioned before, the best knowledge in structural analysis combined with a continuing growth of digital computing has provided an incredible increase in structural optimization research and applications in the field of engineering design. Applied to the case study, structural optimization will allow us to identify optimal geometric layouts. The optimization tools are numerous and their particular uses will depend on the specific application taken into account. The optimization procedure will be conducted combining commercially available codes and custom written programs in order to save a large amount of steel when designing a post-tensioned concrete flat slab. The most efficient disposition of the tendons in-plan and out-of-plan will assist the engineer in reaching the same design objectives for deflection and stress verification while also decreasing the overall amount of steel necessary for each slab. A fundamental concern in the design of high-rise buildings and long spans structures deals with the consumption of resources. Such approaches will allow an increase in the number of floors while yet decreasing the thickness of the slab resulting in a positive economy of material and reducing the global dead load of the building.

The process of optimization will follow all the steps of the design from the concept to the code checks. A focus of the work will be to couple computational and analytical pproaches to achieve a deeper understanding of the structural behavior in order to define a particular methodology in creating a discussion between the optimal procedure and the theory of post-tensioned concrete flat slabs.

Plural optimization methodologies will be investigated such as Rain Flow Analogy, Principal Moments Directions, Topology Optimization and Force Density Method.
The Rain flow analogy normally deals with the phenomenon of fatigue of materials with irregular cycles of loading. Within the rain flow analogy, one imagines the (distributed) load as a rain shower of constant intensity falling down on a surface, representing the sum of curvatures. In contrast, the principal moment directions provides a high concentration of stresses as a path to follow when designing the tendons directions. These 2 previous methodologies lead to overly complex mathematical approaches without furnishing a clear optimal orientation while still requiring significant efforts of interpretation.

5.1 In-Plan Study

As mentioned in the Strategy section (chapter 4.3), three post-tensioned layouts will be analyzed and compared. It is important to clarify that the profiles will always follow the conventional disposition ("Mid-High-Low-High-Mid") as the comparison intends to deal only with the IN-PLAN tendon optimization.

5.1.1 Refined Topology Optimization

Topology Optimization best optimizes the In-Plan aspect. The optimization problem is clearly defined by a given domain, loadings and boundary conditions. Into the topological space the structure is able to carry the loads from the points of application to the supports. Given a certain objective (minimum compliance, target frequency, etc.), the optimization process leads to the best structural system when considering the optimal objective of the system we are considering.

Hyper mesh Application (Seee also Appendix 2):

The principal elements are modelled on HyperMesh Optistruct, i.e. core, columns and slab.

First, the following rule is imposed:

Tx=Ty=Tz=0 for slab columns and core

Then, in order to better reflect reality and to obtain accurate results:

Tx=Ty=Tz=0 for core and on Tz= 0 for columns

In Figure 69 the pins are represented in red. The loads are imposed with a value of 1 kip, as it does not affect the final result. The value applied to the gravity loads orients the direction of the load action on the slab, so to lead to a more realistic path of the forces. In Figure 69, the loads are represented in yellow.

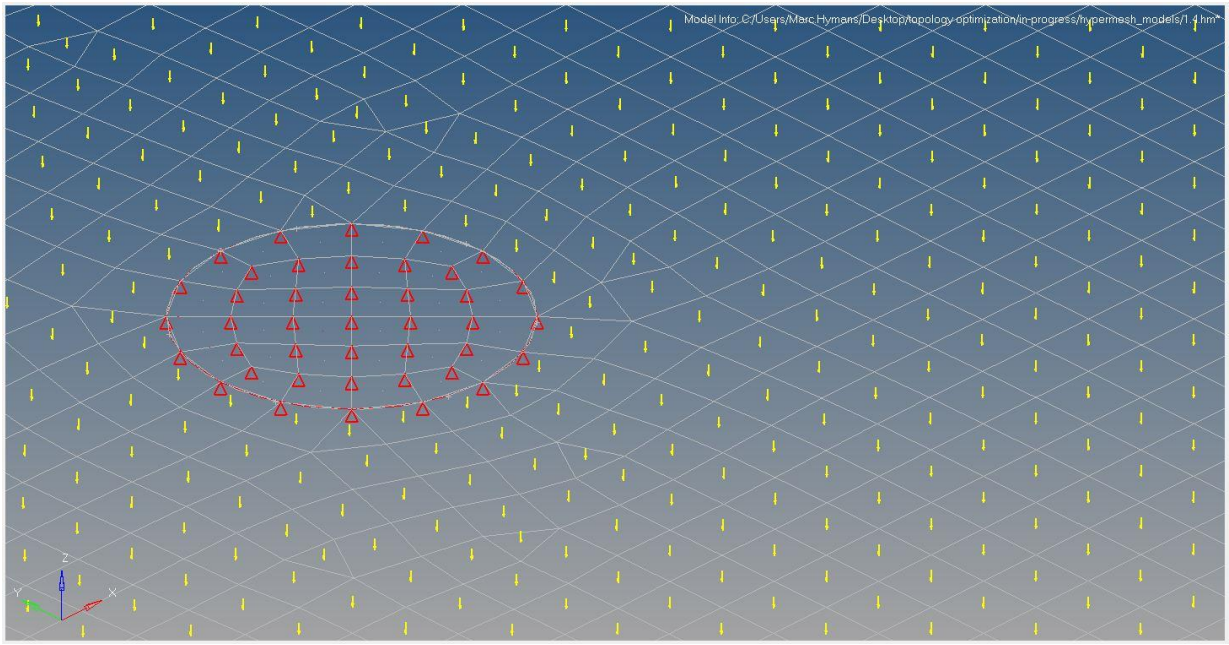

Figure 69: Design procedure with HyperMesh: Supports in red and uniformly distributed gravitational loads in yellow (Source: author, 2015)

A mesh is first applied to the geometry, using the software Hypermesh Optistruct by Altair, a company which enjoys a great reputation for the accuracy of their mesh design.

A mesh of a 6 in slab could obtain a precise optimization output. A smaller mesh would not provide a significant increase in the results convergence accuracy, and, overall, would not allow the most discretized models to run.

The mesh is applied to all the slab, except for the core, as it has not to be included in the optimization process; because when building a post-tensioned concrete slab, it is very rare to have the tendons running through the core. The exception can be for a core with a large span, which does not apply to this case study.

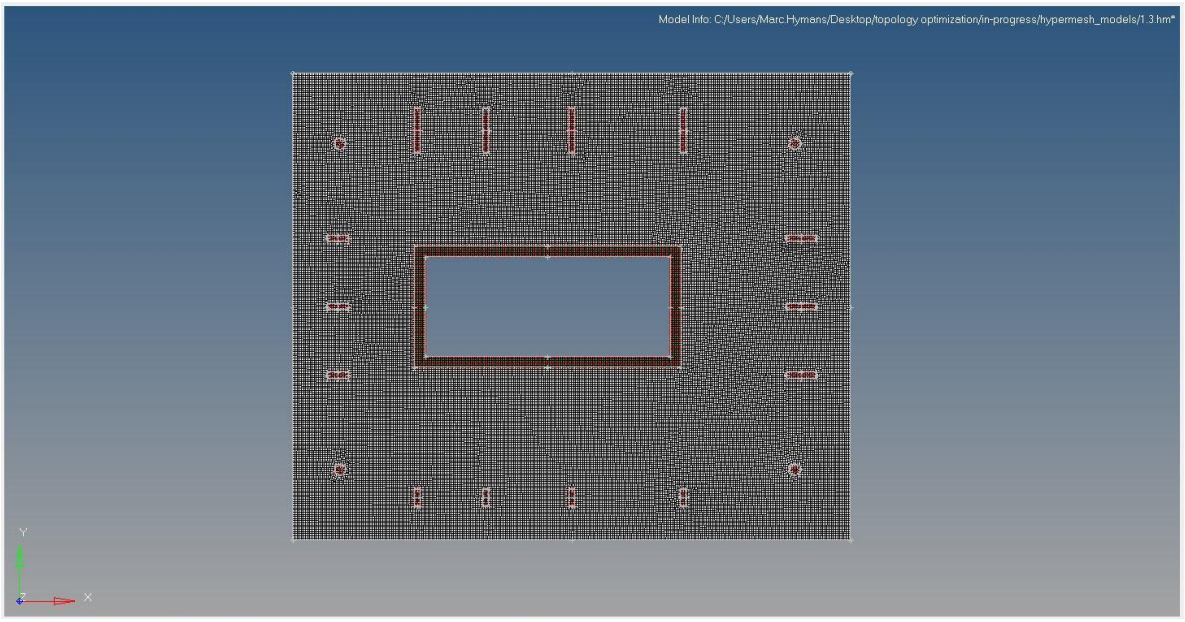

Figure 70: Design procedure with HyperMesh: Meshing along the slab and the supports (Source: author, 2015)

The objective is first to reach the minimum compliance, that is to determine where the maximum stiffness within the slab is located. The second objective is the volume fraction, i.e. to get a minimum quantity of material for a maximum stiffness.

Since the software used for this phase carries out the optimization through the SIMP methodology, the penalization factor varies following a trial and error process. The first step of discretization, p= 1, does not affect the result and with a density of 50 % of material we can proceed.

What can at first be observed is a high concentration of red color at the supports, i.e. around the columns and the core. This result is expected, as the flow of forces always tends towards the stiffest parts, represented by the supports.

A strong red line can also be found running along the edge of the slab where the spans reach high values. A high concentration of red color is even located at the mid-span between the core and the columns, which is directly related to the moment curvature, reflecting the maximum sag at mid-span and the max eccentricity at the supports.

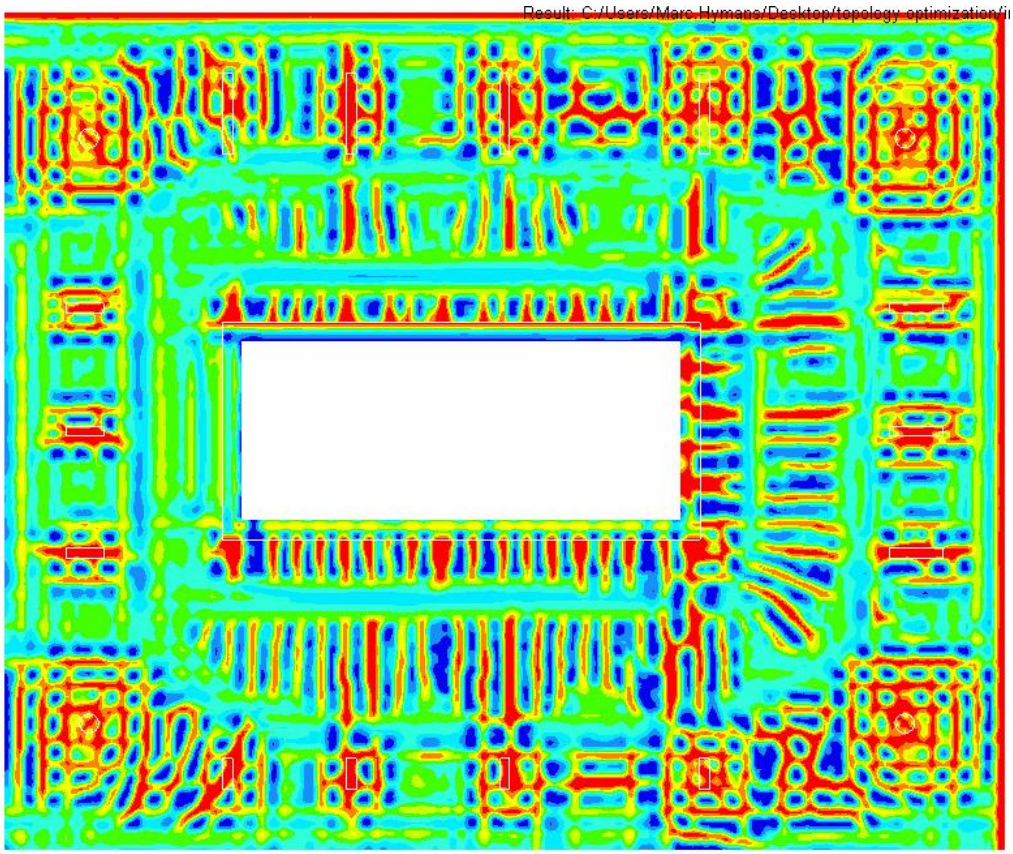

Figure 71: Outcome from HyperMesh, first iteration (Source: author, 2015)

Nevertheless, no clear direction can be observed. This first optimization is not accurate enough to interpret and direct the optimization procedure. All the iterations proceed, which leads to an entire range of possible solutions, containing ρ and p respectively (Table 5), which vary, in order to penalize the density of material with a progressive (step by step) increment. The objective will be reach a compromise between the least amount of material used with the clearest observable pattern.

Model	dconstraints (ρ)	Opticontrol (p>1)
1	0.5	dicrete = 1
2	0.4	dicrete = 1
3	0.3	dicrete = 1
4	0.2	dicrete = 1
5	0.1	dicrete = 1
6	0.5	dicrete = 2
7	0.4	dicrete = 2
8	0.3	dicrete = 2
9	0.2	dicrete = 2
10	0.1	dicrete = 2
11	0.5	dicrete = 3
12	0.4	dicrete = 3
13	0.3	dicrete = 3
14	0.2	dicrete = 3
15	0.1	dicrete = 3
16	0.5	dicrete = 4
17	0.4	dicrete = 4
18	0.3	dicrete = 4
19	0.2	dicrete = 4
20	0.1	dicrete = 4

Table 5: List of the varying iterative parameters to proceed to Optimization (Source: author, 2015)

In this case, the SIMP method used for Topology Optimization is a density method. It can be initiated through a gradient based optimization, which signifies finding the MINIMUM requirement of the objective function. The end objective seeks to make it possible to manufacture, therefore the best approach is to have solid or empty elements with no material in between. In order to reach this result, as described previously in the theoretical part, this method makes use of the penalization factor to penalize intermediate densities (Figure 72). In fact, the cost of intermediate densities is higher compared to the relative stiffness, thus intermediate density becomes unfavorable.

The full range of results can be plotted and observed from HyperMesh. The analysis procures a plurality of models with a high number of branches and stiff lines, ranging from a light blue to a strong red, with red corresponding to max stiff zones. The very light lines result from a tendency to link the stiffest parts.

From the less discretized model at the top left to the most discretized located at the bottom right.

Results confirm that key load patterns observed are indeed viable. Loads are carried to the supports through the material configured in the lines of different colors, thickness and directions, passing from tension to compression, depending on whether situated at the bottom or the upper face of the slab. It also depends on if trying to take the shortest path possible for coupling the loads. There is no solution available for $p = 3$ and $\rho = 0.1$ or $p = 4$ and $\rho = 0.2$, which results from a ratio between the optimization parameters (material quantity through volume fraction) and the refinement of the mesh. The objective works towards a plot with as few intermediate densities as possible, which is possible until a certain criteria. After that point, the results through the Topology Optimization procedure are not attained (no results = no plots).

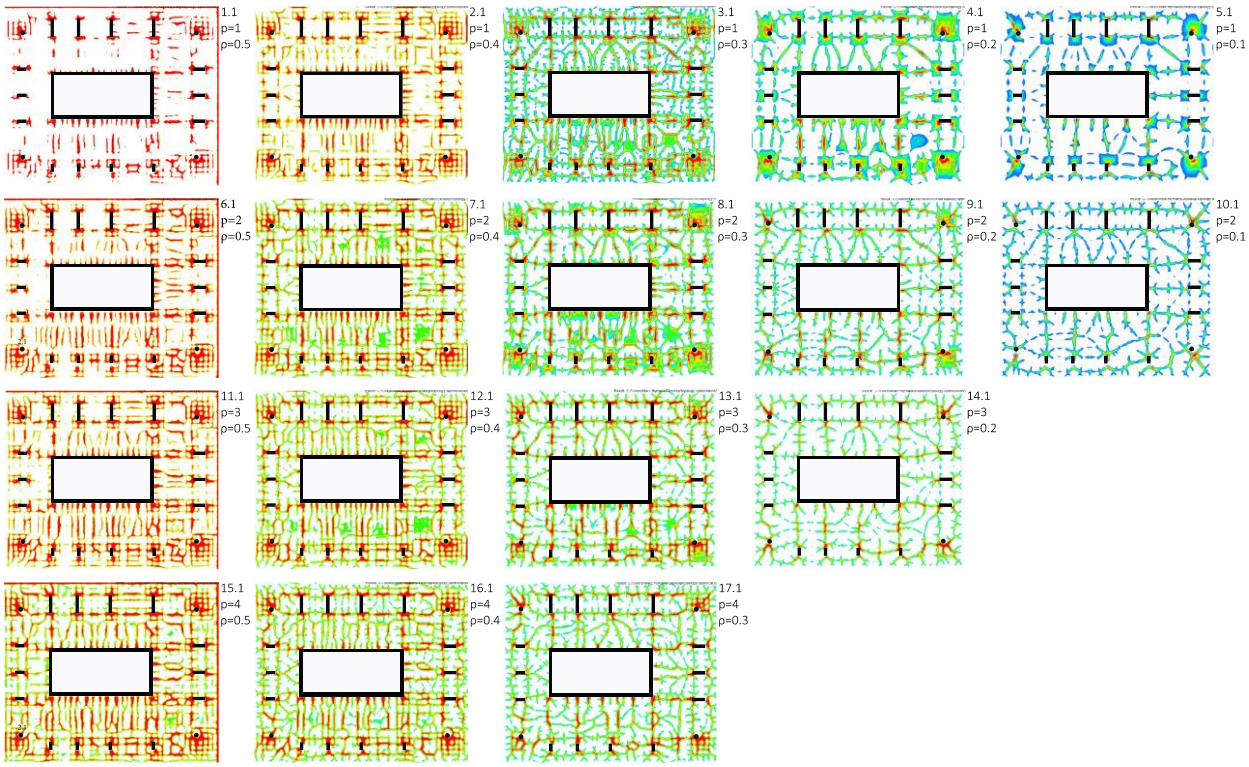

Figure 72: Outcome from HyperMesh: List of the all range of iterations proceeded and permitted by the software (Source: author, 2015)

The fundamental step of the optimization procedure is to move from a continuum structure to a discrete one. The crucial point is to understand and translate the new discrete structures into a realistic one.

5.1.2 Interpretation of the optimization and design of the topology concept

Topology Optimization can be segmented into three phases. First, where the topology of the structure is generated, secondly comes the interpretation of the topology process, where various approaches can be used for to interpret, and finally the detailed designed phase. This section will focus on the second phase and it does not strictly define how to conduct the interpretation. The engineer is responsible to interpret and reengineer the results at the end of the process, but the methodology itself depends only on the specific study being made.

Here, an image interpretation approach will be employed. Graphic aids ranging from trace papers with hand drawings to computer vision technologies will be used to represent the boundaries of the Finite Element results.

5.1.2.1 Step 1 - Selection of the most accurate HyperMesh OptiStruct outcome

It is necessary to choose the most accurate output from Figure 72 in order to develop as far as possible a new method of laying the post-tensioning, which requires a sensitive approach to achieve the desired outcome.

The following figures are regrouped in pairs.
The main difference being that the blue hue has been removed from the figure on the right hand side, which corresponds to the low density contour. This differentiation assists when passing from the HyperMesh output to the new optimized layout. The red colored areas correspond to the high density contour of the Topology baseline layout, while green corresponds to the intermediate contour and white signifying the low density in the right hand model.

The two criteria ρ and p lead to two different physical interpretations.

First, to address the penalization factor effect. A fixed value of $\rho = 0.4$ is applied and the penalization factor varies from $p = 1\ to\ p = 3$. The following plots reveal a rapid increase in highly stiff required lines. In this case, the volume fraction is 40% and the presence of intermediate densities does not provide this study with enough accuracy to properly interpret, as can be observed through the presence of many small branches.

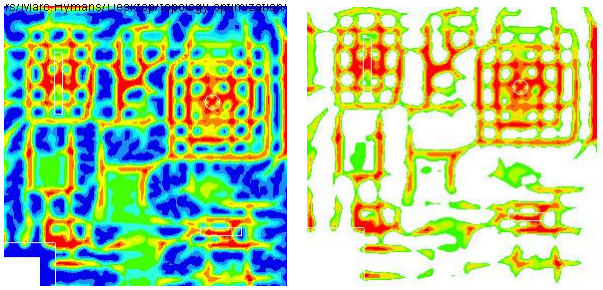

(a)

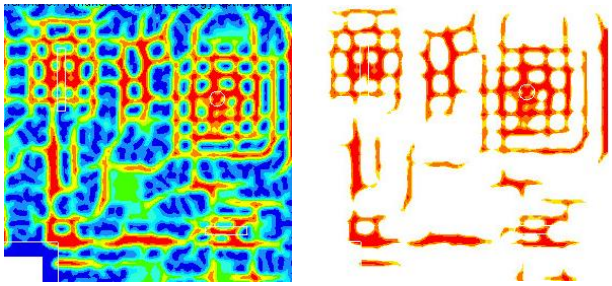

(b)

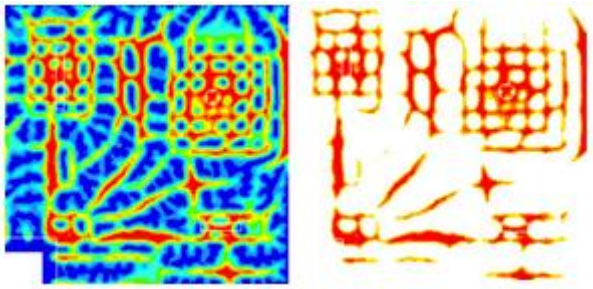

(c)

Figure 73: ρ=0,4 , (a) p= 1, (b) p = 2, (c), p = 3 (Source: author, 2015)

In Figure 74 the effects of the volume fraction can be considered. A fixed value p = 3 is applied and the volume fraction varies from $\rho = 0.5\ to\ \rho = 0.2$. 0. 5 and 0.2 representing 50 % and 20 % of the material respectively. As a matter of fact, the layout sensitivity is explored for values between 20 and 50 %.

Different volume fractions can be explored in order to view the potential load path. These volume fractions visualize the optimal material placement. The load path observed will then be used to perform the interpretation step and obtain a meaningful design. The volume fraction is therefore an important parameter to explore when generating a stiffener layout on a pressurized plate. The load path sensitivity, however, makes it difficult to determine the best possible layout as local optimums exist and their true performance remains unknown until working through the interpretation and sizing phases. However, the less material that exists, the more certain the obtained result will be.

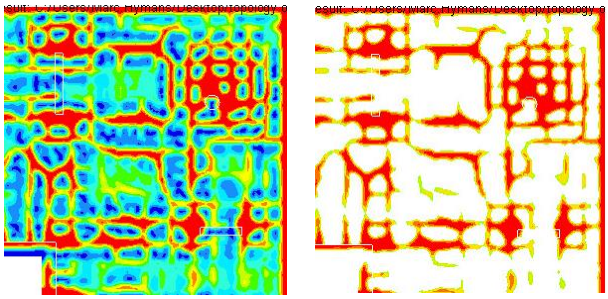

(a)

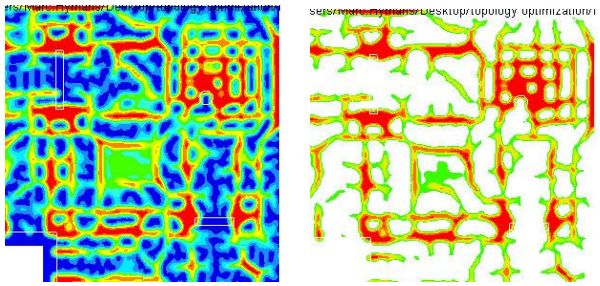

(b)

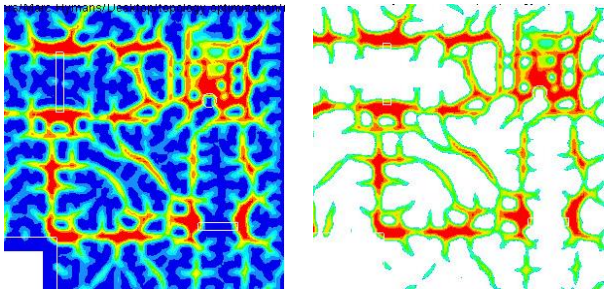

(c)

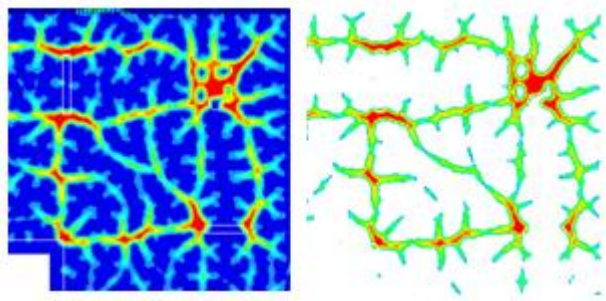

(d)

Figure 74: ρ= 3, (a) ρ=0.5, (b) ρ=0.4, (c) ρ=0.3, (d) ρ=0.2 (Source: author, 2015)

The interpretation depends entirely on the desired objective to be attained. In this case, the goal of the study aims to develop a post-tensioning layout In-Plan profile, using one of the outputs of the Topology Optimization.
To complete this goal, clear lines are required. Couple (d) of Figure displays the most clear and stiff lines, corresponding to model 14. In fact, model 14 (Figure 75) presents a desirable compromise between models 17 and 10. Model 10 contains lines, but with a low contour density, which is not required, as the higher the contour, the more stiff the load path. Model 17, being one the last discretized models, with $p = 4\ and\ \rho = 0.3$ lacks defined lines and contains too much material with 30%.
Model 14 on the other hand, where $p = 3\ and\ \rho = 0.2$, brings to the future interpretation study an excellent understanding of the concrete flat slab behavior in order to optimize as far as possible the post-tensioning layout.

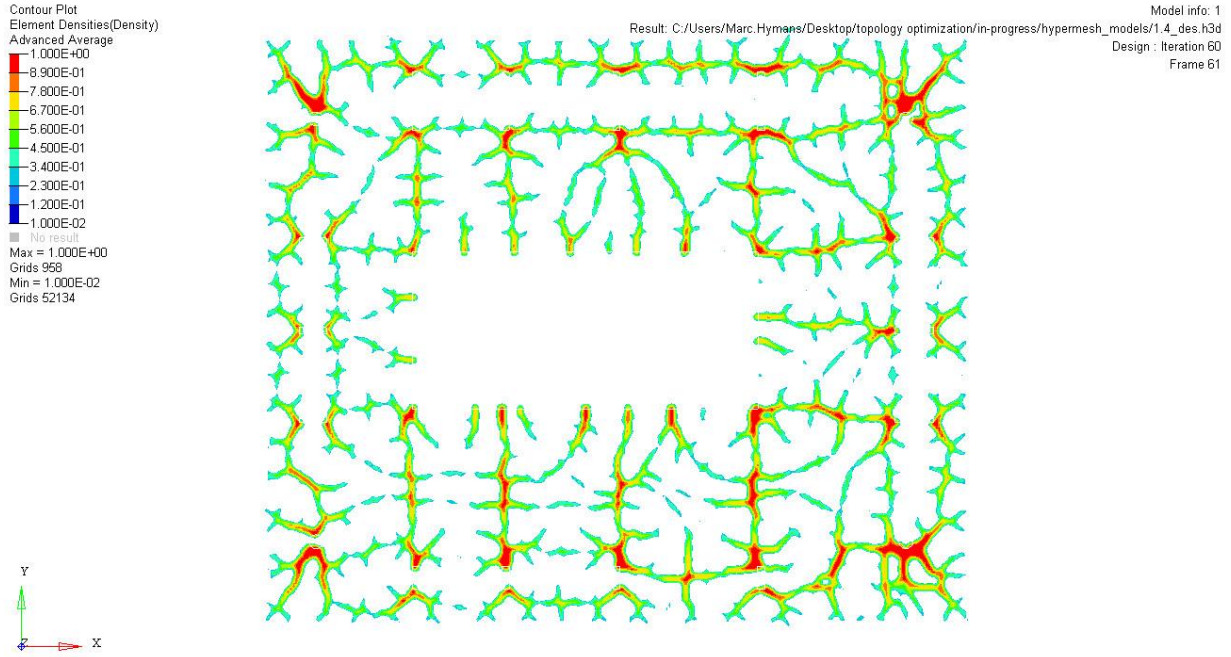

Figure 75: Selected HyperMesh output to be considered for the following analysis (Source: author, 2015)

This HyperMesh result has been attained after 60 iterations.

5.1.2.2 Step 2 - Optimization of the banded tendons

A. Interpretation of the FEM HyperMesh layout

A first remarkable aspect observed through the HyperMesh selected plot is an important concentration of stiff areas surrounding the columns. In post-tensioning concrete the banded

tendons, amongst other things, work to stiffen the slab at the localization of the columns, being located at the interface between the columns and the slab.
To avoid bending of the columns, it is in fact necessary to stiffen the slab at the localization of the columns, thanks to the banded tendons. What can be observed in the following moment's diagrams, the column moment diagram is closely related to the slab behavior.
What has therefore been done is to bring the moments into tributary areas and then distribute that moment into the drapes of the tendons.

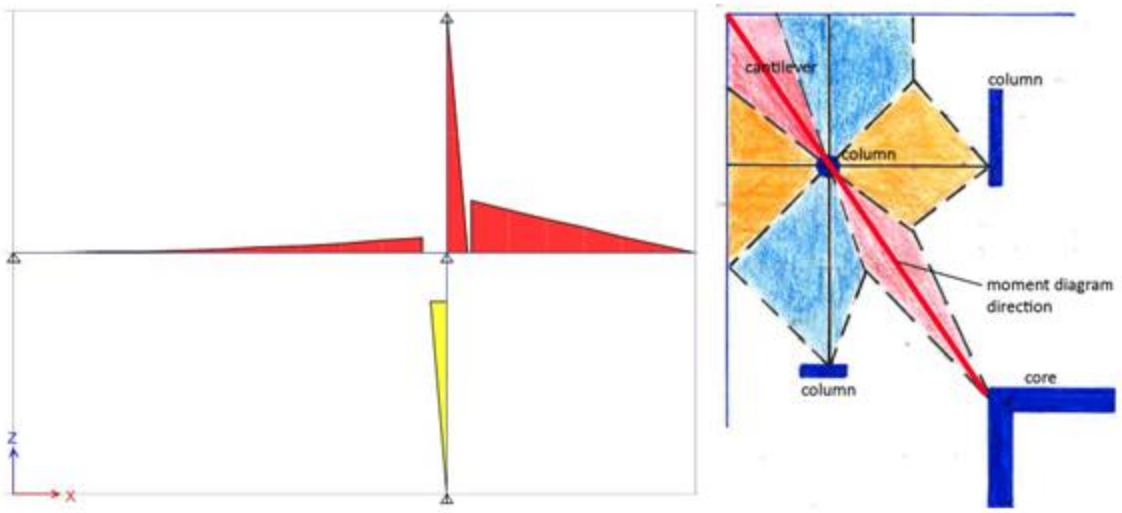

Figure 76: Tappered-column (Source: author, 2015)

This approach leads to considering the banded tendons for a first step of optimization. Not only for their particular structural status in post-tensioning but also for a practical consideration. Referring to the conventional post-tensioned layout, banded tendons are presented in a reduced quantity, with respect to the uniform ones. It is indeed interesting to first force the optimization of the banded tendons without affecting at all the uniform tendons disposition between the comparative models.

Going back to the interpretation, the presence of red lines at the columns' edges leads to split each primary tendon into two pairs of tendons. The tendons follow the top and bottom of the columns. Moreover, instead of trailing straight on the vertical, banded tendons run through the corner columns, with one reaching the slab corner, while the other one will be aligned to the horizontal columns' edges, as manually mapped out on the HyperMesh Output with the use of a trace paper.

Unlike in the conventional approach, where the banded tendon passed through the mid depth of the columns.

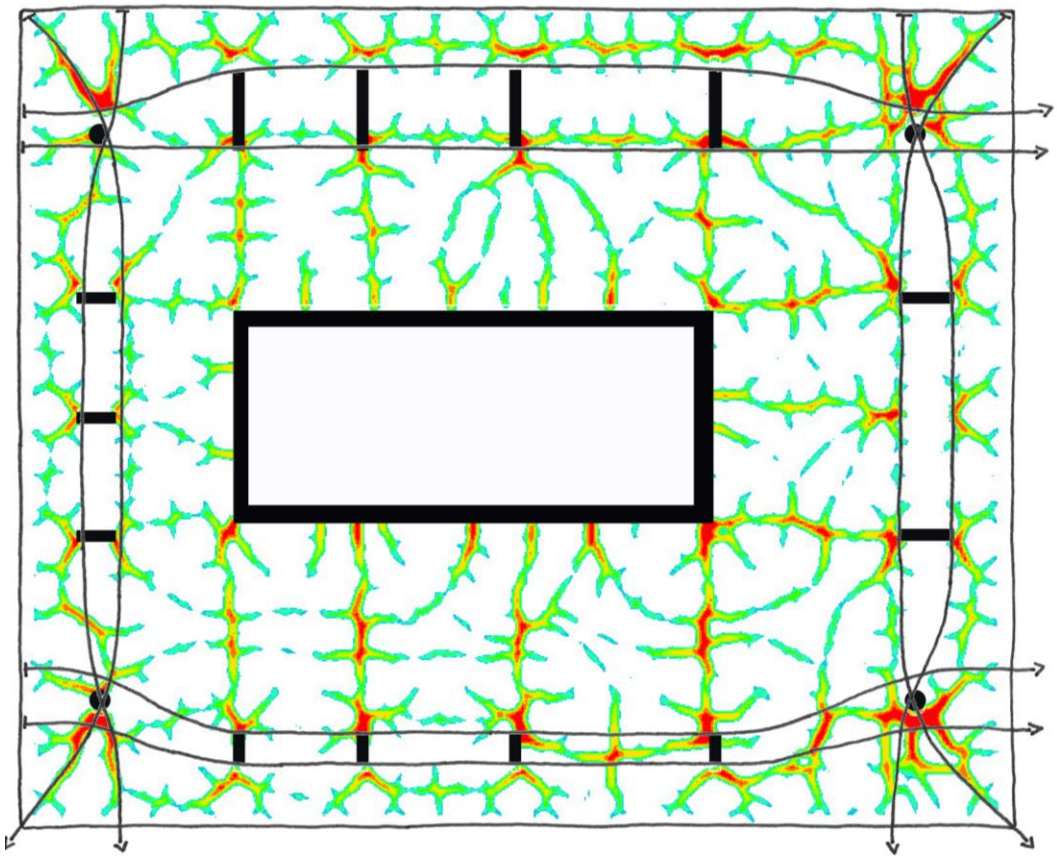

Figure 77: Interpretation of the results from the selected HyperMesh outcome: step 1 (Source: author, 2015)

The next step will be to control the efficiency of this initial optimization proceeding.

B. FEM Verification

The FEM verification consists of confirming the pertinence of the previously obtained optimized results through topology optimization. This comparison of the two post-tensioned concrete flat plates, sharing the same material characteristics, results in a different post-tensioned layout. The first model has been conventionally post-tensioned, while the second model has been obtained after the first step of optimization.

For that reason, the model will be designed in SAFE. The finite element analysis will demonstrate objectively which configuration, among the two identified, performs better.
For a solid comparison, the same long-term deflection at the edges of the two models will be required. Nevertheless, with different cable positions, in order to obtain the exact same profile deflection is impossible because the analysis is based on a finite element analysis. It is obvious that the finite element method is powerful and also versatile [27]. The deflection control with

a maximum of 0.75 inches deflected slab at the edges remains a satisfying criteria for the comparison.

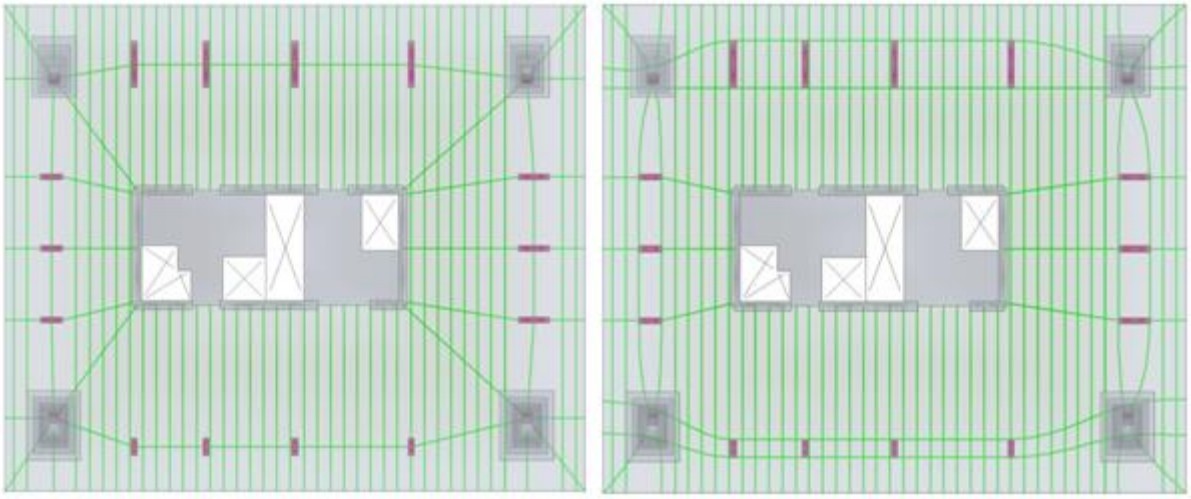

(a) (b)

Figure 78: Tendons layouts: (a) Current scheme, (b) Double-banded optimized scheme (Source: author, 2015)

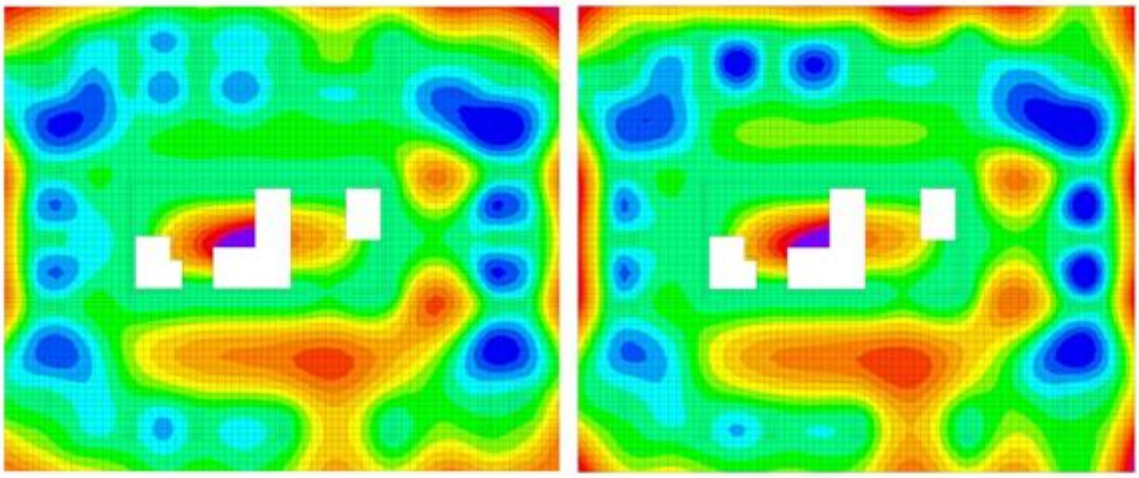

(a) (b)

Figure 79: Long-term deflection: (a) current scheme, (b) Double banded optimized scheme (Source: author, 2015)

The first observation is an approximately equal deflection, even the deflection profile is a bit more homogeneous and favorable at the edges with the optimized scheme. The deflection plot is just slightly better. As soon as the deflection profile objective is attained, a series of criteria will be used to compare the two models.

These criteria result from using the SAFE model, which allows for comparing the weight of utilized post-tensioning, checking the stresses and verifying the rebar's demand.

A. Method to evaluate the accuracy of the optimization procedure: PT Weight

The weight of post-tensioned cables placed into the concrete slab provides a quick and accurate evaluation of the pertinence of the optimization followed until now. The total weight amount of post-tensioning presented into each scheme corresponds to the weight of tendons in pounds and for each square foot. The calculation was made with excel, where the tendon's information spreadsheets are based on the tendon's properties retrieved from SAFE: the tendon's length, the amount of strands to form a tendon or a group of tendons and the tendon's geometrical characteristics with its respective diameter (= $\emptyset = 0.5$ " for all the tendons).

TABLE: Object Geometry - Tendons 03 - Vertical Profile

Tendon	SpanLabel	SpanType	L
Text	Text	Text	In
2	Left Cantilever	Linear	190,4998
2	Span 1	Reverse Parabola	275,6258
2	Span 2	Reverse Parabola	375,392
2	Span 3	Reverse Parabola	283,4829
2	Span 4	Reverse Parabola	182,9995
3	Span 5	Reverse Parabola	159,0002
3	Right Cantilever	Linear	338,4347

(a)

TABLE: Tendon Property Assignments

Tendon	TendonProp	NumStrands	BondType
Text	Text	Unitless	Text
2	0.5" Tendon	3	Unbonded
3	0.5" Tendon	3	Unbonded
4	0.5" Tendon	3	Unbonded
5	0.5" Tendon	8	Unbonded
6	0.5" Tendon	3	Unbonded
7	0.5" Tendon	3	Unbonded
8	0.5" Tendon	3	Unbonded
9	0.5" Tendon	3	Unbonded
10	0.5" Tendon	3	Unbonded

(b)

Table 6: PT weight calculation method: (a) tendons lengths, (b) tendons diameters (Source: author, 2015)

With the help of the builder companies notices to obtain the weight of a commercial tendon, the total weight of cables using into the slab can be easily defined. Which is for example, in the case of the second scheme: 0.84lbs/ft2

Area	14170	Total	11905,4 lbs
Tendon Wt.	0,53	Wt/Area	0,84

Row Labels	Sum of L	Num. Tendons	Weight of Tendons
10	1308,00	3	173,3
105	1308,00	3	173,3
106	1308,00	3	173,3
11	1308,00	3	173,3
12	1308,00	3	173,3
13	1308,00	3	173,3
14	497,43	3	65,9
15	497,43	3	65,9

Table 7: PT weight calculation method: Final result (Source: author, 2015)

The comparison between the two schemes: the conventional and the optimized/double-banded ones would be as following:

- Scheme 1 = Conventional Scheme: $\omega_{PT} = 0.88$ psf
- Scheme 2 = Double banded Optimized Scheme: $\omega_{PT} = 0.84$ psf

The optimization procedure leads to a post-tensioning saving of 4.5 % per slab. It is not negligible, but not completely relevant. In fact, the optimization procedure is time consuming, which translates to more calculations and design process for the engineer. This extra work will definitely result in an increase of the design cost. To be efficient, the PT weight saving resulting from the optimization would have to be of a larger percentage than 4.5%.

5.1.2.3 Step 3 - Enhancing the banded tendons optimization procedure

A. FEM trial and error corner's study

The previous results obtained through step 1 did not entirely justify the advantage of performing a topology optimization. These results could be the consequence of an incorrect interpretation of the outcomes obtained through the topology optimization SIMP method.
The different steps of topology optimization interpretation will help to build, due to a trial and error procedure, a rule to translate the topology optimization results up to the most optimal post-tensioning layout.

Moreover, one particular difficulty of the structure in this project is the presence of large cantilevers located at the slab corners.
This step will focus on the corners to optimize as far as possible the cable distribution in this particular location, i.e. to treat only the tendon part located between the column and the slab edge, which is the segment dealing with the cantilever.
Each cantilever tendon is split in two, imposing a distributing rule to reach an equal span between the tendon anchorage positions. This approach has been taken in order to once again attempt to translate the HyperMesh selected outcome (Figure 89).

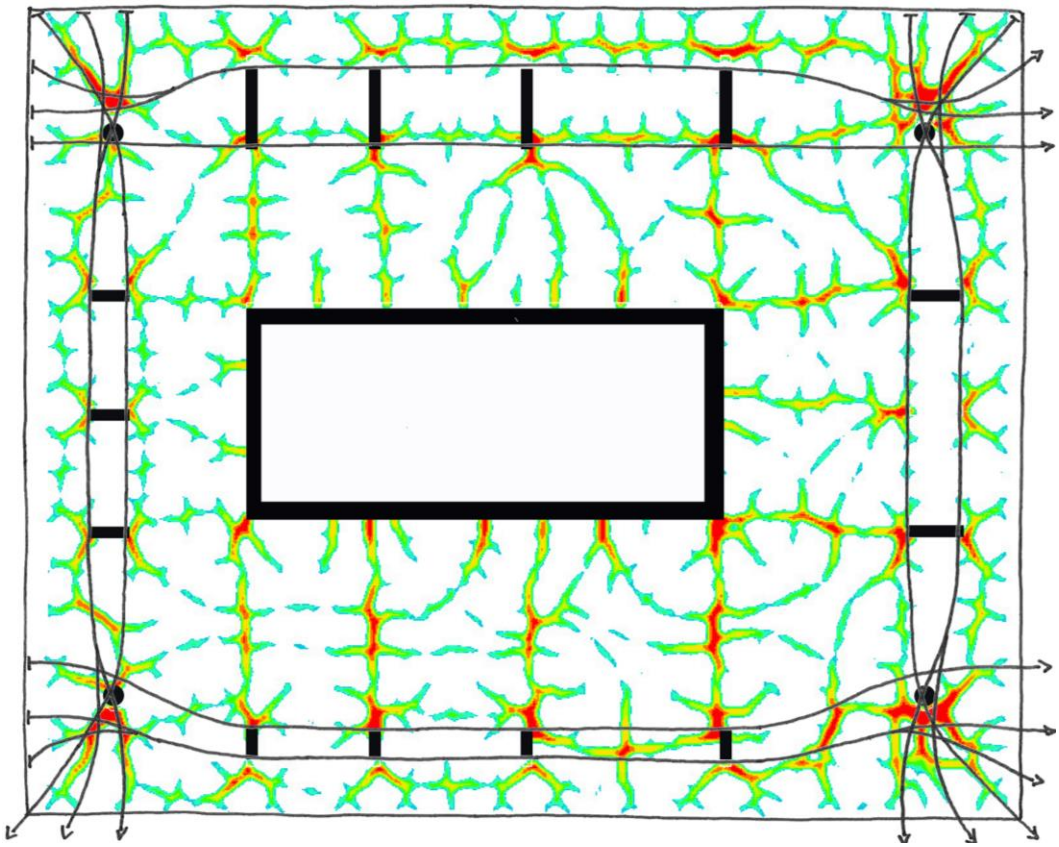

Figure 80: HyperMesh outcome: Enhancing the interpretation methods at the critical zones, the cantilevers (Source: author, 2016)

This step will utilize the finite element method as a trial and error tool with manual increments to reach the final expected deflection result by focusing on the corner deflections maximums. Each FEM model will have the exact same characteristics (number of tendons, materials, loads, etc).

A comparison will then be made between the different models to confirm the accuracy of this optimization step.

Model 1: $\Delta = 0.74\ inches$

Model 2: $\Delta = 0.60\ inches$

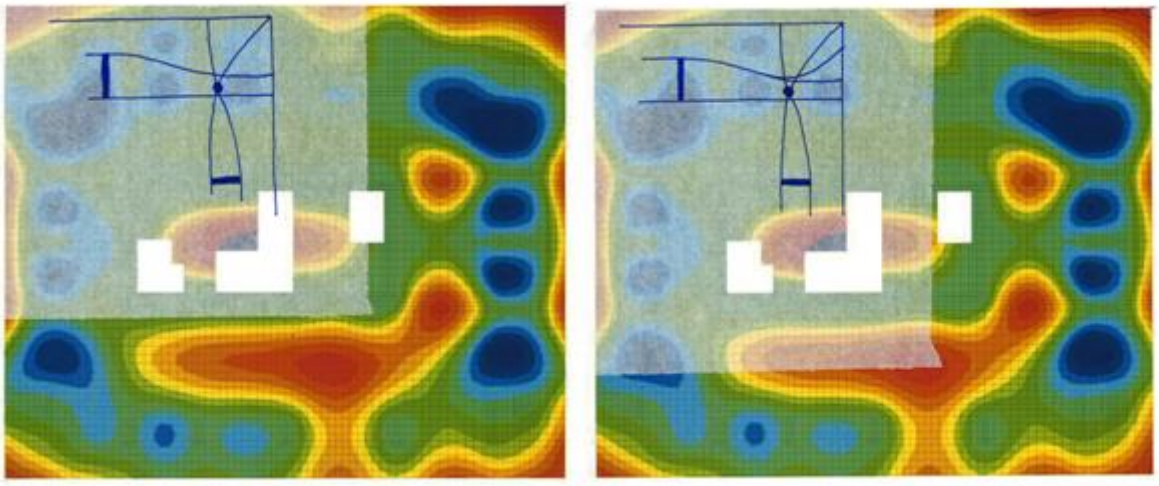

(a) (b)

Figure 81: Tappered-column (Source: author, 2016)

Model 3: $\Delta = 0.44\ inches$

Model 4: $\Delta = 0.45\ inches$

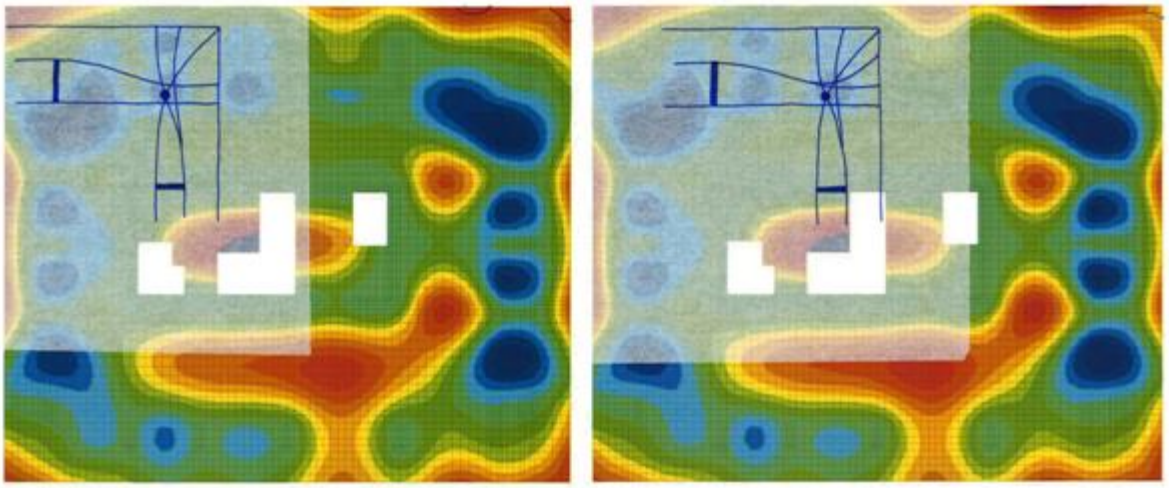

(a) (b)

Figure 82: Tappered-column (Source: author, 2016)

The result is improving, going from a deflection value of 0.74 inches in model 1 up to 0.45 inches for model 4. This result demonstrates that splitting the tendons makes sense. The inquiry raises a question about whether the investigation in step 1, i.e. to double band the tendons, improved the new optimized layout. The analysis conducted in models 5 to 8 will investigate this question further.

Model 5: $\Delta = 1.65\ inches$ Model 6: $\Delta = 0.81\ inches$

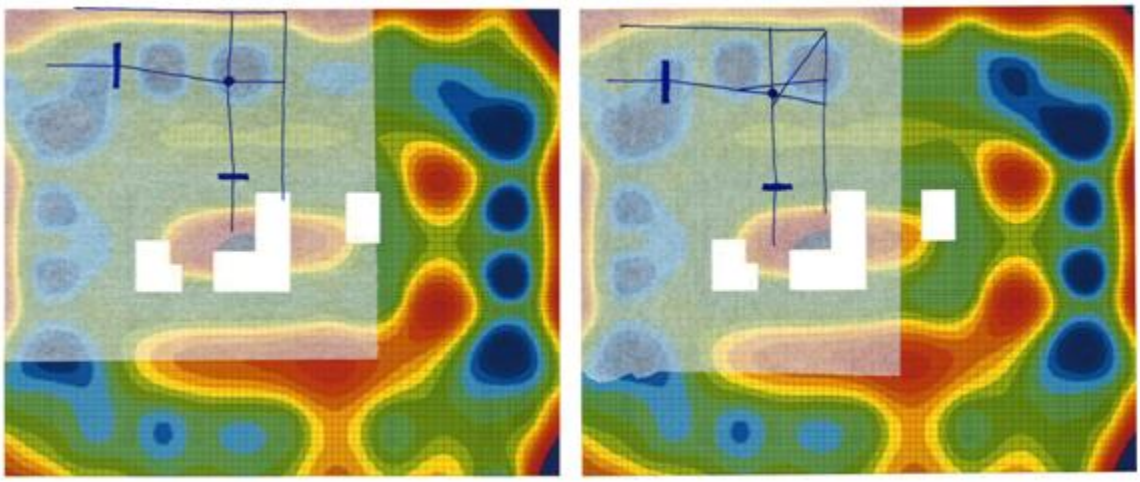

(a) (b)

Figure 83: Tappered-column (Source: author, 2016)

Model 7: $\Delta = 0.78\ inches$ Model 8: $\Delta = 0.74 inches$

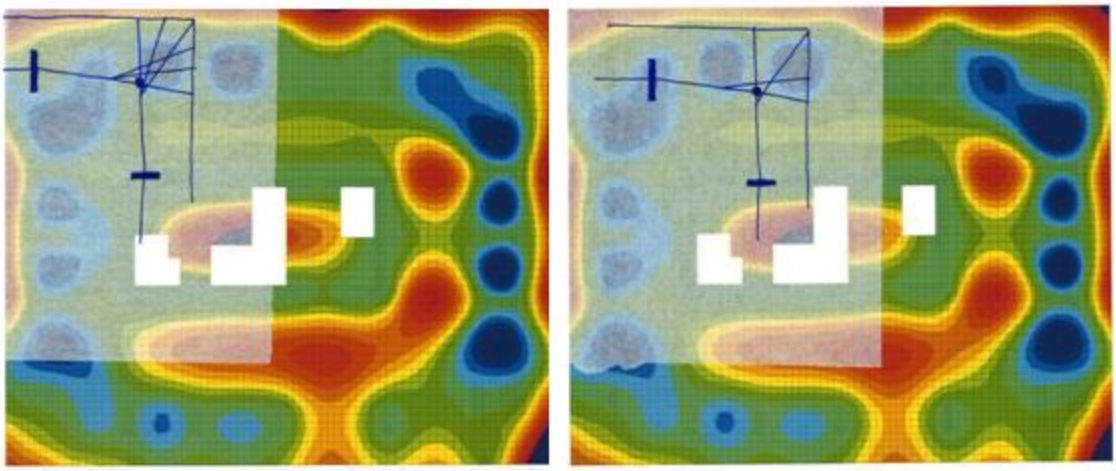

(a) (b)

Figure 84: Tappered-column (Source: author, 2016)

This „artisanal" FEM procedure helps us to demonstrate the necessity to combine double banded and split tendons to find the most optimal deflection values.

B. FEM Verification

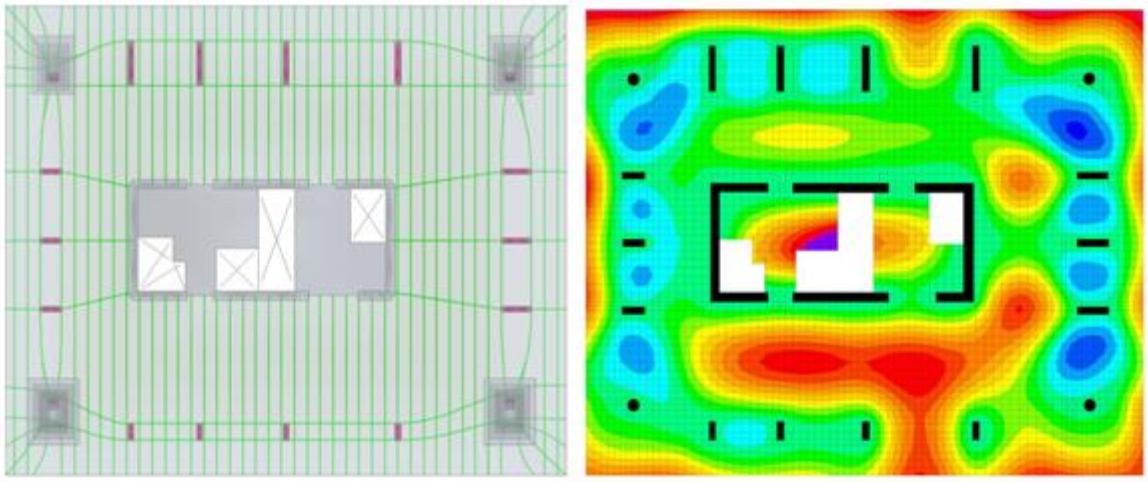

(a) (b)

Figure 85: Tappered-column (Source: author, 2016)

The finite element analysis conducted with SAFE again allows to plot the long-term deflection profile.
The deflection profile is much more regular with less uplift observed. An homogeneous deflection profile is especially desired when designing a residence building. In fact, the issue of irregularity of loads becomes more significant in the case of residential buildings than for office buildings.
An important increase of strongly non-symmetric changeable loads would definitely increase stresses more dramatically in some parts of the floor system. Stress creep also increases in displacement under stress. In the case of high-rise programs this problem could develop structural irregularities resulting in serious concerns and a larger cracking of the slab.

Additionally, there is an important decrease in the amount of PT required.

The weight of post-tensioning per square foot $\omega_{PT} = 0.68$ psf as opposed to $\omega_{PT} = 0.88$ psf obtained through the first step of optimization.

5.1.2.4 Step 4 – Optimization of the entire post-tensioned layout: Banded + Uniform tendons

The objective of the third step is to be as experimental as possible.
The building restrictions (awkward layout to build) as per the code´s restrictions (max permissible curvature for tensile forces losses) will not be taken into consideration, because the objective will be to optimize as far as possible the post-tension layout.

A. Interpretation of the FEM HyperMesh layout

Curved lines appear on the HyperMesh outcome. The model allows for shortening the span between the core and the columns. These lines grant the point of departure for the new optimization step.

The rules to distribute the tendons satisfy the following criteria:

- To follow the branches of the HyperMesh output without making any distinction between the line colors (strong red, orange, green). The color intensity will provide information on the number of tendons to assign to each pair of tendons.
- To pass through the column edge and then reach the slab edge
- The spacing between two columns must be divided by three

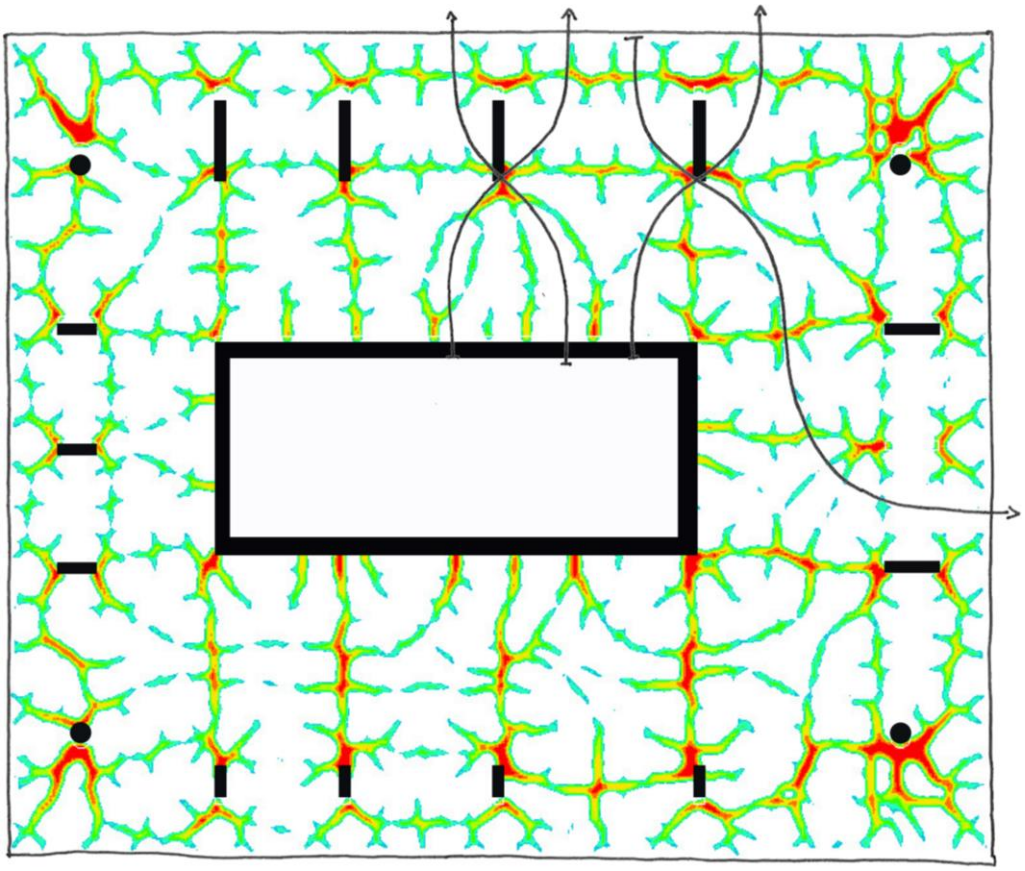

Figure 86: Tappered-column (Source: author, 2016)

The result obtained, as opposed to the two first schemes, comprises both banded and uniform tendons, a post-tensioned scheme with only banded tendons. This scheme was quickly named the biomimicry scheme in order to traduce its truly organic shape (Figure 87).

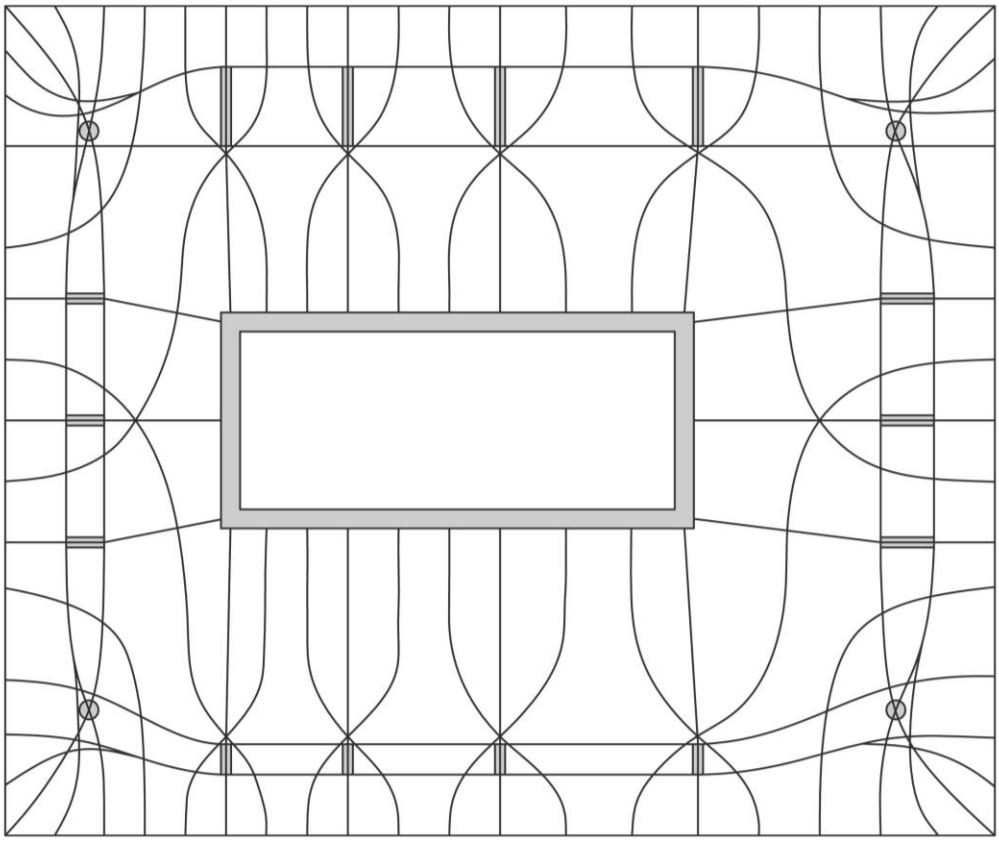

Figure 87: Only banded scheme drawing (Source: author, 2016)

This optimal layout recalls the ribbed concrete floor slab systems of Pier Luigi Nervi, developed for example in the floor system of the Gatti wood factor. He relied on theoretical calculations developed along with Arcangeli to determine the isostatics of principal moments.

B. FEM Verification

Once again, for the finite element control the banded locations are brought into SAFE. The deflection of the 2 first schemes is enhanced at its maximum in order to be as close as possible to scheme 3, which is in the end impossible.

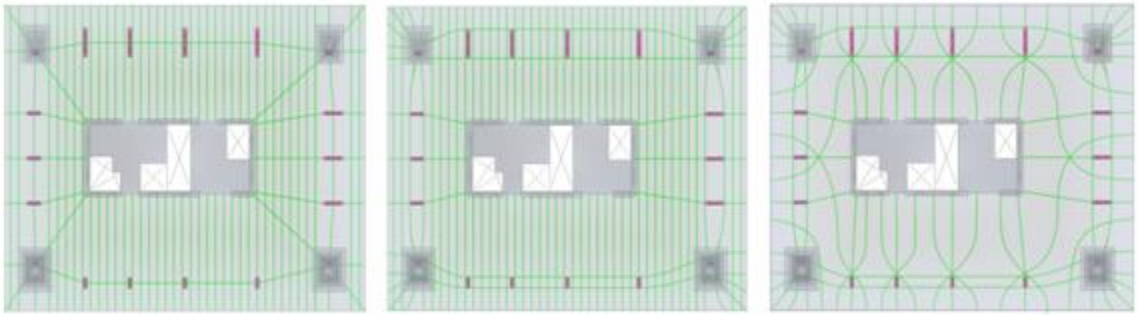

(a) (b) (c)

Figure 88: Tappered-column (Source: author, 2016)

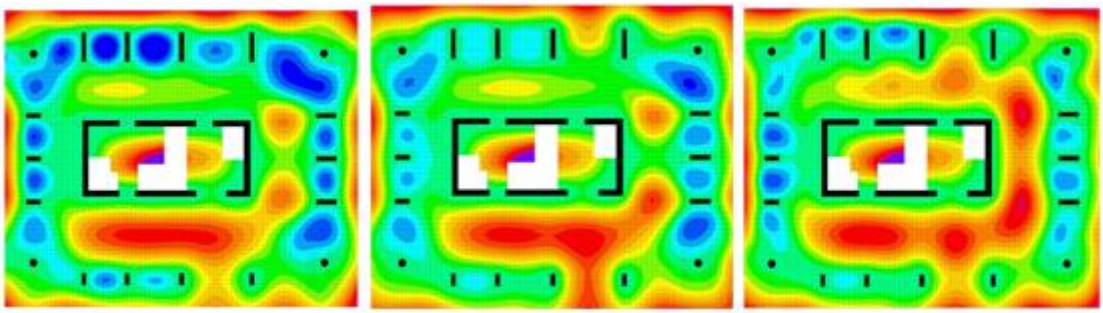

(a) (b) (c)

Figure 89: Tappered-column (Source: me, 2016)

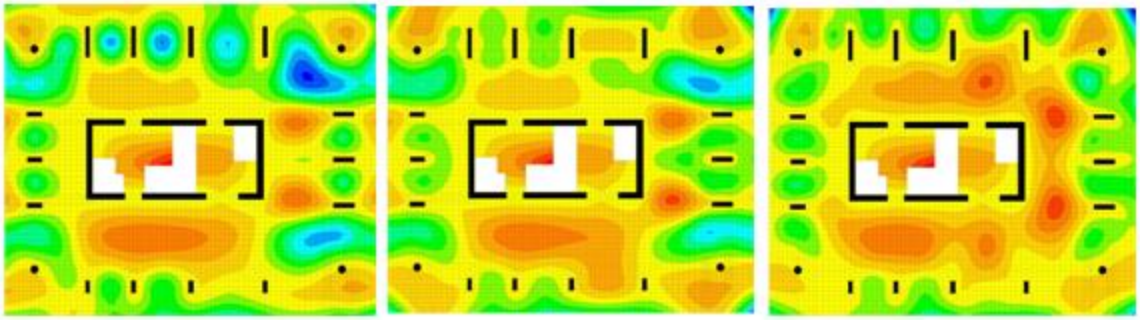

(a) (b) (c)

Figure 90: Tappered-column (Source: author, 2016)

The maximum acceptable deflection value in the long-term is $\Delta_{LT} = 0.75\ inches$ and the instantaneous deflection, with the load combination SW + PT, is $\Delta_{LT} = 0.125\ inches$.

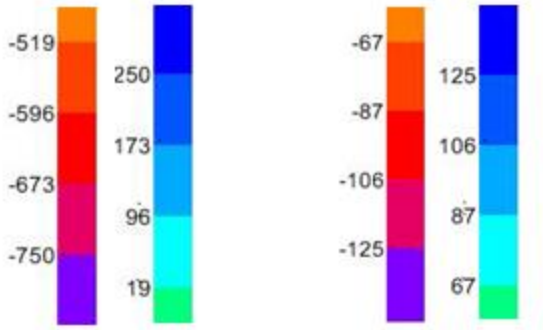

(a) (b)

Figure 91: Colors indications for deflections values, on the left hand side the max permissible deflection and on the right the max admissible uplift: (a) Long-term deflection, (b) Initial deflection (Source: author, 2016)

5.1.3 Comparison between the three schemes: conventional, double banded and only banded schemes

5.1.3.1 PT Weight

A comparison between the conventional scheme, the double banded optimized scheme and the only banded optimized scheme is conducted.

	Scheme 1	Scheme 2	Scheme 3
PT Weight	0.80 psf	0.68 psf	0.58 psf
		15 % PT SAVINGS	**28 % PT SAVINGS**

Table 8: PT weight comparison between the 3 schemes (Source: author, 2016)

The third scheme provides an excellent result. 28% of savings for each slab means this optimization promises much in terms of future feasibility of building. These initial savings will be followed by a series of additional savings, primarily on the column size and the foundations.

However, though such positive performances are attained, these results must be validated through additional verifications.

5.1.3.2 Check of Stresses

This part refers directly to the recommendations made in chapter 2.8.2.2. B, according to ACI 318-08.

The objective is not to conduct a precise study of the stresses check, but it must ultimately verify that the two optimized models do not find their stress values increasing highly, i.e. those of models 2 and 3, and in order to demonstrate that even when optimized, the concrete post-tensioned slab behavior continues to behave following the expectations of the codes.

The verification will be made of the long-term for the principal deflection profile study, and the following values will be brought into the FEM model.

At Total service limit state:

Top and Bottom fiber tensile stresses $\leq 6\sqrt{f_{ci}'}$

Extreme fiber compressive stress $\leq 0.6\sqrt{f_{ci}'}$

The red hue indicates values exceeding the code requirements. The result is not worrying as an increase in the concentration of stresses can be explained through the tendon profiles having not been adjusted in this first In-Plan study.

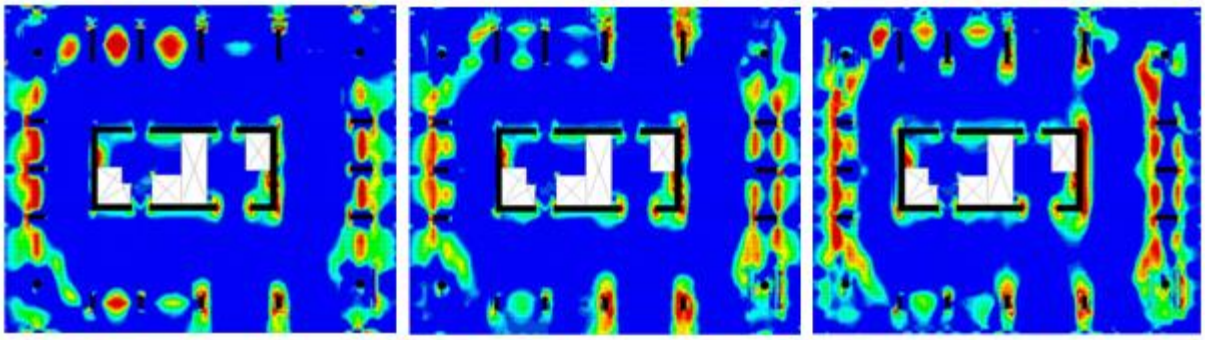

(a) (b) (c)

Figure 92: Top Stresses demands in direction 1/ along x: (a) current scheme, (b) Double banded optimized scheme, (c) Only banded optimized scheme (Source: author, 2016)

On the top slab a strong difference between the three schemes cannot be observed. Scheme 2 presents better results. What can be found in scheme 1 is a high concentration of stresses between the columns which is more disturbing than in scheme 3. In fact, a high concentration of the stresses at the support locations could develop into small fissures and a long term weakening of the entire structure.

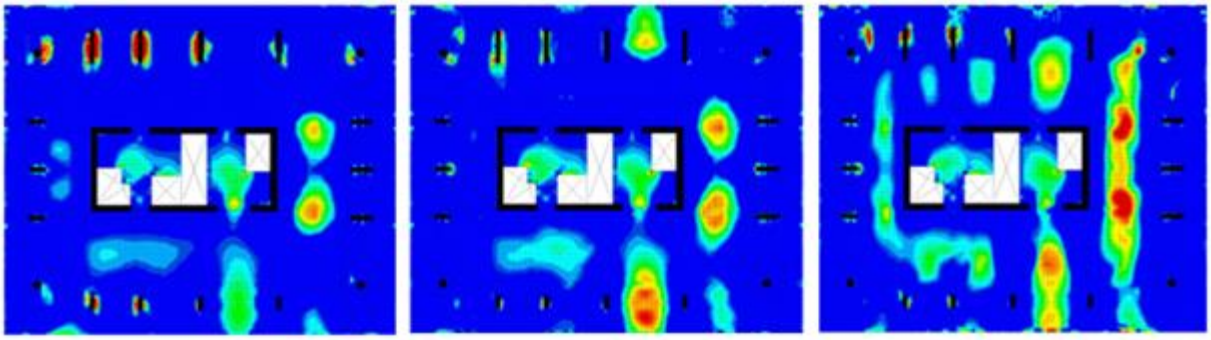

(a) (b) (c)

Figure 93: Bottom Stresses demands in direction 1/ along x: (a) current scheme, (b) Double banded optimized scheme, (c) Only banded optimized scheme (Source: author, 2016)

The bottom plot reveals an increase of stresses at the mid span, resulting from a small amount of post-tensioning tendons. This result could be due to rebar or adjusting the tendon profiles.

The stresses verification shows that the optimization does not really affect the post-tensioned slab behavior in a major way, a promising result in terms of the optimization procedure.

5.1.3.3 Quantity of rebars: Calculation by self-developed code

Post-tensioning offers direct cost reduction over conventionally reinforced slabs primarily by reducing concrete and rebar material quantities as well as rebar installation labor. A post-tensioned slab will have substantially less rebar than a conventional system, which is one of the main causes of an economic benefit.

It is required to evaluate the amount of rebar, because if we can experience significant savings through post-tensioning, this amount has to be confirmed by a non-increasing quantity of rebar. This measure holds true especially for the third scheme where the absence of distributed tendons to balance the gravity loads could produce a large increase of rebar in the bottom part of the slab.

A minimum amount of rebar/bonded reinforcement is required in the negative moment regions of the slab at the column supports (section 18.9.3.3 of ACI 318-08) and in the positive moment regions at the midspan of the extreme tensile stress in the concrete when service loads exceed $2\sqrt{f_c'}$ (section 18.9.3.2 of ACI 318-08) [1]. Defining the amount of rebar in a slab is a long calculation procedure, and not the aim of the study.

A methodology to quickly evaluate the amount required for the slab has yet to be found. For that purpose, a MatLab code has been written. From SAFE, it is possible to plot the density of the rebar demand, having as a maximum #4 bars with a 12” space (Figure 94).

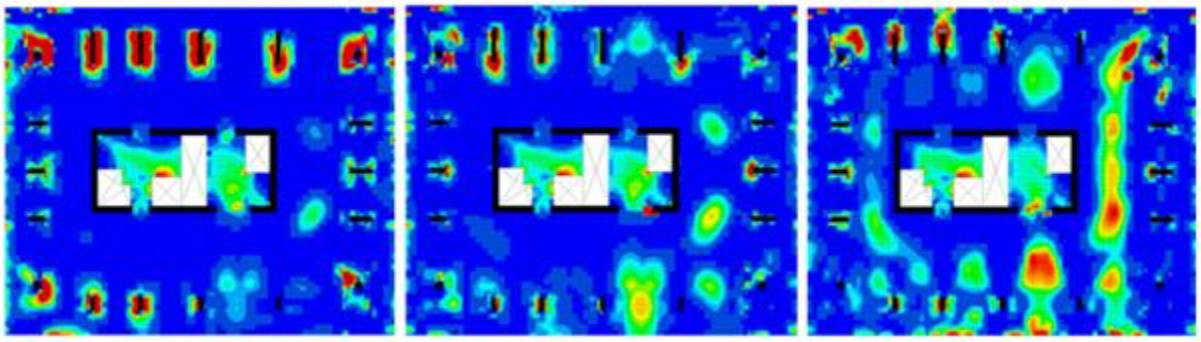

(a) (b) (c)

Figure 94: Bottom Rebars demands in direction 1/ along x: (a) current scheme, (b) Double banded optimized scheme, (c) Only banded optimized scheme (Source: author, 2016)

The MatLab code developed for this purpose reported Appendix 3 converts the jpeg plots with RGB colors into three separate matrices to define the colors range. The objective is to calculate the red, i.e. to cancel the blue and the other colors, so as to count those that will not be taken into account (count=0).
The loop is repeated for each pixel of the plot. As an exit value, the code gives a red color ratio for the three schemes to compare, in summing for each scheme the proper amount of red and then dividing it by the total amount of red. The red color corresponds to the value exceeding the #4 bars. The higher the red ratio is important as the less the post-tensioned performs well.

		Scheme 1	Scheme 2	Scheme 3
Direction 1	Top Bars	3.11 %	1.85 %	3.4 %
Direction 2	Top Bars	2.46 %	1.55 %	2.78 %
Direction 1	Bottom Bars	1.89 %	0.36 %	0.67 %
Direction 2	Bottom Bars	1.49 %	1.03 %	0.9 %
	Total	8.95 %	4.79 %	7.75 %
			40 % SAVINGS	**14 % SAVINGS**

Table 9: Rebars ratio (Source: author, 2016)

What can be observed is a large savings with the two optimized schemes. Nevertheless, there are better savings with the second scheme, which can be explained by the fact the profiles are not accurate nor adapted to each tendon layout. It will be important to confirm these results to understand what the optimal tendon profiles are.

5.1.4 Consolidation of the methodology

As soon as the third optimized scheme might produce some desired results in terms of post-tensioning savings, the next steps could be taken. However, this would require around 28% of the tendons weight by slab without any increase of the rebar consumption with respect to the conventional scheme and, at the contrary of some savings, also verify the codes' restrictions of the stresses. The next step would be go from a very experimental optimized scheme to a more realistic an optimized scheme in terms of the ACI codes requirements. Of course, this would have to be done without losing any benefits from the tendons weight savings.

One of the important parameters to enhance in the third scheme would be the tendons curvatures. One advantage of post-tensioning is the possibility of the post-tensioning reinforcement to be placed in horizontal curves. An excess in the tendons curvatures, however, would have multiple impacts:

1) To strongly increase the losses
2) To expand the amount of hairpins demand
3) Lack of improper use of the curvatures can result in cracking or concrete failure, particularly at slabs openings [2]

To counteract point 1), a parameter would need to be imposed into the optimization procedure, which will take into account the friction losses code requirements (ACI-318_08: 18.6.2):

$$P_{px} = P_{pj}\, e^{-(K\, l_{px} + \mu_\rho\, \alpha_{px})}$$

Concerning point 2) and the hairpins demand, a quick verification can be made thanks to the SAFE model.
As for the rebars, the hairpins demand can be extracted as a color plot (Figure 95):

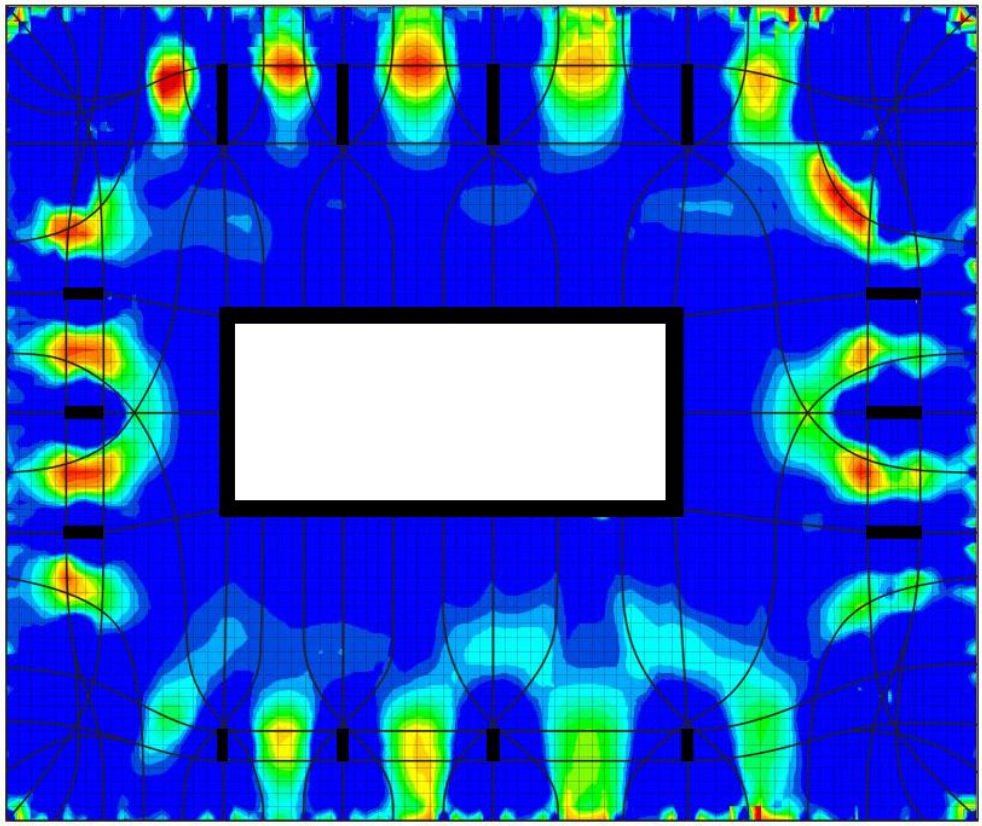

Figure 95: Hairpins demand (Source: author, 2016)

The red color here corresponds to the value exceeding the codes requirements:

$$\sigma_{rupture} = 7.5\ {f_{ci}}' = 503\ psi$$

All the values which are exceeding $\sigma_{rupture}$ concern the locations in the slab where hairpins are required, i.e. in the red zones. As in Figure 95, the post-tensioning layout is superimposed on the hairpins plot demand, helping to confirm the accuracy of the FEM analysis and the demand of hairpins matching the high curvatures.
This step makes sense as the curve moves along the tendon the more you produce excessive compression axial stresses into the slab (Figure 96).

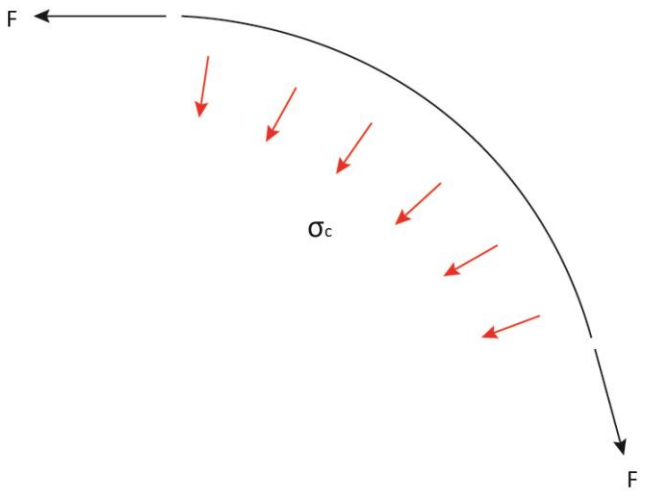

Figure 96: Compression axial stresses (Source: author, 2016)

For example, the amount of hairpins required for the tendon on the high right hand side, with a high red plot value, would require the placement of 12 supplementary hairpins compared to the normal requirement.
The length of the tendon affected by the red color being 44”/12” (spacing between two hairpins) = 12 hairpins to ad (Figure).
#3 hairpins at 12 inches on-center for each should be installed, transferring the horizontal radial force via the hairpin reinforcing the concrete.

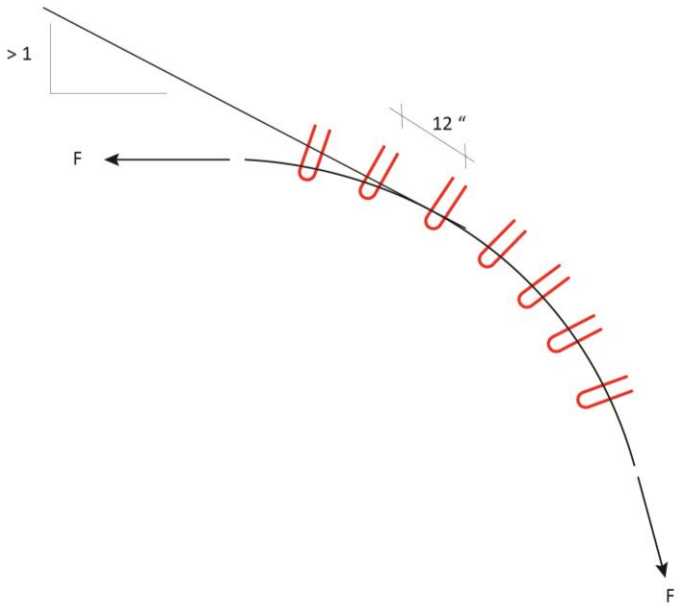

Figure 97: ACI codes requirements for hairpins disposition (Source: author, 2016)

This awareness would contribute to also develop a parameter which limits the hairpins demand.

5.2 Profiles Study

5.2.1 Force Density Method

The applied model to be now considered will be the optimized post-tensioning layout, found through the previous In-Plan study.
Following the new disposition of the tendons into the concrete slab, the objective will consist of defining the most optimal tendon profiles in order to again minimize the weight of post-tensioning the slab.
The goal is also to distribute the tendons height so that the deflection profile becomes much more homogeneous if not optimal and adapted to the required design, i.e. the engineer could request the design he thinks to be the most appropriate to its particular building use.

Force Density Method seems to be an interesting and potential methodology to use. The ratio between the length of the cable and the maximum deflected point allows to also define the tensile stresses inside the cables.

$$q = \frac{F}{L};\ F = q.L$$

However, applying Force Density to this geometry will be a hard task and first a methodology must be determined to understand how Force Density will interact with the case study model.

To describe the tendons profiles as precisely as possible, each tendon will have to be divided into x number of points (Figure 98). This division is assumed for practical considerations, i.e. each node will be connected respectively to the other node with a line/branch of 3 feet length.

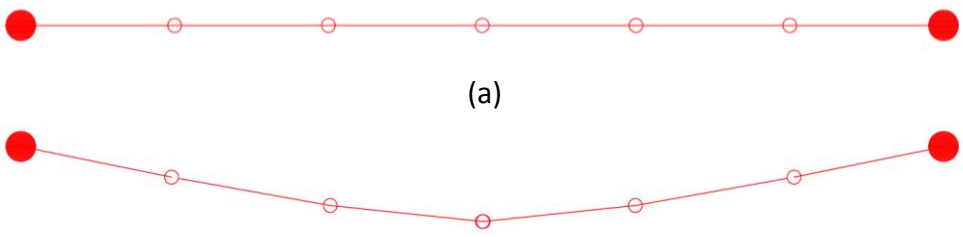

(a)

(b)

Figure 98: tendon discretized in an x number of nodes: (a) Shape before the loads application, (b) deformed shape (Source: author, 2016)

This procedure will be done on a CAD file, i.e. the new In-Plan PT layout will be completely drawn on Autocad, with as many branches as the number of nodes.

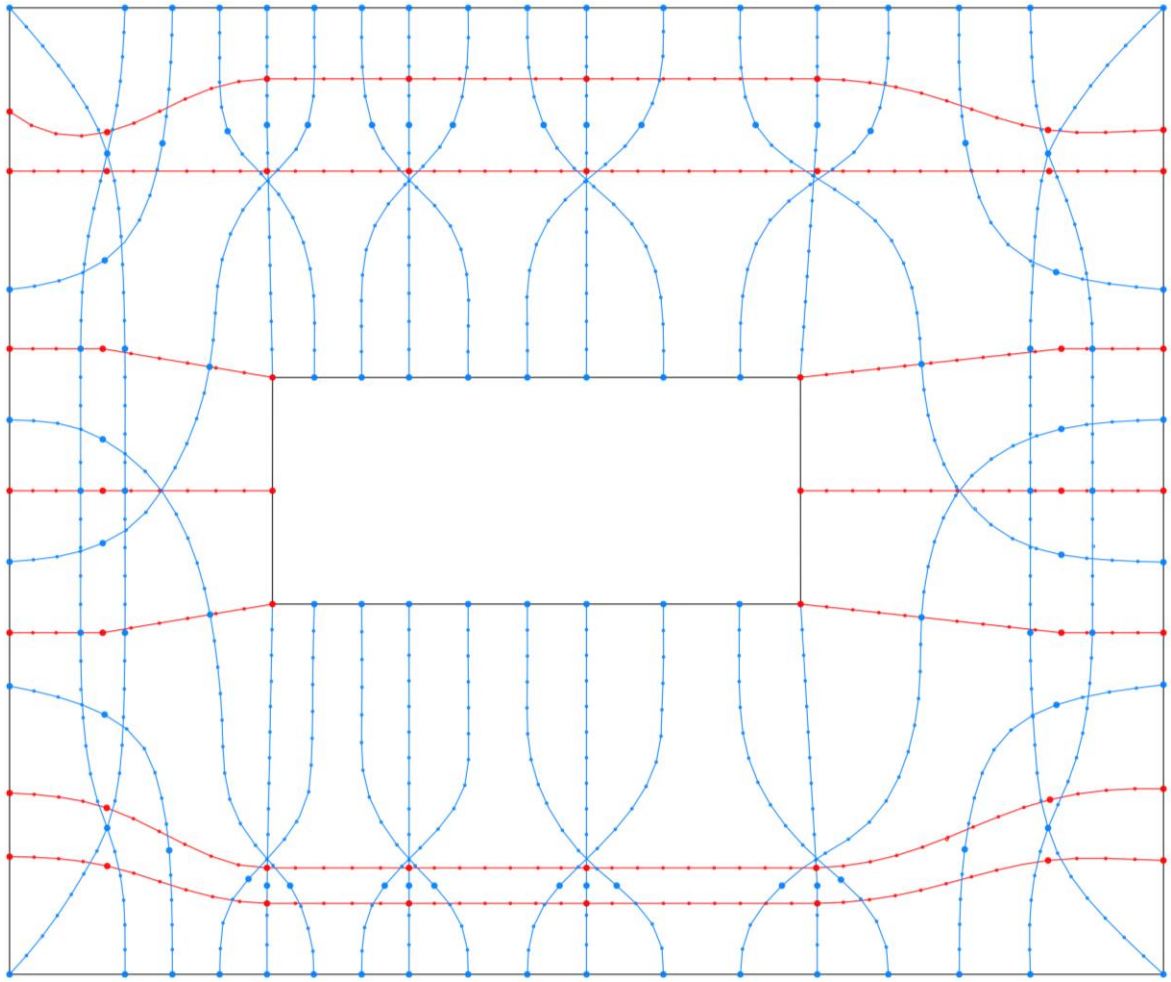

Figure 99: Post-tensioning layout discretized on a CAD file in nodes and bars, underlining of the supports (Source: author, 2016)

One of the first difficulties is to define the tributary loads in order to then apply the tributary load values to each nodal element. It is quite impossible to determine the tributary areas by a hand calculation due to the complexity of the geometries.

The procedure is as follows:

- Use the Altair program, the same used for the In - Plan optimization procedure.
- Import first the dxf file with the optimized layout divided in branches (Figure 99)
- Generate a mesh (15 inches is reasonable)
- Ensure the mesh passes through the nodes (Figure 100)

As soon as the layout is correctly meshed, the next difficulty to tackle deals with a software issue, i.e. to find a way to pass from HyperMesh to a dxf file. In fact, to apply Force Density will require importing the required Force Density software into a dxf file.

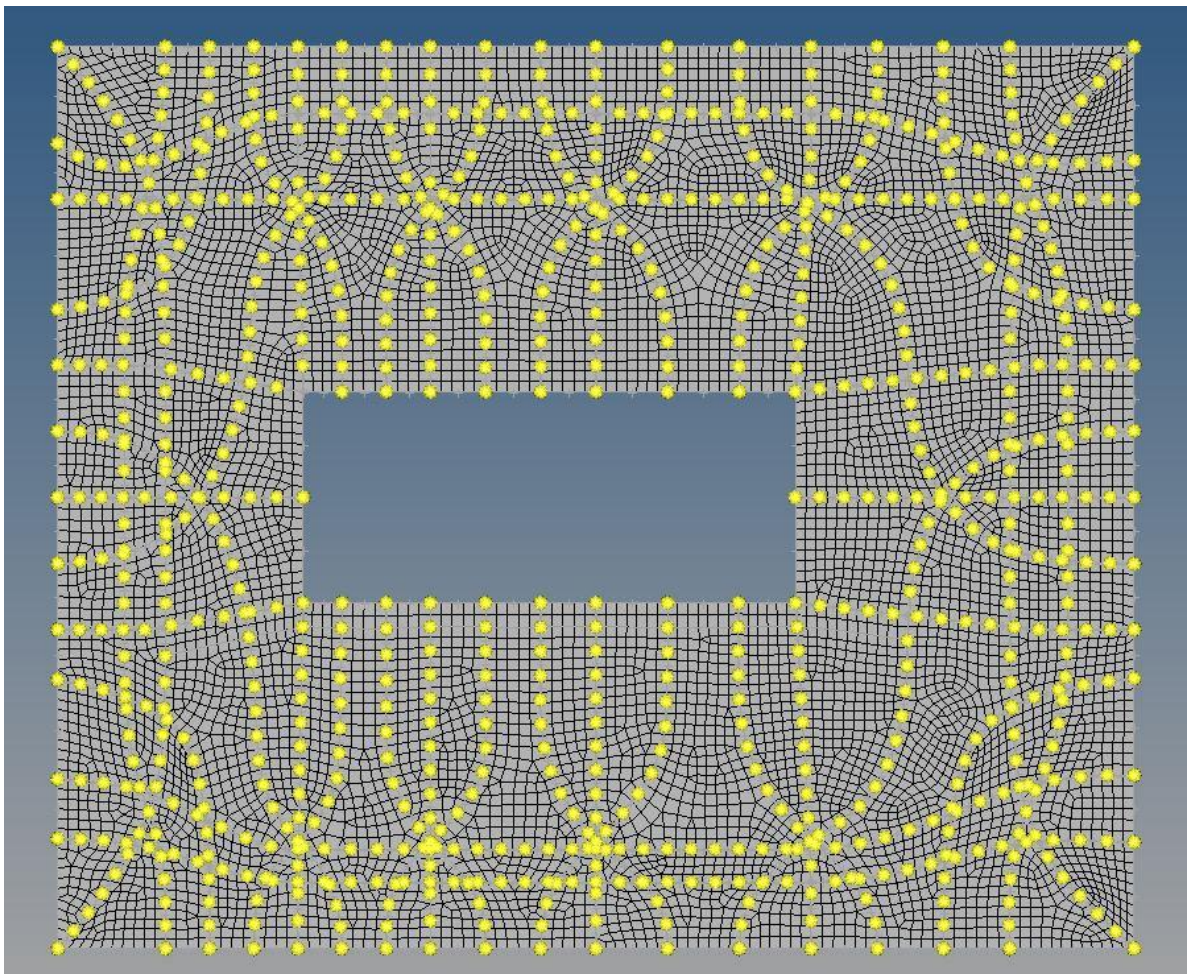

Figure 100: Mesh generation on HyperMesh (Source: author, 2016)

A possible method to pass from hypermesh to a dxf file is:

- Export the file in Nastran .dat
- Open the file on strand
- Ensure the mesh is correct/contains no error, in running an analysis (this is very important)
- Finally, export the file in dxf

The entire following procedure will be realized on the S-Frame software. The strategy to find the final tributary loads for each node proceeds as follows:

- Apply to each node a support, blocked in the three directions, x=y=z= 0 (Figure 101)
-

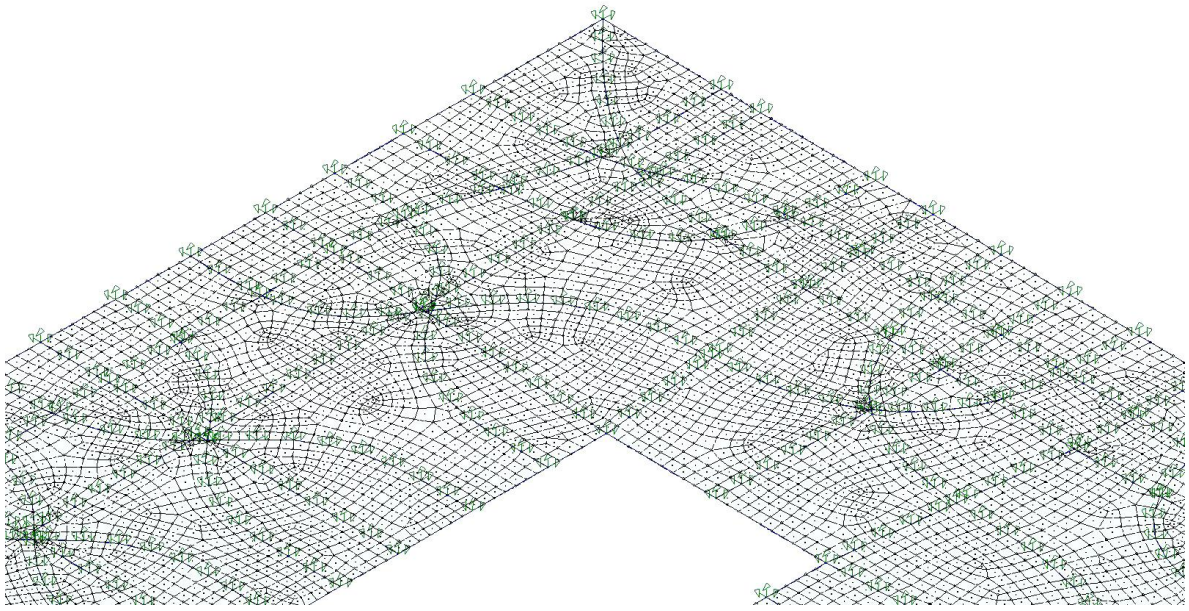

Figure 101: Nodes with their respective applied supports (Source: author, 2016)

- Apply uniform gravity loads to the entire plate (Figure 102)

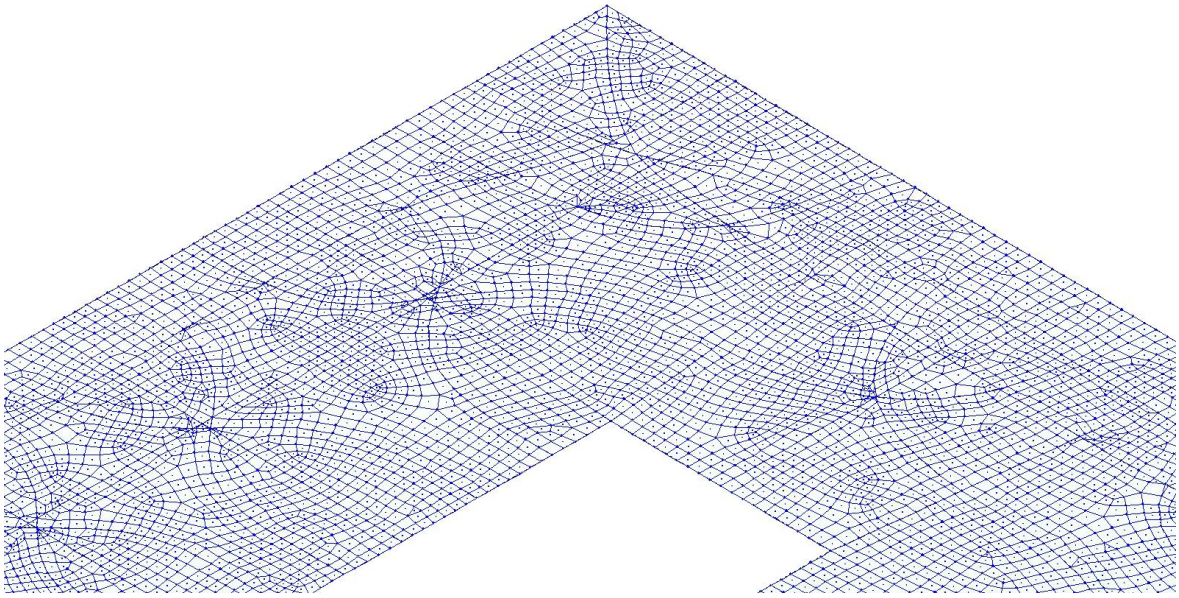

Figure 102: Self-weight (Source: author, 2016)

- A spreadsheet is available on S-Frame where are all the support reaction values are available with as many values as there are number of nodes.

These values are exported to an excel spreadsheet, then inverted to become load values, which are the tributary areas.

The next stage is to apply the previous results of tributary area loads to a new model (Figure 103).
First, the supports on this new model must be defined, which are composed of the optimized tendon layout, divided into a number of bars and nodes.
The x y z constraints are defined where the supports are located. These supports are the 0 coordinates and correspond to the high points of the drapes. All the other nodes are free to move on the z axis, but are blocked on the x and y in order to fix the tendon IN-PLAN profile and to measure only the drapes. Concerning the supports at the edges (core and slab edge extremity), a deflected value of 4 inches is imposed. This value of 4 inches derives from being the perfect mid-height of the slab thickness.

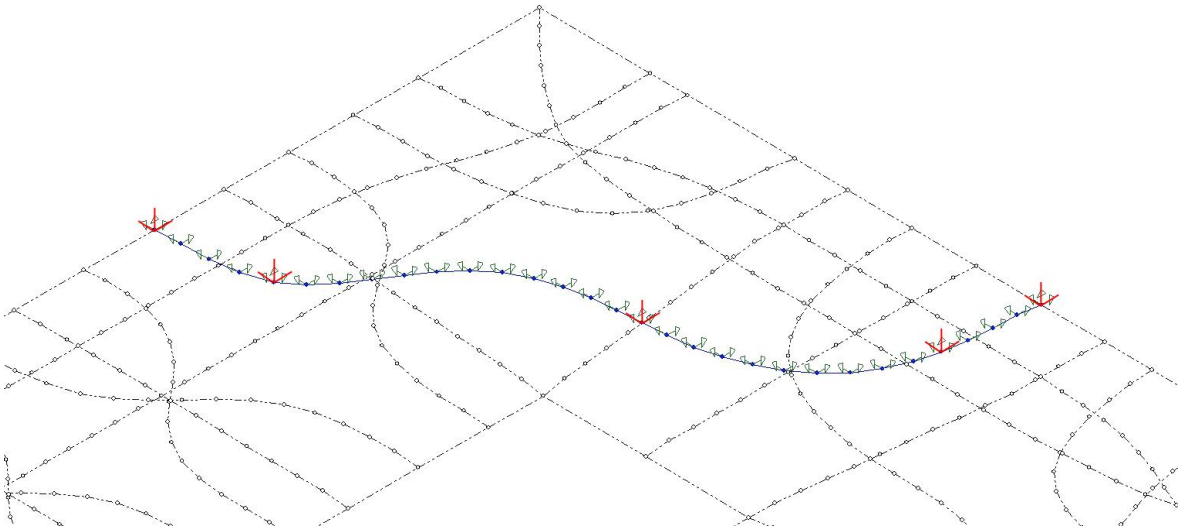

Figure 103: Supports assignation (Source: author, 2016)

Next, the tributary area loads are imposed on the nodes using the same spreadsheet as before in order to affect each value with its corresponding node (Figure 104).

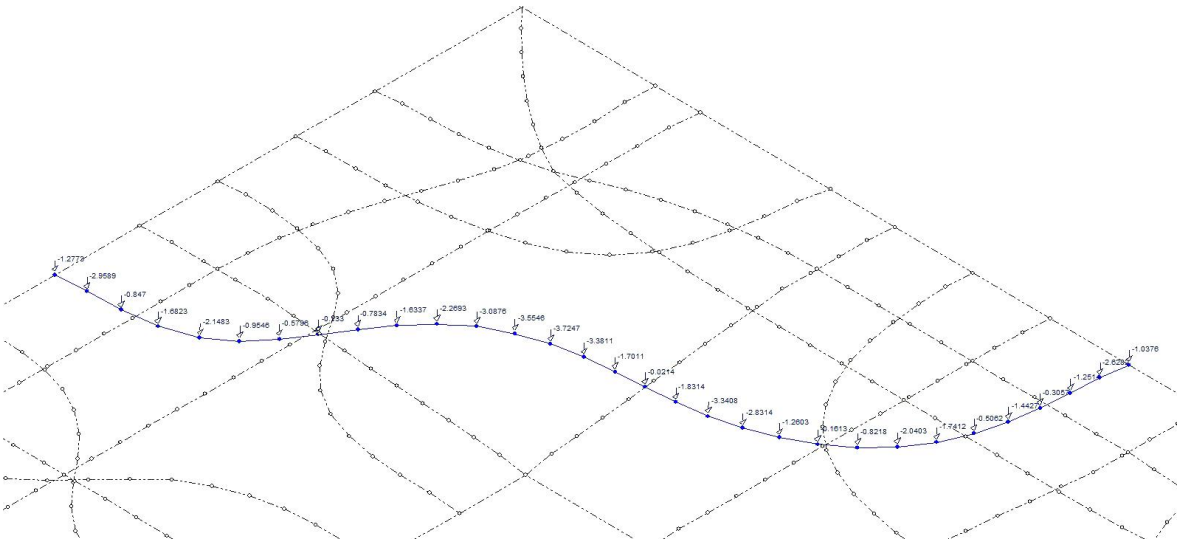

Figure 104: Gravity tributary loads applied to each node (Source: author, 2016)

Another complexity lies in understanding how to optimize the drapes. A target of 6 inches maximum (high point to low point) is aimed for because:
Slab thickness = 8” and cover = 1” both on top and bottom part of the slab. Max possible drape therefore becomes 6”.
To estimate the max drape a trial and error process is applied to optimize tendon by tendon. Effective tendon forces of 27 kips are imposed, which is the effective force of each tendon. The deflection is measured for each multiple of 27 kips to be the closest as possible to a 6” deflection value.
The trial and error procedure is then stopped at a max value very close to 6 inches, but without exceeding this value.

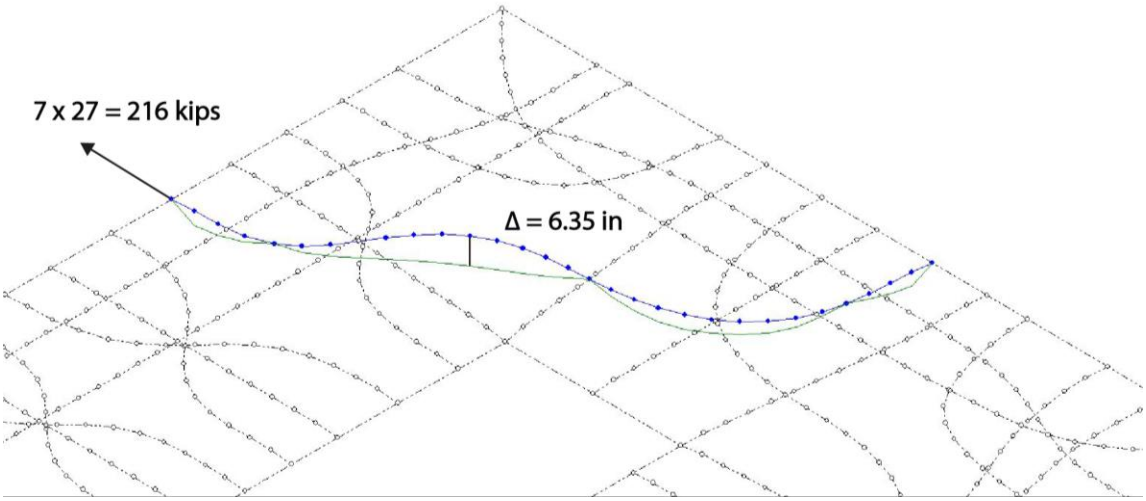

Figure 105: Optimal drape research procedure: too high deflection value (Source: author, 2016)

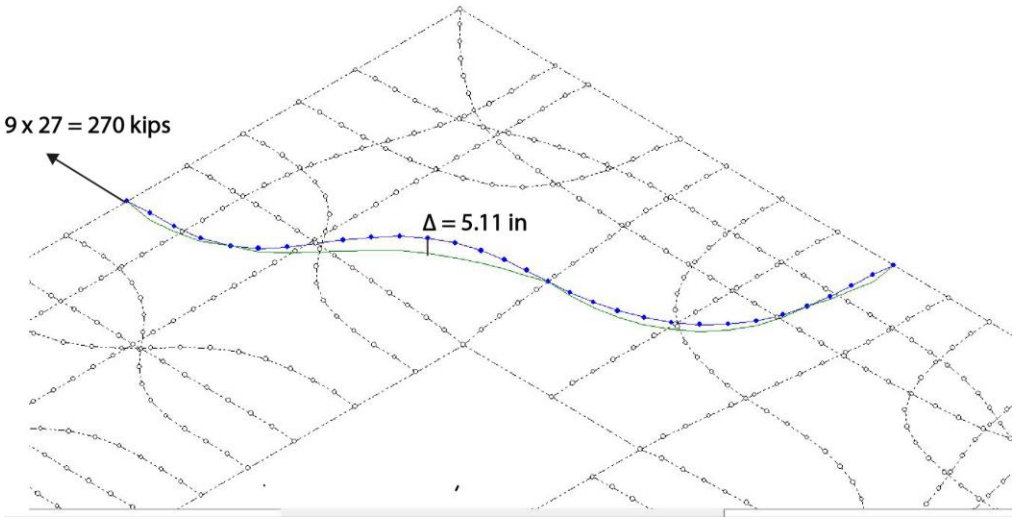

Figure 106: drape research procedure: too low deflection value (Source: author, 2016)

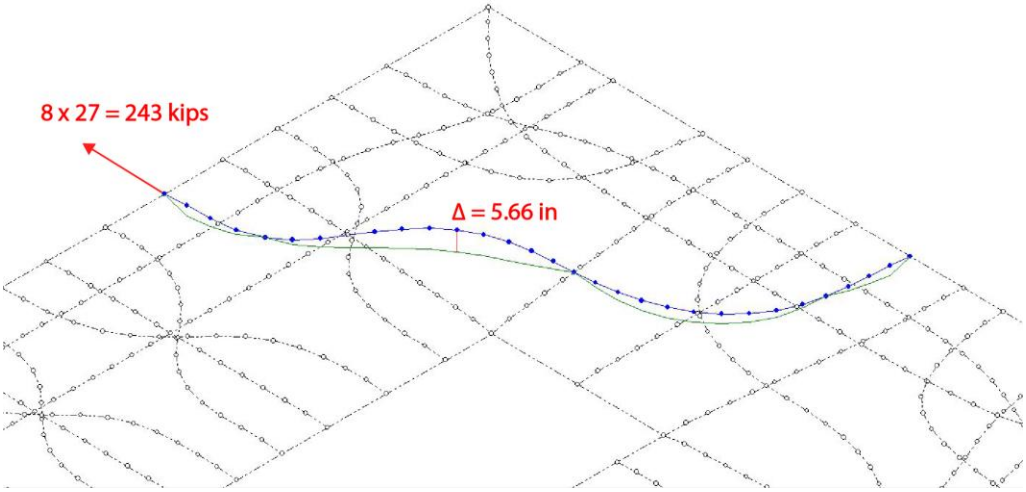

Figure 107: Optimal drape research procedure: deflection value in-between: Selected values (Source: author, 2016)

The following table presents the hold deflection prestress values for each tendon.
This table proves useful when going back to the IN-Plan procedure to assign the correct number of tendons for each group of tendons.

# Tendons	loads (kips)	Prestress (kips)	Tend.	Max deflection (in)	Min deflection (in)
1	14.37	81	3	5.50	1.61
2	16.28	135	5	5.34	1.28
3	19.69	135	5	5.70	1.33
4	20.25	162	6	5.69	1.26
5	10.49	135	5	5.31	1.34
6	17.07	189	7	5.65	1.28
7	18.04	216	8	5.66	1.28
8	21.57	270	10	5.86	1.23
9	14.07	108	4	4.35	1.40
10	14.46	81	3	5.74	1.59
11	16.91	81	3	5.42	1.48
12	27.40	216	8	5.90	0.99
13	25.86	216	8	5.91	0.90
14	27.14	216	8	6.00	0.99
15	19.87	189	7	5.56	0.96
16	42.95	162	6	5.65	1.07
17	23.15	216	8	6.00	1.08
18	21.54	189	7	5.74	1.21
19	28.73	297	11	5.94	1.04
20	25.49	243	9	5.66	0.98
21	50.18	243	9	5.66	0.86
22	27.51	270	10	5.92	0.90
23	15.08	216	8	5.83	0.97
24	40.37	189	7	5.82	0.74
25	25.14	297	11	5.86	0.91
26	21.36	216	8	5.98	1.01
27	31.35	405	15	5.86	0.31
28	26.07	270	10	6.00	1.04
29	53.57	297	11	5.95	0.68
30	28.99	324	12	5.89	0.95
31	20.28	54	2	4.49	1.85
32	26.88	81	3	5.08	1.67
33	20.79	54	2	5.35	1.62
34	26.89	81	3	5.35	1.61
35	45.88	81	3	5.20	1.08
36	43.30	108	4	5.51	1.05
37	52.71	135	5	5.52	0.66
38	51.60	81	3	5.52	1.31
39	44.82	81	3	5.44	0.75
40	60.01	162	6	5.73	0.82
41	60.95	135	5	5.47	0.72
42	38.88	81	3	5.00	0.67

Table 10: Loads, Prestress, Number of tendons, max and min deflection values corresponding to each group of tendons (Source: author, 2016)

5.2.2 FEM Verification

Once a specific height is assigned to each node value, this following phase enters those values into the Finite Element Model. This section was particularly time consuming because of the technical restrictions of the software.
In fact, SAFE does not define precise points along the cables nor does it permit a z coordinate to be attributed to these points. The process was an elementary process if not an artisanal one. In order to target the nodes, it was decided to create fictive columns. The positioning of the columns corresponds to the location of each node, i.e. each 3' along the tendon length (Figure 108).

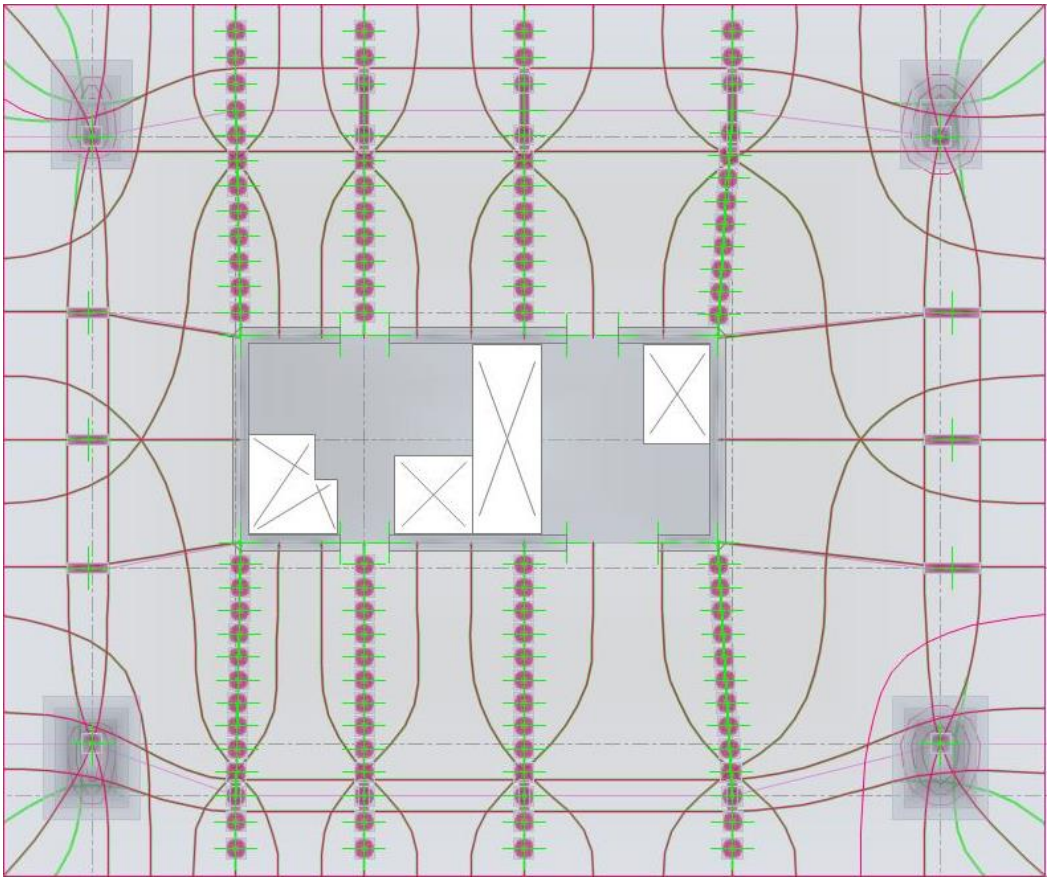

Figure 108: Method to manually create some new points on SAFE, In-plan view (Source: author, 2016)

The presence of the fictive columns allowed for new points on the tendon, with the spacing between each node the imposed length was then the total length between two high points (a high point corresponding to a support). This length was then divided by the number of spacings found between the nodes (Figure 109) composing this length. The heights' values for each node could have been entered into the tendon vertical profile SAFE window.

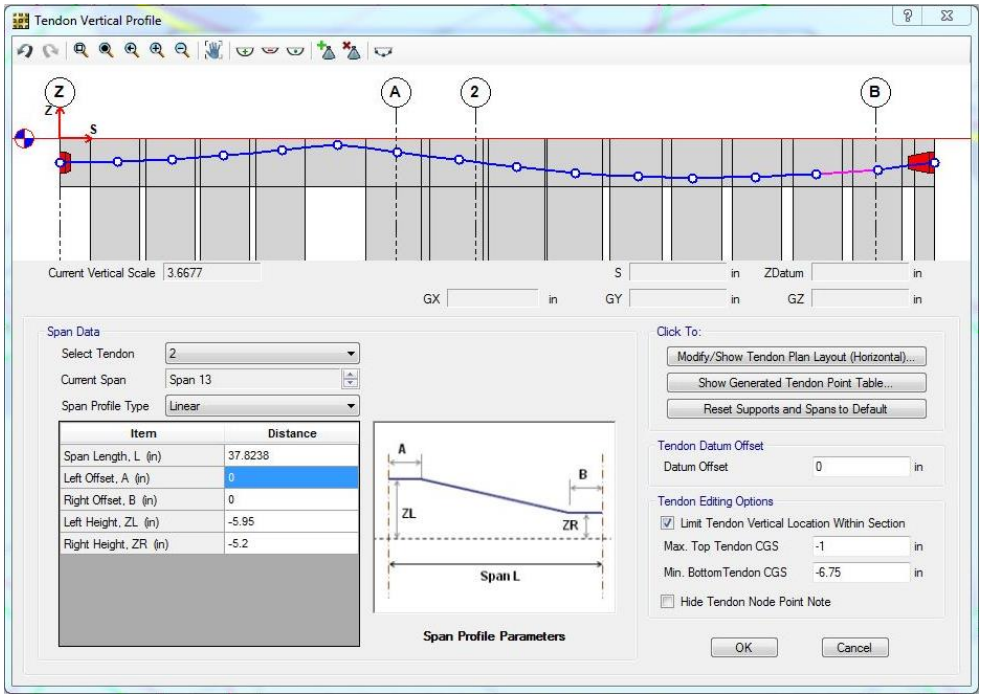

Figure 109: Method to manually create some new points on SAFE, Profile view (Source: author, 2016)

The columns were deleted just after the respective heights were defined. At the end of this process, the profile is able to be sufficiently well determined (Figure 110).

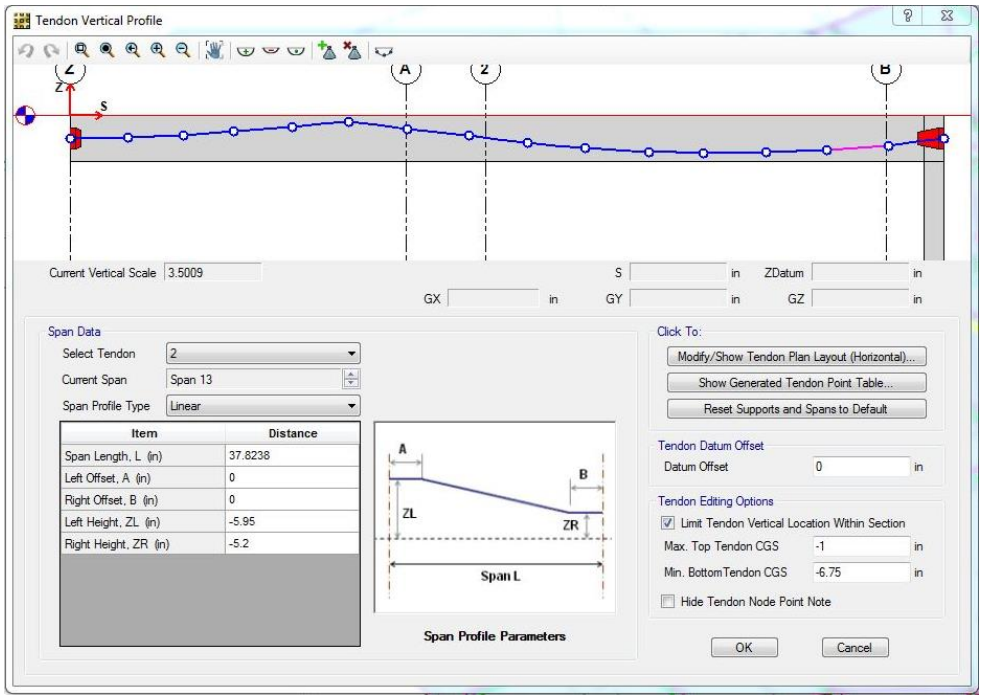

Figure 110: New optimized profile (Source: author, 2016)

While this methodology has worked, some uncertainty yet remains. I contacted the CSI technical support, asking them if there was a better way to proceed. They answered me the software did not allow to modify precisely the z coordinate of a point and I assume the very time consuming methodology I have just introduced was therefore only way and best way to proceed in the meantime.

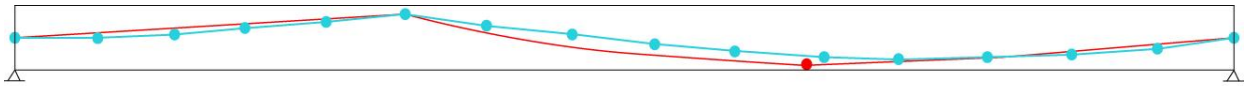

Figure 111: Comparison of the conventional profile (in red) and the optimized profile (in blue): Example of a straight tendon (Source: author, 2016)

There is not such a significant difference between the conventional tendon profile and the optimized one (Figure 111). This is due to dealing with a straight tendon. In fact, the tributary loads applied to the nodes are far more regular than the one applied to a curved tendon (Figure 112).

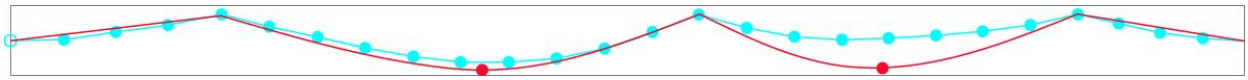

Figure 112: Comparison of the conventional profile (in red) and the optimized profile (in blue): Example of a curved cable (Source: author, 2016)

All of the profiles have been modified into the FEM model and it is now possible to run the analysis in order to observe the performance obtained through the Force Density Method optimization.
The comparison was made also for the previous models with a long-term deflection output.

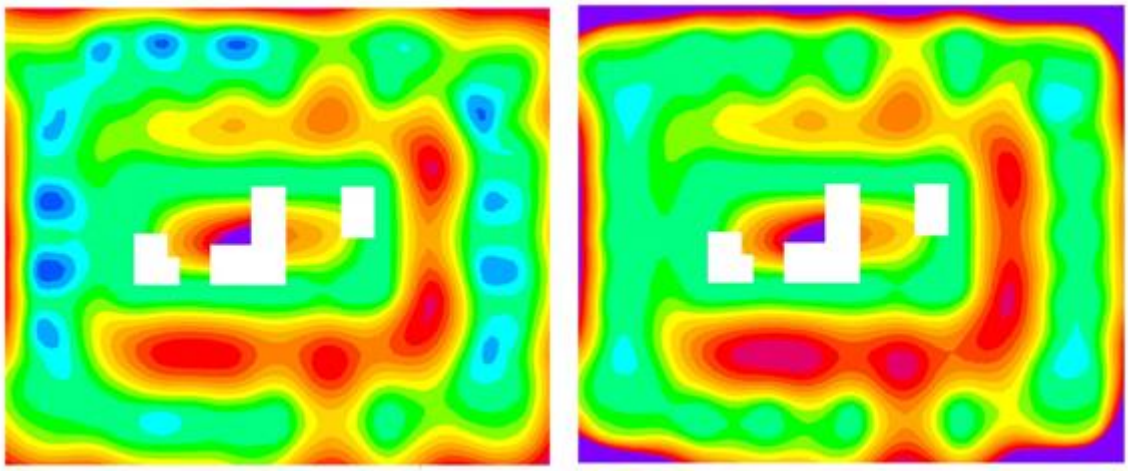

(a) (b)

Figure 113: Long-term deflection profile: (a) Conventional post-tensioned layout, (b)Post-tensioned layout optimized both in plan and in profile (Source: author, 2016)

A strong similarity is noticed between the two deflection profiles (Figure 113). They have exactly the same shape, except the optimized long-term deflection profile is worse than the layout without optimization of the profiles. For the same amount of PT between the TO layout, optimizing does not increase the deflection of the slab.

The positive aspect is no longer having uplift which is the normal consequence of a more deflected plate.

6 Conclusions and future developments

According to the United Nations Environment Programme (UNEP), buildings consume about 40% of global energy, 25% of global water, 40% of global resources and they emit approximately one third of the greenhouse gas emissions, the principal cause of the greenhouse effect.
There is not one good solution to build with less environmental impact, but the combined efforts of many small actions could allow the building sector to perform positively on behalf of the planet, especially when it is well established that cement production is responsible for around half of the industry's CO2 output. This figure includes both the energy required to produce cement as well as the CO2 given off as a by-product due to the chemical reactions involved.

Architecture, which aims to develop a coherent attitude, must find new forms, expressions and materials not only in reference to traditional forms and classical use of materials, but each building project should provide an opportunity to develop a new way of building the future.

The innovative methodology developed by the structural engineering team of the Skidmore Owings & Merrill LLP San Francisco office has all throughout the research has contributed to inventing a new way to achieve post-tensioned concrete flat slabs.
Post-tensioning is in fact commonly used in the bay area construction as it is a way to build very thin slabs allowing buildings to get more floors within the same overall height, which is economically relevant. Post-tensioning compared to traditional reinforced concrete brings many advantages such as larger spans with thinner slabs, less cracking and shrinkage effects, etc.
Nevertheless, it has been stated at the beginning of the study that the conventional approach for post-tensioning, especially when applying it to complex architectural shapes, is a very time-consuming procedure. This process in no way assures achieving the best method or location to place the cables into the concrete slab.

To counteract this problem, new innovative tools have been developed through a number of consecutive steps with a final objective of optimizing post-tensioning in concrete flat slabs. This method has been pursued through the design phase of a real case study, i.e. a luxury 20-story housing situated in the south of market area of San Francisco.

For this case study, methods of optimization have been investigated and more particularly the Topology optimization and the Force Density Method. It was decided to proceed with a comparative approach of three different schemes: a conventional, an optimized one but realistic for construction and a highly optimized one which would not take into account too many ACI codes and technical restrictions.

The first approach has been the In-Plan optimization study pursued mainly with an Altair software, HyperMesh Optistruct. The study with HyperMesh procured a wide range of outputs. It has been important to develop some interpretation methodologies, allowing to step accurately from the optimization results to the new optimal post-tensioning layout.
Also, it was necessary to bring into the first optimized layout a new placement of the banded tendons into the slab as the uniform tendons remained similar between the conventional scheme and the first optimized scheme. For this reason, one was termed the double-banded optimal scheme. In fact, in this scheme, with respect to the conventional one, the banded tendons were split into a pair of 2 tendons.
The first results brought through a deflection profile control realized with the FEM software SAFE did not provide any great ameliorations from the first to the second scheme. The comparison was made with the help of the post-tensioning weight amount present in each scheme. The saving with the optimal scheme was only 4.5%.

An amelioration of the methodology led to once again splitting the banded tendons at the corners proceeding to a trial-and-error procedure of the deflection at the corners. These were problematic zones because of large cantilevers up to 11 feet. In this trial a 15% saving of post-tensioning between the conventional and the optimal scheme was found.

The following step has been to optimize as much as possible the PT layout. Interpreting again the output from the Topology Optimization led to a biomimicry scheme, composed of only banded tendons, with tendons of increased curvatures.
The final savings was found at 28%, an important amount to achieve when considering just the slab of the building.

This high savings of post-tensioning allows to say that the methodology used is reliable and applicable within engineering practice. Nevertheless, to master it in its entirety the optimization procedure has been submitted to different checks; such as verifying if the amount of rebar would not greatly increase in the case of an optimal scheme, or if the demands on hairpins due to the high curvatures of the tendons would produce new compressive stresses within the slab. A MatLab code has been written by the author to determine easily and quickly the amount of rebar demand in the three schemes. This has resulted in observing that even when the post-tensioning is optimized, as is the amount of rebar. The demand on hairpins is increasing into the high curvature location of the only banded scheme, which surely would become a new parameter to take into account in order improve the optimization procedure.

Also, improving the results would cause them to pass through the optimization of the profiles. For the In-Plan profiles optimization, the drape profiles of the cables have been the same at mid-thickness of the slab as at the edges and high at the supports while low at the mid-spans.
This optimization step has been conducted with the help of the Force Density Method combined with MatLab codes, the S-Frame software analysis in order to study the force density

and HyperMesh and the Strand software to define the accurate tributary loads . In fact, one of the main difficulties has been to find the way to calculate the adequate tributary load at each node and for each cable as the tendons geometry in the optimized layout became quite complex. The cables have been discretized into a number of nodes in order to study quite precisely the deflection of the profiles and then compare it with the conventional profiles. This study was followed only for the most optimal scheme, the only banded one. A ratio between a max permissible deflection of each node and the tension applied to each cable (27 kips by cable and multiplied as soon as the correct deflection had been reached), allowed for the determination of the correct amount of strands for each cable as the new deflection profile of each tendon. A limit a deflection of 6 inches was kept with the slab thickness being of 8 inches, 1 inch at the top and 1 inch at the bottom of the slab were required for the concrete cover.

As for the In-Plan study a FEM verification has been made with SAFE. The results obtained were better without an optimization of the profiles. The optimization procedure with the Force Density Method did not procure any amelioration of the final defected shape of the slab, and as proceeding towards an optimization, the contrary would have been expected, i.e. to save again some tendons and to improve the deflected shape.
This finding questions the time passed to proceed to the optimization of the profiles. As stated by Werner Sobek “Research must not be afraid of failing. That’s the most important thing to tell people: it’s not a problem if you work for six, eight or twelve months on something and then it doesn’t work out because the path you took was not in vain.” In fact, the results achieved through FDM should assist the research in continuing to progress and improving the methodology of the profile optimization.
Force Density Method appears to be the best methodology, but there is a need to identify what else can be used to further improve it.
In fact, one possible development could be, instead of applying tributary loads onto the cable nodes with the concrete self-weight slab combined with the post-tensioning cables weight, to instead apply the moments’ values corresponding to each node position, which would reflect more realistically the drape behavior of the tendons. This method would find a way to extract the moment value at each coordinate of the slab. One further step for the research would consist of considering construction constraints (construction techniques, feasibility, time and cost) to adapt the obtained optimized profiles to a possible utilization on site.
Moreover, it is important to recall that the optimization method has been pursued in the elastic domain for simplifications and so one of the possible deepening would also be to control the results in an Ultimate Limit State, because the real behavior of the plate has to be considered within the Ultimate limit state case.
It could be also interesting to go in a further way towards developing a methodology to optimize the rebar in order to fit perfectly in the new optimal placement of the post-tensioning tendons.

As said by Hegel it is "…that the fear of being wrong constitutes an error in itself". Research for new forms has to follow not just a rational procedure but it is necessary to also follow intuition and to be fundamentally aware of all kinds of inspirational inputs. The key is to pass beyond existing borders.

Figure 114: All kinds of inspirations can contribute to develop new ideas: Iranian tiling, 17th century (Source: Photo taken by Mark Sarkisian in the Louvre department of Islamic arts,Paris, 2016)

Bibliography

Post-tensioning

[1] ACI 318-08, Building code requirements for structural concrete, American concrete institute, 2008.

[2] O. Aalami, Bijan, *Post-tensioned buildings Design and Construction,* US Edition, 2014.

[3] O. Aalami, Bijan, Gail, S. Kelley, Design of concrete floors, With particular reference to post-tensioning, *Pti techincal notes*, Issue 11, january 2011.

[4] O. Aalami, Bijan, Gail, S. Kelley, Unbonded and bonded post-tensioning systems in building construction, A design and performance review, *Pti techincal notes*, Issue 11, september 1994.

[5] Bondy, Kenneth, Post-tensioned concrete: Five decades of American Building construction, *Concrete construction*, december 2001.

[6] Bondy, Kenneth, The state of post-tensioned concrete education, *Concrete international,* october 2014.

[7] Guyon, Yves, *Béton précontraint: étude théorique et expérimentale*, Paris : Eyrolles, 1958.

[8] Gupta, Pakwan R., Watry, C. Nicholas, Sustainable design of buildings by post-tensioning concrete, *Concrete international,* october 2012.

[9] Huang, Yu, Kang, Thomas, Computer modeling of post-tensioned structures, *Singapore : IPCSIT*, vol. 22, 2012.

[10] Lefebvre, Denis, Effets du retrait-fluage sur les structures en béton pécontraint, *4th Structural specialty conference of the Canadian society for civil engineering*, june 5-8, 2002.

[11] Lin, T.Y., Burns, Ned H., *Design of prestres sed concrete structures*, US : John Wiley & Sons, 1981.

[12] Miller, Dane, Doh, Jeung-Hwan, Peters, Tim, Environmental impact assessment and conventional reinforced concrete slab design, *ISEC-7, Honolulu June 18-23*, 2013.

[13] Nawy, Edward G., *Prestressed Concrete: A Fundamental Approach.* Fifth Edition. Upper Saddle River, New Jersey: Pearson Prentice Hall, 2006.

[14] Post-tensioning institute, *What is post-tensioning?,* december 2000.

[15] SAFE, Post-tensioned concrete, Design manual, CSI Computers and structures, Berkeley, California,

USA, december 2010.

[16] VSL, *Post-tensioned in buildings,* 1985.

[17] VSL, *Post-tensioned slabs,* 1985.

Plates theory

[18] Belluzzi, O., *Scienza delle Costruzioni, vol.3*, Italy: Zanichelli, 1966.

[19] Timoschenko, Stephen, Woinowsky-Krieger, Serge, *Theory of plates and shells*, US : McGraw-Hill, 1959.

Optimization

[20] ALTAIR ENGINEERING. Optistruct. 2013.

[21] Beghini, A., Stromberg, L. L., Baker, W. F., Paulino, G. H., Mazurek, A., A New Frontier in Modern Architecture: Optimal Structural Topologies.

[22] Beghini, A., Sarkisian, M., Geometry Optimization in structural design, *SEAOC 83rd annual convention,* 2014.

[23] Beghini, L. L., 2013, Building science through topology optimization, *Doctoral dissertation*, University of Illinois at Urbana-Champaign.

[24] Baker, William F., Beghini, Alessandro, Beghini, Lauren L., Mazurek, Arkadiusz, Carrion, Juan, Combining classical theories with new technologies, *The Higgins lecture,* 2013.

[25] Gründig, Lothar, Moncrieff, Erik, A history of the principal developments and applications of the force density method in germany 1970-1999, *IASS-IACM 2000*, Fourth international colloqium on computation of shell & spatial structures, 2000.

[26] Halpern, Alsion B., Billington, David P., Adriaenssens, Sigrid, The ribbed floor slab sytems of Pier Luigi Nervi, *Proceedings of the international association for shell and spatial structures (IASS) Symposium 2103 « Beyond the limits of man »,* 2013.

[27] Ho-Le, K, Finite element mesh generation methods : a review and classification, *Computer-aided design*, vol. 20, 1988.

[29] Krauser, Gaelyn, Optimization of two-way post-tensioned concrete floor systems, *Thesis presented to the faculty of California Polytechnic State University, San Luis Obispo*, october 2009.

[30] Sigmund, Ole, Bendsoe, Martin Philip, *Topology Optimization, Theory, Methods and Applications*, Germany : Springer Science & Business Media, 2003.[34] Tarisciotti, C., Biancolini, M. E., Quando le equazioni dell'elasticità progettano strutture, *A&C Analisi e calcolo*, Num.59, november/dicember 2013.

[31] Vanderbergh, T., De Wilde, W.P., Latteur, P., Optimization at the conceptual design stage with morphological indicators : design for strength or design for stiffness ?, *WIT Press*, Vol 97, 2008.

[32] Veenendal, D., Block, P., An overview and comparison of structural form finding methods for general networks, *International journal of solids and structures*, 2012.

[33] Johnsen, Stephen, Structural topology optimization, Basic theory, Methods and Applications, 1988.

APPENDICES

APPENDIX 1

Project: 75 HOWARD
Subject: To optimize the corner tappered columns curves
Date: 8/12/2015
By: M.H.

Material Properties

Wc =	150	pcf
f'c =	5	ksi
b=	12	in
As =	0.153	in2
fy =	245	ksi

Slab thickness

t=	8	in

Loads

SDL=	45	psf
SWT=	100	psf
W(psf)=	145	psf
curtain L=	385	p/ft

Methodology

Mn=As*fy*(d-a/2) with a = (As*fy)/(0.85*f'c*b)

Mn=As*fy*(d-0.57*(As *fy/f'c*b))

Mx known

And : Mn = Mx

If d is found , so h can be found too, in varying x, y and z values

d=0.59*(As*fy /f'c *b) + (Mx/As*fy)

h= d + cover with cover = 0.75 in

Strip 1 (Z direction):			**Strip 2 (X direction):**		
N tendons	3		N tendons	3	
Asz =	0.459	in2	Asx =	0.459	in2
Z	M(z) (kft)	h (in)	X	M(x) (kft)	h (in)
0	0	1.82	0	0	1.82
2	-0.5	1.76	2	-2.56	1.55
4	-1.37	1.67	4	-6.98	1.07
6	-2.97	1.50	6	-15.12	0.20
8	-5.64	1.22	8	-28.84	-1.26
10	-9.75	0.78	10	-49.97	-3.51
12	-15.54	0.16	12	-78.95	-6.61
14	-23.67	-0.71	14	-113.98	-10.34
16	-34.21	-1.83	15	-133.5	-12.43
18	-47.6	-3.26	15.5	-143.27	-13.47
20	-64.2	-5.03	16	-153.03	-14.51
22	-84.04	-7.15	16.5	-163.3	**-15.61**
24	-106.75	-9.57	17	-173.57	-16.70
26	-131.66	-12.23	17.5	-183.83	-17.80
28	-156.16	-14.85	18	-194.1	-18.89
28.1	-159.52	-15.20	18.5	-182.73	-17.68
28.6	-166.31	-15.93	19	-171.48	-16.48
29.1	-173.11	-16.65	19.5	-160.17	**-15.27**
29.6	-180.05	**-17.39**	20	-149	-14.08
30.1	-188.99	-18.35	20.5	-138.12	-12.92
30.6	-193.93	-18.88	21	-127.23	-11.76
31.1	-198.17	-19.33	23	-85.97	-7.36
31.6	-191.6	-18.63	25	-49.68	-3.48
32.1	-185.02	-17.93	27	-20.36	-0.35
32.6	-178.45	**-17.22**	29	0	1.82
33.1	-171.9	-16.53			
33.6	-165.43	-15.83			
34.1	-158.96	-15.14			
34.6	-152.5	-14.45			
35.1	-146.06	-13.77			
35.6	-139.8	-13.10			
35.9	-136.04	-12.70			
36	-134.79	-12.57			
38	-110.34	-9.96			

Strip 3 (Y direction):		
N tendons	5	
Asy =	0.765	in2
y	M(y) (kft)	h (in)
0	0	2.53
2	-5.94	2.15
4	-13.42	1.67
6	-24	0.99
8	-39.22	0.02
10	-60.62	-1.35
12	-89.68	-3.21
14	-126.41	-5.56
16	-169.33	-8.31
18	-216.88	-11.36
18.91	-239.93	-12.83
19.41	-252.59	-13.64
19.91	-265.25	-14.45
20.41	-278.23	**-15.28**
20.91	-291.27	-16.12
21.41	-304.32	-16.95
21.91	-317.37	-17.79
22.41	-308.47	-17.22
22.91	-294.76	-16.34
23.41	-281.02	**-15.46**
23.91	-267.35	-14.59
24.41	-253.96	-13.73
24.91	-240.56	-12.87
25.41	-227.16	-12.01
25.91	-214.1	-11.18
26.41	-201.36	-10.36
26.91	-188.61	-9.55
27.41	-175.86	-8.73
27.91	-163.98	-7.97
28.41	-152.2	-7.21
28.91	-140.42	-6.46
29.41	-128.95	-5.73
29.91	-118.47	-5.05
30.41	-108	-4.38
32	-77.39	-2.42

APPENDIX 2

HyperMesh Simple Guide

Steps for HyperMesh Optistruct

- Import Geometry from autocad (xref file)
- Define components: Slab, Core, Columns)
- Create then assign component to each surface (surface edit)
- Trim surfaces with lines to obtain a perfect mesh
- Create the mesh (Automesh): Here mesh of 6 inches
- Create the boundary conditions (load collectors)
- Create loads cases (pressure)
- Create material
- Create properties referred to the material
- Assign properties to components
- Define load step
- Run first analysis to verify if is the load is applied correctly
- Define the optimization parameters:

Responses/create:

1) VOLFRAC (volume fraction)
2) COMPL (compliance)

Dconstraints/create:

1) constraint = VOL CONST
2) response = VOL FRAC

Objective:

COMPL (compliance)

Then vary the density and the penalization factor:

- Run analysis for each different case an plot the results

Density = dconstraints

Upperbound: 0.1 à 0.5

Penalization factor = Opticontrol

Discrete : 1 à 4

APPENDIX 3

```
%%%%%%%%%%%%%%%%%%%%%%%%%%%%%%%%%%%%
%                  Post-Tensioning                  %
%                  Rebars quantity                  %
%%%%%%%%%%%%%%%%%%%%%%%%%%%%%%%%%%%%

clear all;
close all;

%read and post the input jpg obtained with hypermesh/optistruct

A1=imread ('scheme1.jpg');
A2=imread ('scheme2.jpg');
A3=imread ('scheme3.jpg');

% store number of red pixel for each area selection
countBlu = zeros(3,2);

for k=1 : 3

   expression= strcat('A=A',num2str(k));
   eval(expression);

   figure;
imshow(A);

% Convert R,G,B from input image to three seperate matrices, uint8 data
imageR = A(:,:,1);
imageG = A(:,:,2);
imageB = A(:,:,3);

% dim of the figureb (pixel)
dim = size(A(:,:,1));

% Rlimit, Glimit, Blimit
Rlimit = 50;
Glimit = 50;
Blimit =102;

% reset nonBlu count to zero for each loop
count = 0;

% for each pixel within the selected area in current loop, determine if it is red, if not, change RGB to white
for m = 1: dim(1)

   for n=1: dim(2)

if imageR(m,n) < Rlimit && imageG(m,n) < Glimit && imageB(m,n) > Blimit
```

```
   % count if Blu
count = count+1;

else

imageR(m,n) = 255;
imageG(m,n) = 255;
imageB(m,n) = 255;


end
end

end

countBlu(k,1) = count;

Bluratio(k,1)=count/(dim(1)*dim(2));

A = cat(3,imageR,imageG,imageB);
imshow(A)

end
```

APPENDIX 4

This self-developed code was elaborated as a tool to quickly determine the number of tendons to be implemented for each of the cables participating in a post-tensioning layout.

```
%%%%%%%%%%%%%%%%%%%%%%%%%%%%%%%%
%                Post-Tensioning                %
%              Banded tendons quantity          %
%%%%%%%%%%%%%%%%%%%%%%%%%%%%%%%%

clear all;
close all;

%read and post the input jpg obtained with hypermesh/optistruct
A=imread ('image3.jpg');

figure;
imshow(A);

% Convert R,G,B from input image to three seperate matrices, uint8 data
imageR = A(:,:,1);
imageG = A(:,:,2);
imageB = A(:,:,3);

% dim of the figureb (pixel)
dim = size(A(:,:,1));

% number of total loops - user input
nloop = 2;

% Rlimit, Glimit, Blimit
Rlimit = 200;
Glimit = 50;
Blimit =50;

% store number of red pixel for each area selection
countRed = zeros(nloop,1);

% define variable storing matrices for each mask (from ROIPOLY, type logic)
totalMask = zeros(dim(1), dim(2), nloop);

% select area for each loop
for k = 1 : nloop
B=roipoly(A);

% convert logic data type to uint8 data type (0s and 1s)
newB=uint8(B);

% store matrix from each loop to totalMask
```

```
totalMask(:, :, k) = newB;
end

% variable for suming all masks for plots
newB1plot = zeros(dim(1), dim(2));

% filter and count number of red pixel for each loop
for q = 1: nloop
% extract mask
newB = totalMask(: , :, q) ;

% summing mask for plot
newB1plot = newB1plot +newB;

% reset nonRed count to zero for each loop
count = 0;

% find index for nonzero(selected area) pixels in the current loop
[row,col] = find(newB);

% for each pixel within the selected area in current loop, determine if it is red, if not, change RGB to white
for m = 1: length(row)
    i = row(m);
    j = col(m);
if imageR(i,j) < Rlimit || imageG(i,j) > Glimit || imageB(i,j) > Blimit
imageR(i,j) = 255;
imageG(i,j) = 255;
imageB(i,j) = 255;

% count if nonRed
count = count+1;

end
end

% find red pixel by subtracting the number of nonRed pixel from the total number of pixel selected from current
loop
countRed(q) = length(row)-count;
end

%% PLOT
% adjust RGB based on overlay of masks, if mask = 0 at the pixel (i.e. not selected), then R=G=B =0 = Black
newimage1=A(:,:,1).*uint8(newB1plot);
newimage2=A(:,:,2).*uint8(newB1plot);
newimage3=A(:,:,3).*uint8(newB1plot);
% determine the red pixel to plot within the selection
[rownew,colnew] = find(newB1plot);
for m = 1: length(rownew)
    i = rownew(m);
    j = colnew(m);
if newimage1(i,j) < Rlimit || newimage2(i,j) > Glimit || newimage3(i,j) > Blimit
```

```
newimage1(i,j) = 255;
newimage2(i,j) = 255;
newimage3(i,j) = 255;
end
end
newimage=cat(3,newimage1,newimage2,newimage3);
imshow(newimage);

totalarea = sum(countRed);
percentage=countRed/totalarea;
```